NASA CR-177,344

NASA-CR-177344
19850024798

A Reproduced Copy

OF

NASA CR-177,344

Reproduced for NASA

by the

NASA Scientific and Technical Information Facility

NASA CONTRACTOR REPORT 177344

Fixed Gain and Adaptive Techniques For Rotorcraft Vibration Control

R. H. Roy
H. A. Saberi
R. A. Walker

CONTRACT NAS2-11548
May 1985

NASA

NASA CONTRACTOR REPORT 177344

Fixed Gain and Adaptive Techniques For Rotorcraft Vibration Control

R. H. Roy
H. A. Saberi
R. A. Walker
Integrated Systems Inc.
Palo Alto, California

Prepared for
Ames Research Center
under Contract NAS2-11548
May 1985

National Aeronautics and
Space Administration

Ames Research Center
Moffett Field, California 94035

TABLE OF CONTENTS

TABLES

FIGURES

LIST OF SYMBOLS

$a_{(x,y,z)}$	axial, lateral, and normal specific forces at the pilot location
$A(j\omega)$	frequency dependent cost on system
A_{mp}	six-vector of the amplitude of the of the vibration responses at the pilot location due to equal forces in all six directions at the hub for the m^{th} mode
A_i	lagged output coefficient matrices in autoregressive model
A_{1_s}, B_{1_s}	cyclic swashplate controls
b_i	numerator coefficient of frequency-shaping filter in discrete form
$B(j\omega)$	frequency dependent cost on system imputs
B_i	lagged input coefficients of matrices in autoregressive model with exogenous inputs
$C(k)$	controller feedback gain matrix
D	feedforward output distribution matrix
F	system dynamics matrix
$F_{(x,y,z)}$	axial, lateral, and normal forces at the rotor hub
G	control distribution matrix
h_i	frequency shaping filter numerator coefficients in continuous time domain
H	measurement distribution matrix
K	symmetric stiffness matrix
$\bar{K}$	generalized stiffness matrix
$K(k)$	Kalman gain matrix
L,M,N	roll, pitch, and yaw torques at the rotor hub
M	symmetric mass matrix

$\tilde{M}$	generalized mass matrix
$P(k), P(k\|k)$	filtered state (parameter) estimate error covariance matrix at indexed time point K
$P(j\omega)$	frequency shaping filter transfer function in continuous time domain (SISO)
$P_\eta(j\omega)$	matrix square-root of frequency dependent output cost function in continuous time domain
$Q(k)$	process noise covariance matrix
R	measurement noise covariance matrix
$R_\nu(\kappa)$	innovations covariance matrix
R_{mp}	approximate amount of vibration excitation of mode m at the rotor hub assuming equal forces and moments in all directions
RSS	root-sum-square
T	matrix relating inputs and outputs in the static model of vibration valid at a single frequency only
T	force distribution matrix
$u(k)$	dynamic system control imput vector
$v(k)$	measurement noise vector
VEQ	equivalent airspeed
$x(k)$	dynamic system state vector
$y(k)$	vector of system output measurements
z	Frequency variable in discrete time domain
$\varepsilon(\kappa), \nu(\kappa)$	predicted data residuals (innovations)
ζ	damping coefficient (>0⇒ stability)
η	vector of generalized coordinates
θ	vector of parameters to be estimated in
$\theta_{c,tr}$	{collective, tail rotor} controls

$\lambda(k)$	"forgetting factor"
$\phi(k)$	vector of lagged inputs and outputs
ϕ_{mp}	vector of modal deflections at the hub
ψ	rotor shaft angle
ω	frequency variable in continuous time
ω_m	frequency of m^{th} vibration mode
Ω	fundamental vibration frequency (N/rev)
Ω_ρ	pre-warped Ω (bilinear transform)
Ω_r	rotor angular velocity
$(\cdot)_{fs}$	frequecncy shaping filter state/parameter
$(\cdot)^T$	vector/matrix transpose
$\hat{(\cdot)}$	estimated quantity

SECTION 1
INTRODUCTION

This report presents the results of an analysis effort performed to demonstrate the feasibility of employing approximate dynamical models and frequency-shaped cost functional control law design techniques for helicopter vibration suppression. Both fixed-gain and adaptive control designs based on linear second-order dynamical models were implemented in a detailed Rotor Systems Research Aircraft (RSRA) simulation to validate these active vibration suppression control laws. Approximate models of fuselage flexibility were included in the RSRA simulation in order to more accurately characterize the structural dynamics. The results for both the fixed-gain and adaptive approaches are promising and provide a foundation for pursuing further validation in more extensive simulation studies and in wind tunnel and/or flight tests.

1.1 BACKGROUND

One of the important improvements which will influence a wide acceptance of rotorcraft for both commercial and military applications is the reduction of the mechanical vibration level. Reducing the vibration level will effect ride quality both directly and indirectly through its affect on noise level, as well as providing a more stable weapon delivery platform, and may reduce maintenance, cost, and weight.

There are several significant sources of vibration in rotorcraft including rotors, transmission systems, and engines. The dominant source of vibration for most helicopters in forward flight, however, is the periodic loading of the rotor blades. When a helicopter transitions from hover to forward flight, it loses polar symmetry of the airflow through the rotor disc. The relative velocity of the air which the blades encounter is (to

first order) a sinusoidal function of the blade azimuth with respect to the direction of flight. These differences are further augmented by a helically shed trailing vortex system, resulting in a rough ride for the blades and consequently the aircraft, even in smooth air. Vibration at high forward speed is further accentuated by compressibility and stall effects.

Basically, the vibrating loads are periodic with the majority of the power concentrated around frequencies which are harmonics of Ω, the rotor angular velocity (Ω_r) times the number of blades (N).

$$\Omega = N\Omega_r \tag{1.1}$$

Though vibration can occur at frequencies other than Ω, 2Ω, 3Ω, etc., due to structural resonances in the airframe and the blades, the disturbance power at frequencies other than harmonics of Ω is significantly below that near Ω and its harmonics. This results in significantly lower vibration levels. Near Ω and its harmonics, however, rotor and fuselage flexible modes can transmit the rotor hub loads to various locations in the airframe with significant increases in amplitude and alterations in phase.

Uncontrolled vibration levels in rotorcraft can exceed 0.25 g, a level significantly higher than that for fixed-wing aircraft. A example of uncontrolled vibration for a MBB BO 105 helicopter in steady-state forward flight at 70 knots and during some maneuvers is shown in Figure 1-1 (taken from reference [1]). Notably, the accelerometer and rate gyro outputs have been pre-filtered with a three-pole analog filter with cutoff frequency 16 Hz, yet the vibration level remains quite high. Current methods for reducing these vibration levels involve the use of mass-spring-damper systems for isolating and/or absorbing the vibrational energy. These passive control systems are heavy, and are only effective at a few operating conditions. This has led to considerable research into 'active' techniques, where the rotor blades are excited at harmonics of Ω in order to reduce the aerodynamic loads. A summary of the findings of this research is given next.

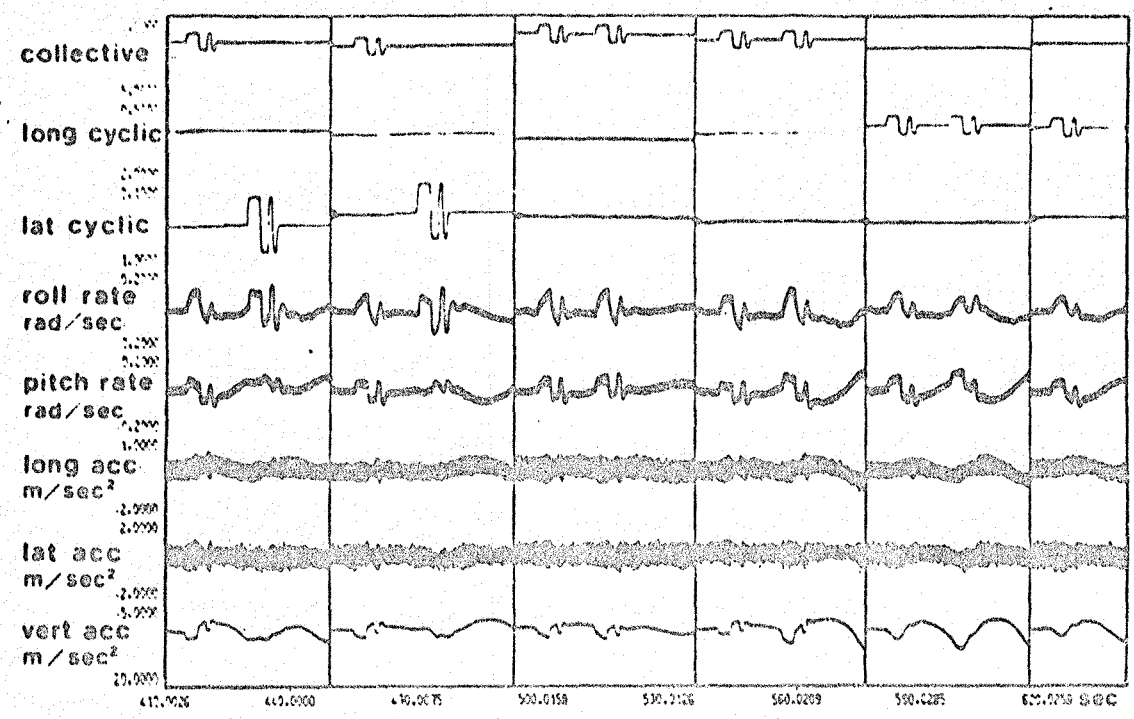

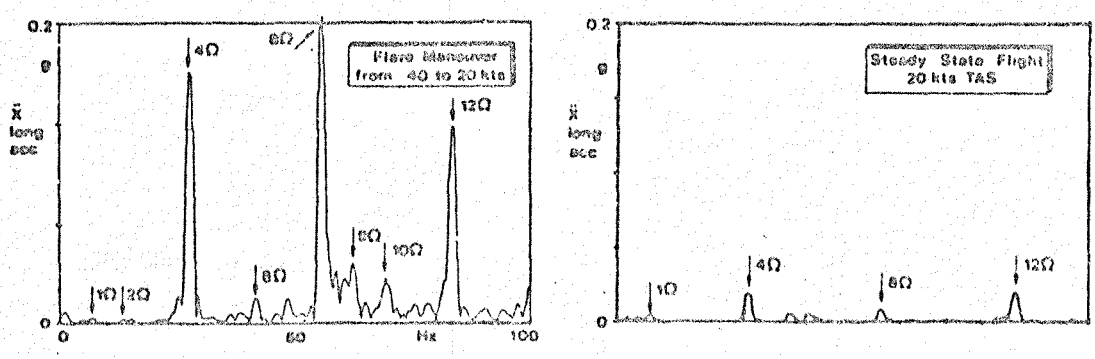

Figure 1-1: Uncontrolled Vibration of MBB MO 105 Helicopter

1.2 ACTIVE CONTROL OF ROTORCRAFT VIBRATION

Most of the research to date on active control of rotorcraft vibration has focused on multicyclic (or higher harmonic) control (N/rev and its harmonics) since the pioneering work of McCloud and Kretz [2]. An excellent review of the state-of-the-art in multicyclic control as of 1982 was given by Johnson [3]. He characterized multicyclic control as that with: (1) a linear, quasi-static, frequency domain model of the helicopter vibration response to control; (2) identification of the helicopter vibration model by least-squared error or Kalman-filter methods; and (3) a minimum variance or quadratic performance function controller. Johnson also presented a tutorial on such control algorithms that use recursive parameter identification with linear feedback, algorithms which are generally termed self-tuning regulators. Discussions of other feedback strategies and helicopter vibration in general can be found in Johnson's text [4].

The linear, quasi-static, frequency domain model of helicopter vibration referred to requires further elaboration in order to accurately express the differences between this model and the linear second-order dynamical model employed in this analysis. This linear quasi-static model, referred to in the literature as the 'T-matrix' model, is quite simply a linear static model of the input-output relationship expressing the observed accelerations (z) as constant linear combinations of the inputs (u):

$$z = Tu \, . \tag{1.2}$$

This is clearly not a valid model over the entire frequency range of helicopter operation, but can be used to accurately express the input-output characteristics at a single frequency. As discussed by Gupta in [5], restriction of an arbitrary transfer function description of the input-output relationship results in such a static relationship (enlarging the the field of scalars to include complex numbers).

Since the static model is unknown a priori, it must be identified, and since helicopter dynamics are inherently nonlinear, the identification must be performed adaptively (on-line) or at a prespecified number of flight conditions within the flight envelope. In order to restrict the identification

to a specific frequency (or frequencies), the data input to the various identification algorithms are effectively bandpass filtered by transforming into the frequency domain (FFT) and retaining only the responses (magnitudes and phases) at the frequencies of interest. Thus, to state explicity what is meant by the terminology "linear, quasi-static, frequency-domain model", the reference is to a static linear model relating the inputs and outputs which is designed to be valid only at a specific frequency (or frequencies).

In this analysis, the linear static model has been extended to include second-order dynamics between the inputs and outputs. This broader class of dynamical models is used in order to account for input lags due to blade dynamics as well as the effects of fuselage flexibility over a finite bandwidth near Ω (N/rev). Coupled with an appropriate control strategy, this class of models will admit identification and control of non-minimum phase systems (systems with transfer function zeroes in the right half-plane). Non-minimum phase systems are commonly found in the relationships between control surface deflections and achieved accelerations on rotorcraft, aircraft and missiles.

Both linear time-invariant controllers and adaptive controllers were studied. The application of 'optimal' regulator theory to the helicoptor vibration control problem was successful primarily due to the utilization of frequency-shaped cost functions in the linear-quadratic regulator (LQR) design procedure [6,7]. These cost functions lead to control feedback whose energy is concentrated in the frequency band or bands of interest. Time-invariant controllers were tested on the RSRA simulation both with and without fuselage flexibility effects included [8]. As expected, fuselage flexibility radically altered the input-output dynamical relationships, indicating the need for considering these effects in any control design. Furthermore, the input-output characteristics (of the nonlinear RSRA simulation) were shown to vary significantly with flight condition. Though gain-scheduling techniques can be used to update the controller as the flight conditions change, other considerations such as configuration change which alter the input-output characteristics make investigation into the use of adaptive control laws potentially useful.

The research reported here and by Gupta [5], differs from previous approaches in two principal ways--in the model form and in the control cost

functional formulation and resulting mechanization. Previous work has concentrated on static models in which the inputs and outputs are directly related by a coefficient matrix (T) whose parameters (elements of T) are modeled as stochastic random-walk processes. As outputs of an identification algorithm, these parameters may slowly vary with time. In this analysis, the input-output model is augmented to include second-order dynamics. This more complex model more accurately characterizes the helicopter's input-output relationships near N/rev. Using frequency weighted cost functionals in the estimation and control law synthesis places increased emphasis on errors in the frequency bands of interest.

1.3 SUMMARY OF RESULTS

Fixed-gain and adaptive control laws were designed for suppression of the narrowband vibration (at the pilot location) resulting from periodic loading of the rotor blades in a simulation of the rotor systems research aircraft (RSRA). The particular version of the simulation used did not include blade dynamics or aeroelastic effects, however the simulation was augmented with a model of eight flexible modes of the fuselage near Ω (N/rev). The results of the fixed-gain control design indicate a significant 'robustness' with respect to changes in flight conditions including speed, altitude, and weight (disc loading).

The adaptive controller also performed remarkably well at all flight conditions, including a 35 second transition from 80 knots to 125 knots. In general, the convergence times for the adaptive controller were larger than those for the fixed-gain controller, but the steady-state RSS (root-sum-squares) acceleration at the pilot location was insignificantly different in most cases. Further comparisons of results for the two strategies are difficult to justify in light of the fact that different control configurations were used for the two cases (four controls including the tail collective were used in the fixed-gain design while the tail collective was eliminated in the adaptive controller), and more fundamentally since the solutions to the vibration control problem used two different sets of underlying assumptions. However, it is interesting to note that in most cases the

However, it is interesting to note that in most cases the adaptive controller required less control authority to accomplish the same reduction in vibration level at the same flight conditions.

The absence of a detailed rotor model including aeroelastic effects may have conributed strongly to the similarity in performance of the two algorithms. It is likely that the inclusion of higher order aeroelastic effects would have resulted in more pronounced model variations as a function of flight condition than were realized in the RSRA simulation. The more pronounced model variations would have led to increased performance degradation of the fixed-gain controller away from the design point. However, due to the periodic nature of the disturbances, the approximate model of the vibration dynamics is adequate for periodic disturbance suppression in spite of the underlying complexity (nonlinearity) of the actual helicopter vibration dynamics.

1.4 SUMMARY OF REPORT

The report is organized as follows. Section 2 describes the addition of fuselage flexibility equations to the GENHEL simulation of RSRA. Section 3 discusses the fixed-gain control law design, its performance, and presents some preliminary results on robustness of the control law with respect to variations in flight conditions away from the design point. A discussion of frequency shaped cost functions is also included in Section 3. Section 4 describes the adaptive control algorithm in detail, and presents the results for various flight conditions. Section 5 summarizes the results and key features of the adaptive and fixed-gain algorithms with performance comparisons where appropriate. Section 6 contains recommendations for future work.

SECTION 2
MODELING RSRA ROTORCRAFT VIBRATION DYNAMICS

A previous study ([8]) and this current research have used a detailed Rotor Systems Research Aircraft (RSRA) simulation (GENHEL) to validate the effectiveness of frequency-shaped cost functional control laws for helicopter vibration suppression. Since flexibility effects can dramatically change the dynamical relationship between control inputs and observed vibrational accelerations, several fuselage flexible modes near Ω (N/rev) were added to the GENHEL simulation of the RSRA. While the GENHEL rotor model was not as complete as it might have been, the basic rigid body rotorcraft simulation with fuselage flexibility calculated accelerations similar in magnitude to those observed on the actual rotorcraft. Unmodeled actuator and blade dynamics coupled with nonlinear aeroelastic effects certainly would result in different magnitude and phase (most significantly transmission zeroes) relationships between the inputs and the outputs of the simulation model from those of the actual helicopter in the narrow band of frequencies around Ω and its harmonics. However, the dynamical model used in the control designs has sufficient degrees of freedom (poles and zeroes) to accurately characterize the input-output relationships in the frequency intervals of interest for the purpose of periodic disturbance rejection!

2.1 THE NASTRAN MODEL AND VIBRATION EQUATIONS

The GENHEL helicopter simulation program assumes the fuselage is rigid, ignoring the effects of fuselage flexibility on vibration. In order to include these effects, a finite element modeling program (NASTRAN) was used to estimate the natural frequencies and mode shapes in a finite element model of the helicopter. An appropriate subset of the modes was chosen for inclusion into the GENHEL program, effectively replacing the rigid body with an appropriate flexible fuselage. This section provides a mathematical description of the flexible fuselage and its inclusion into the GENHEL program.

For a set of dynamical equations of the form:

$$M\ddot{x} + Kx = 0 \tag{2.1}$$

where M is a symmetric mass matrix, and K is a symmetric stiffness matrix, the NASTRAN program computes the natural frequencies (ω's), a generalized stiffness matrix $\tilde{K}$, a diagonal generalized mass matrix $[\tilde{M}]$, and the generalized eigenvector matrices (ϕ's), such that:

$$\phi^T K \phi = \tilde{K}, \tag{2.2}$$

$$\phi^T M \phi = \tilde{M}. \tag{2.3}$$

NASA Ames provided a NASTRAN model for the flexible fuselage of the RSRA helicopter. For the first 34 (lowest frequency) vibrational modes, natural frequencies, generalized stiffnesses, generalized masses and mode shapes (generalized eigenvectors) at various locations throughout the fuselage were calculated. The results are summarized in Appendix A.

The effects of external forces applied at various locations on the fuselage can be considered by modifying equation (2.1) to include a non-zero forcing term:

$$M\ddot{x} + Kx = TF, \tag{2.4}$$

where T is a force distribution matrix, and F is a vector of external forces (in the x, y, and z directions in a body-fixed coordinate system) and moments (about the x, y, and z axes denoted L, M, and N respectively):

$$F^T = [\, F_x, F_y, F_z, L, M, N \,] .$$

Note that since the z-axis is coincident with the rotor shaft, no yaw moments (neglecting bearing friction effects) are transmitted to the fuselage. Using equations (2.2) and (2.3), equation (2.4) can be written in modal form:

$$\tilde{M}\ddot{\eta} + \Omega^2 \eta = \phi^T TF, \tag{2.5}$$

where

$$x = \phi\eta. \tag{2.6}$$

Since M is a positive, diagonal matrix, its inverse is well-defined and the differential equations can be written:

$$\ddot{\eta} + \tilde{M}^{-1}\Omega^2\eta = \tilde{M}^{-1}\phi^T TF, \tag{2.7}$$

where

$$\tilde{M}^{-1}\Omega^2 = \mathrm{diag}\{\omega_i^2\} \tag{2.8}$$

is a diagonal matrix of the natural frequencies. For the RSRA helicopter, these modal differential equations can be written:

$$\begin{bmatrix} \ddot{\eta}_1 \\ \ddot{\eta}_2 \\ \cdot \\ \cdot \\ \cdot \\ \ddot{\eta}_n \end{bmatrix} + \underset{M}{\overset{--1}{}}\ \underset{K}{\overset{-1}{}} \begin{bmatrix} \eta_1 \\ \eta_2 \\ \cdot \\ \cdot \\ \cdot \\ \eta_n \end{bmatrix} = \underset{M}{\overset{--1}{}}\ \underset{\phi}{\overset{T}{}} \overbrace{\begin{bmatrix} 0 & 0 & 0 & 0 & 0 & 0 \\ \vdots & \vdots & \vdots & \vdots & \vdots & \vdots \\ 1 & 0 & 0 & 0 & 0 & 0 \\ 0 & 1 & 0 & 0 & 0 & 0 \\ \cdot & \cdot & \cdot & \cdot & \cdot & \cdot \\ \cdot & \cdot & \cdot & \cdot & \cdot & \cdot \\ 0 & 0 & 0 & 0 & 0 & 1 \\ \vdots & \vdots & \vdots & \vdots & \vdots & \vdots \\ 0 & 0 & 0 & 0 & 0 & 0 \end{bmatrix}}^{T} \begin{bmatrix} F_x \\ F_y \\ F_z \\ L \\ M \\ N \end{bmatrix}; \tag{2.9}$$

where T is a rectangular (34 x 6) matrix of zeroes with an imbedded 6 x 6 identity matrix which picks out of ϕ^T the vectors associated with the modal deflections at the hub. Thus, defining the columns of T as T_{F_x}, T_{F_y}, T_{F_z}, T_L, T_M, T_N, we can identify, for example, $T_{F_x}^T \phi$ as the NASTRAN state at the hub, where the x-direction force is applied. Similar identifications hold for the other five degrees of freedom. Using the fact that the mass and stiffness matrices in equation 2.9 are diagonal, the equations decouple yielding:

$$\ddot{\eta}_m + \omega_m^2 \eta_m = \phi_{mh}^T F/\tilde{M}_m, \tag{2.10}$$

where

$$\phi_{mh}^T = [\phi_{mh}(F_x), \phi_{mh}(F_y), \phi_{mh}(F_z), \phi_{mh}(L), \phi_{mh}(M), \phi_{mh}(N)],$$

and F is applied at the rotor hub. The vector ϕ_{mh} is the vector of modal deflections at the hub for mode m.

The outputs of interest are translational accelerations (specific forces) at the pilot's location. In terms of the vibration states at a particular location on the fuselage, these outputs can be written as follows:

$$y_p = H\ddot{x}_p, \tag{2.11}$$

where x_p is the displacement of the fuselage at point p (eg. the pilot location) as a function of time, and $\ddot{x}_p$ is the resulting acceleration. These measurement equations can be written in terms of the modal states as follows:

$$y_p = H[\phi_{1p}\ \phi_{2p}\ \phi_{3p} \cdots \phi_{np}]\ddot{\eta}\ , \tag{2.12}$$

where y_p are acceleration measurements at the pilot location and ϕ_{ip} is a column vector whose six elements are the deflections of the i^{th} mode at the pilot location for each of the six degrees of freedom. The measurement distribution matrix H specifies the contribution of each degree of freedom to the accelerometer output. For an accelerometer mounted along the x-direction, the H-matrix would be proportional to:

$$H_x = [\,1\ 0\ 0\ 0\ 0\ 0\,]\ .$$

Up to this point, the effects of structural damping have been ignored. In order to include these effects, a term proportional to $\dot{\eta}$ is added to the modal equations. The constant of proportionality is in turn proportional to the damping coefficient. Since typical structural damping ratios are between 3% and 5%, the modal equations were augmented with a damping term giving 5% damping. These equations were discretized using zero-order hold

equivalence and a sample interval equal to the GENHEL simulation time step. The resulting discrete equation is of the following form:

$$y_{k+1,i} = a_{1i}y_{k,i} + a_{2i}y_{k-1,i} + b_{0i}u_{k+1} + b_{1i}u_k + b_{2i}u_{k-1};$$

where k is a time index, i is a mode index, u_k is the applied force at the hub at time k, and $y_{k,i}$ is the contribution to the accelerometer output at the pilot location at time k from mode i. The coefficients a_{1i}, a_{2i}, b_{0i}, b_{1i}, and b_{2i} are the polynomial coefficients in the discrete-time z-transform transfer function representation of the zero-order hold equivalent input-output relation (rotor hub forces to pilot location accelerometer outputs). This equation was coded and added to the GENHEL simulation program.

2.2 MODAL CONTRIBUTION AND MODE SELECTION

The NASTRAN finite element modeling program was used to calculate the first 34 (lowest frequency) modes for a finite element model of the fuselage of the RSRA helicopter. However, not all of these modes contribute substantially to the vibration at the pilot's location. In order to significantly reduce the computational load, only a small subset of the modes which effectively contribute to the total vibration was chosen for inclusion into the GENHEL simulation.

To select the modes with the greatest effect on the vibration at the pilot location, the amplitude of the response of each mode at the pilot location was estimated. The eight (8) modes with the largest responses near Ω were included. The modal responses were estimated by assuming that the vibrational forces in all six directions (three forces and three moments) were of equal magnitude and phase at Ω where for the five-bladed RSRA;:

$$\Omega = N\Omega_r = 110.7 \text{ rad/sec},$$

N is the number of blades, five, and Ω_r is the rotor angular velocity. Then, using reciprocity, the amount of excitation of each mode due to the

six forces and moments was estimated by the sum of the modal responses at the hub:

$$R_{mo} = \frac{\sum_{k=1}^{6} \phi_{mh}(k)}{\tilde{M}_m[(\omega_m^2 - \Omega^2)^2 + (2\zeta\Omega\omega_m)^2]^{1/2}} \quad . \tag{2.13}$$

The sum in the numerator is over the six degrees of freedom. The steady-state response in each direction (in the force and moment 6-space) was then easily calculated using the corresponding modal amplitude at the pilot location ($\phi_{mp}(.)$);

$$A_{mp} = R_{mp}\phi_{mp} \quad . \tag{2.14}$$

$A_{mp}(k)$, the k^{th} element of A_{mp}, is a quantitative measure of the amplitude of the vibration response at the pilot location due to equal forces in all directions at the hub. The sum over k of the absolute values of $A_{mp}(k)$ (i.e. the L_1-norm of A_{mp}) was used as a cumulative measure of the vibration contribution from each mode. A summary of these values for the 34 NASTRAN modes is presented in Tables 2-1 and 2-2.

In order to minimize the computational load in the controller implementations, only significant modes near Ω were included in the GENHEL simulation. This resulted in the majority of the vibrational energy in the outputs of the simulation appearing at Ω with greater than 10dB of attenuation at the higher harmonics. This, in turn, allowed the controllers to concentrate soley on vibration suppression at a single frequency Ω, thus minimizing the dimensionality of the problem to be solved and hence the computational load. The six modal displacements for the eight selected modes at both the rotor hub and pilot location are given in Table 2-3.

TABLE 2-1. ESTIMATED MODAL RESPONSE A_{mp} AT THE PILOT LOCATION

Mode No.	ω (rad/s)	Relative Modal Deflection at Pilot Location					
		F_x	F_y	F_z	L	M	N
1	0.000	0.1753E-05	-0.1149E-14	0.1078E-12	0.1959E-17	0.5540E-15	0.
2	0.000	-0.3613E-14	0.1753E-05	0.1468E-13	-0.4493E-15	0.4782E-17	0.
3	0.000	-0.7756E-14	-0.4419E-15	0.1804E-05	0.1794E-16	0.4382E-15	0.
4	0.000	-0.2549E-06	-0.4852E-06	0.1903E-05	-0.6406E-07	-0.6473E-10	0.
5	0.000	-0.2340E-06	-0.1829E-08	0.1167E-05	-0.2413E-09	0.6593E-08	0.
6	0.000	0.1964E-06	-0.1459E-05	0.2975E-06	-0.9897E-08	0.7151E-11	0.
7	27.607	0.2585E-06	-0.1359E-07	-0.1389E-05	-0.1702E-08	-0.1492E-07	0.
8	31.032	-0.1472E-06	0.6566E-06	-0.6418E-07	0.2661E-08	0.4340E-09	0.
9	48.046	0.8669E-06	-0.9367E-08	-0.2234E-05	-0.7277E-08	-0.3833E-07	0.
10	59.661	-0.5715E-07	0.2454E-06	0.2132E-07	-0.1350E-08	0.5435E-10	0.
11	64.732	0.1202E-06	-0.3873E-06	-0.1571E-06	0.4274E-08	-0.1506E-08	0.
12	81.099	0.2014E-05	0.4426E-06	0.5238E-05	0.3207E-07	0.1620E-06	0.
13	93.432	0.1774E-05	-0.2830E-05	-0.1734E-05	0.7584E-07	-0.4433E-09	0.
14	97.437	-0.1501E-05	-0.1436E-05	-0.1672E-05	0.4431E-07	-0.2491E-08	0.
15	110.946	-0.4510E-06	0.7916E-06	0.1178E-05	-0.3922E-07	-0.1100E-07	0.
16	117.015	-0.3616E-06	0.5935E-06	0.1908E-05	-0.6044E-07	0.4243E-07	0.
17	120.364	-0.1605E-05	0.3858E-05	0.9501E-06	-0.4727E-07	0.1134E-06	0.
18	126.158	0.1242E-05	-0.1530E-05	-0.2936E-05	0.7637E-07	0.5620E-07	0.
19	131.114	-0.4241E-06	0.2202E-05	-0.9575E-05	0.3122E-06	-0.4344E-07	0.
20	140.716	-0.2529E-06	-0.2940E-06	-0.1396E-05	0.4816E-08	0.7312E-07	0.
21	156.112	-0.7499E-07	-0.2949E-08	0.1900E-06	0.1255E-08	-0.3997E-08	0.
22	165.927	0.5657E-08	0.1051E-07	0.3677E-07	-0.3662E-09	0.5093E-10	0.
23	167.502	-0.1889E-07	-0.1642E-06	-0.3803E-06	0.1593E-07	-0.1186E-07	0.
24	169.942	0.2746E-06	-0.2435E-07	-0.4696E-06	-0.1108E-07	0.7121E-08	0.
25	182.112	0.2157E-08	-0.2633E-07	0.3616E-06	0.1212E-07	0.3313E-08	0.
26	187.013	0.2073E-06	0.1869E-07	0.8997E-06	-0.5178E-08	0.1967E-07	0.
27	191.659	-0.1984E-06	0.5399E-07	0.1230E-06	-0.2249E-07	0.5680E-09	0.
28	200.185	0.3109E-06	0.3674E-05	0.6034E-06	-0.1066E-07	0.4049E-08	0.
29	217.018	-0.2072E-06	-0.3360E-07	0.3674E-07	0.3218E-08	-0.2383E-07	0.
30	224.810	0.1177E-05	-0.1146E-05	0.4677E-05	-0.1370E-06	0.1586E-06	0.
31	229.737	-0.1478E-05	0.3923E-06	0.3691E-05	-0.1105E-06	-0.1136E-07	0.
32	237.447	0.1505E-06	0.9853E-07	-0.1292E-05	0.5755E-07	-0.7304E-07	0.
33	238.716	0.3586E-06	0.9177E-07	0.7429E-06	-0.2431E-07	0.1233E-07	0.
34	243.707	-0.1378E-06	-0.4246E-06	-0.[illegible]68E-06	0.6102E-08	0.1193E-07	0.

TABLE 2-2. CUMULATIVE AMPLITUDE RESPONSE AT THE PILOT STATION R_{mp}

Mode No.	ω (rad/s)	$\lvert A_{mp}(k)\rvert_{L_1}$	R_{mp}
1	0.000	0.1753E-05	0.1753E-05
2	0.000	0.1753E-05	0.1753E-05
3	0.000	0.1804E-05	0.1804E-05
4	0.000	0.2709E-05	0.4662E-05
5	0.000	0.1410E-05	0.5121E-06
6	0.000	0.1963E-05	0.6519E-06
7	27.607	0.1677E-05	0.9495E-05
8	31.032	0.8711E-06	0.5623E-05
9	46.046	0.3158E-05	0.1177E-04
10	59.661	0.3953E-06	0.3293E-05
11	64.732	0.6704E-06	0.1084E-05
12	81.099	0.7909E-05	0.3717E-04
13	93.492	0.4415E-05	0.2285E-04
14	97.437	0.4955E-05	0.3297E-04
15	110.946	0.2471E-05	0.2134E-04
16	117.015	0.2966E-05	0.2101E-04
17	120.364	0.6604E-05	0.2942E-04
18	126.158	0.5843E-05	0.1657E-04
19	131.614	0.1256E-04	0.2987E-04
20	140.716	0.1931E-05	0.1347E-04
21	156.612	0.2332E-06	0.2016E-05
22	165.927	0.5335E-07	0.1123E-05
23	167.592	0.5912E-06	0.5671E-05
24	169.942	0.7857E-06	0.2632E-05
25	182.112	0.4055E-04	0.3333E-05
26	187.013	0.1151E-05	0.5342E-05
27	191.659	0.3954E-06	0.3040E-05
28	200.185	0.9329E-06	0.8302E-05
29	217.018	0.3046E-06	0.2961E-05
30	224.810	0.7296E-05	0.1490E-04
31	225.737	0.5683E-05	0.8874E-05
32	237.447	0.1671E-05	0.7019E-05
33	238.716	0.1230E-05	0.3728E-05
34	243.707	0.7472E-06	0.1817E-05

TABLE 2-3. MODAL DISPLACEMENTS OF SELECTED MODES AT HUB AND PILOT LOCATION

Mode	Displacement at Hub					
No.	F_x	F_y	F_z	L	M	N
12	0.346E+00	0.160E-01	0.254E-01	0.388E-03	-0.880E-02	0.335E-03
13	0.106E+00	-0.427E-01	-0.128E-02	-0.237E-02	-0.314E-02	-0.496E-03
14	-0.231E+00	-0.389E-02	0.396E-01	-0.374E-03	0.617E-02	-0.214E-03
15	0.490E-01	0.513E-01	0.109E-02	0.203E-02	-0.113E-02	0.655E-04
16	-0.381E-01	-0.673E-01	-0.629E-02	-0.241E-02	0.140E-02	-0.976E-03
17	-0.150E+00	0.522E-01	-0.571E-01	0.282E-02	0.546E-02	-0.559E-02
18	-0.139E+00	0.265E-01	-0.990E-01	0.081E-03	0.434E-02	0.229E-02
19	0.178E-02	0.464E+00	0.124E-02	0.199E-01	-0.398E-04	-0.106E-01

Mode	Displacement at Pilot Location					
No.	F_x	F_y	F_z	L	M	N
12	-0.542E-01	0.119E-01	-0.141E...	-0.863E-03	0.490E-02	0.000E+00
13	-0.783E-01	-0.125E+00	0.766E-01	-0.335E-02	-0.196E-04	0.000E+00
14	0.455E-01	-0.435E-01	0.568E-01	-0.134E-02	-0.755E-04	0.000E+00
15	0.211E-01	0.371E-01	-0.552E-01	0.184E-02	-0.515E-03	0.000E+00
16	0.172E-01	0.283E-01	-0.908E-01	0.289E-02	0.202E-02	0.000E+00
17	0.516E-01	0.132E+00	-0.323E-01	0.161E-02	0.385E-02	0.000E+00
18	-0.750E-01	-0.923E-01	0.177E+00	-0.461E-02	0.351E-02	0.000E+00
19	0.142E-01	0.737E-01	0.321E+00	-0.105E-01	-0.145E-02	0.000E+00

Figures 2-1 and 2-2 compare the rigid body vibration at the pilot location (a root-sum-square (RSS) of the three force components) with the same vector sum of accelerations at the pilot location with fuselage flexibility modeled with the eight selected modes. The erratic behavior during the first second is due to the transients in the GENHEL simulation. The states in the GENHEL model are not initially in steady-state. A comparison of these two figures clearly indicates the importance of fuselage flexibility in terms of its contribution to the vibration at the pilot location (at least for this simulation!).

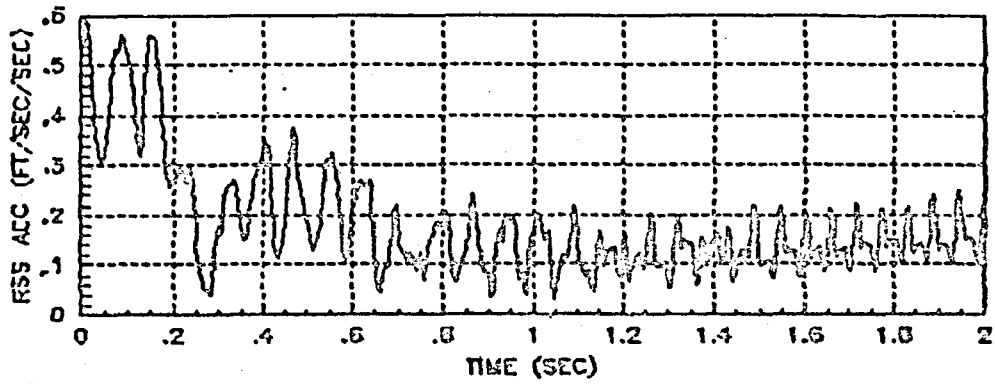

Figure 2-1. RSS Acceleration at the Pilot Location for Rigid Body Model (120kts/100 ft)

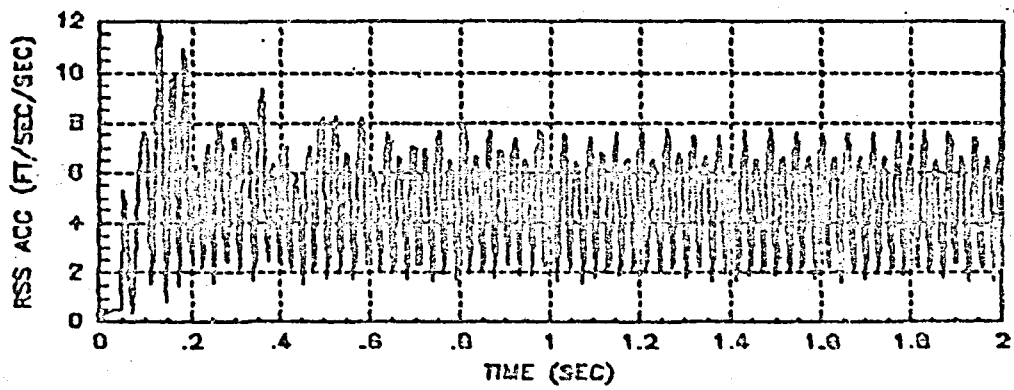

Figure 2-2. RSS Acceleration at the Pilot Location for Rigid Body with Eight Mode Fuselage Flexibility Model (120 kts/100 ft)

Figure 2-3 shows the output of the GENHEL simulation with the eight flexible modes included at a flight condition of 120 knots forward speed and an altitude of 1000 feet. FFT's of the last three (3) seconds of the accelerometer outputs clearly manifest the concentration of vibrational energy at Ω. The power at harmonics of Ω is more than 10dB below that at Ω, as it was designed to be. Inclusion of fuselage flexible modes at or near harmonics of Ω would certainly have contributed to increased power at those frequencies, resulting in a increase in the computational load in the control implementations.

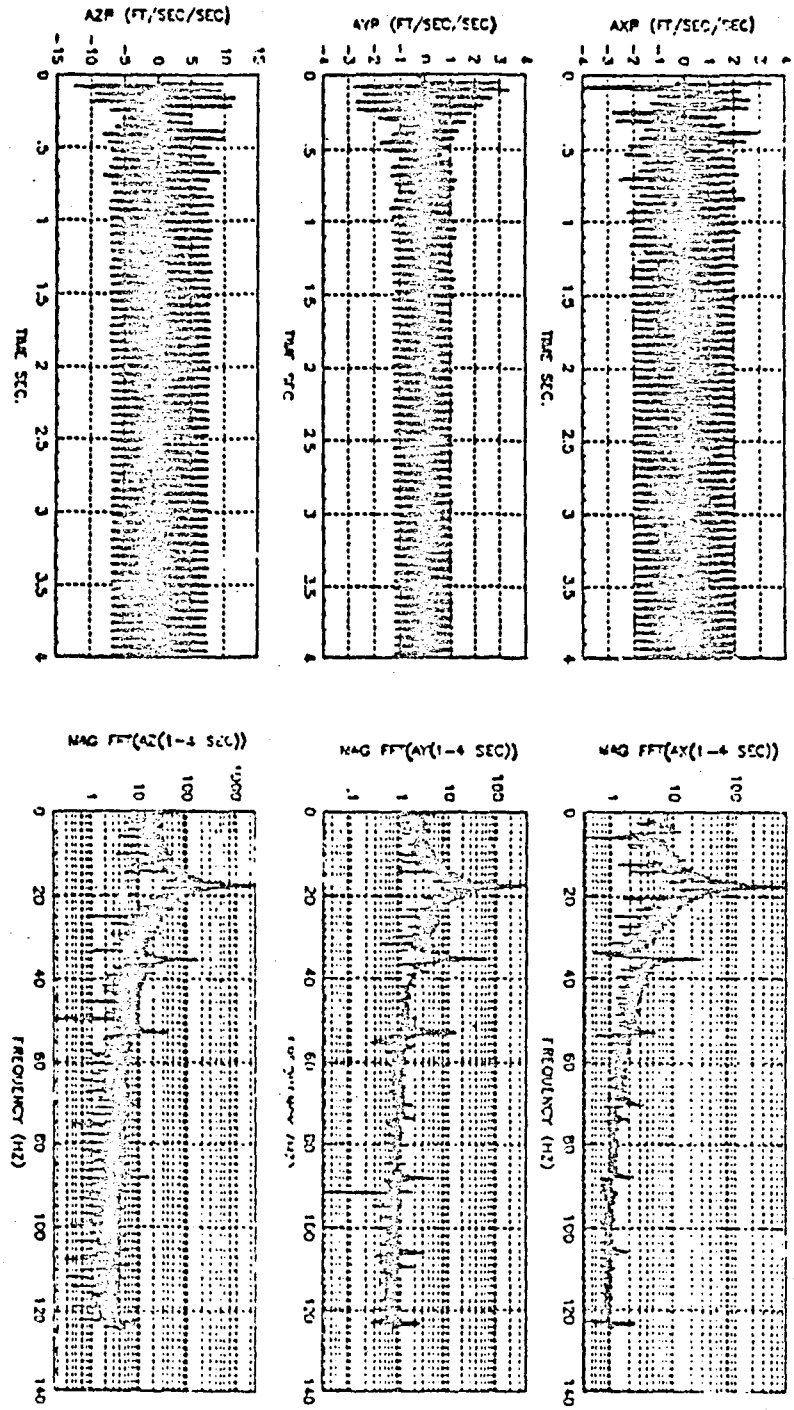

Figure 2-3: Acceleration Outputs and Power Spectra at Pilot Location with Eight Mode Fuselage Flexibility Model (120 kts/1000 ft)

SECTION 3

FIXED-GAIN CONTROLLER FOR RSRA ROTORCRAFT VIBRATION SUPPRESSION

The basic steps involved in the design of the fixed-gain controller include linearization of the nonlinear model of the helicopter vibration dynamics about the desired operating point and measurement model linearization at the same operating point. Appropriate performance specifications are selected, a controller structure chosen, and parameters in that structure such as estimator and controller gains calculated based on an optimization procedure. In modern control theory, the LQR (linear-quadratic-regulator) design procedure leading to steady-state solutions of Riccati type equations is a common choice for controller design. The minimization of a weighted squared error results in a linear state feedback control law with constant gains in steady-state. In estimation theory, the dual concept is linear-quadratic-Gaussian (LQG) estimator design. Thus, the two major steps in fixed-gain controller design are:

1) Generation of linearized dynamical and measurement models, and

2) LQ design for estimator and controller feedback gains.

There are several methods for generating linear models from nonlinear dynamical systems. The basic differences involve the choice of the approximating model form. Utilizing most of the physics underlying the problem, complex model forms can be arrived at and the parameters in these models (stability derivatives) identified from input-output measurements at desired operating points. This method was used in preliminary analysis and will be discussed in a little more detail in Section 3.1. However, such models usually involve a large number of states and questions of observability, controllability, and computability become salient issues. A second approach involves identifying parameters in a low order input-output equivalent model form. This naturally reduces the required computational load since fewer parameters are involved, at the price of a more approximate dynamical model whose ability to predict future system outputs given the past states and inputs will certainly be inferior to that of the more complex higher order model forms. However, as alluded to earlier on several occasions, the helicopter vibration problem is one of controlling outputs at

a few known frequencies. The approximate model of the helicopter vibration dynamics is therefore required to be accurate only at those frequencies. A globally valid model is not necessary as long as the control authority is limited to those frequencies as well.

3.1 IDENTIFICATION OF LINEARIZED MODELS OF THE RSRA VIBRATION DYNAMICS

This subsection presents an overview of the detailed linearization procedure used as a first attempt at obtaining a linearized model of the RSRA vibration dynamics. With the addition of eight fuselage flexible modes, however, the detailed linearized model became excessively large and subsequently a low order input-output equivalent model was identified. The details of this procedure are also discussed. With the model parameters identified, LQR control design was performed by choosing costs on the frequency-shaping filter states and solving for the optimal gains as discussed in the next subsection. The fixed-gain controller design procedure is outlined in Figure 3-1.

3.1.1 Stability Derivative Estimation Using the RSRA Simulation

Based on the approach described in [2], linear models of the RSRA helicopter were constructed by computing stability derivatives of the helicopter rigid fuselage and rotor model at various operating points. Small perturbations in the states of the model which included states associated with the six rigid body degrees of freedom and a flapping mode for each of the five blades resulted in variations in the forces and moments at the hub, leading directly to an estimate of the associated stability derivatives. The performance of controllers designed with these models was entirely satisfactory when applied to the nonlinear, rigid body simulation of the helicopter. However, severe degradation in performance resulted when flexible modes were added to the simulation. In fact, the fixed-gain rigid body model controller design was destabilizing at several flight conditions when applied to the flexible helicopter model.

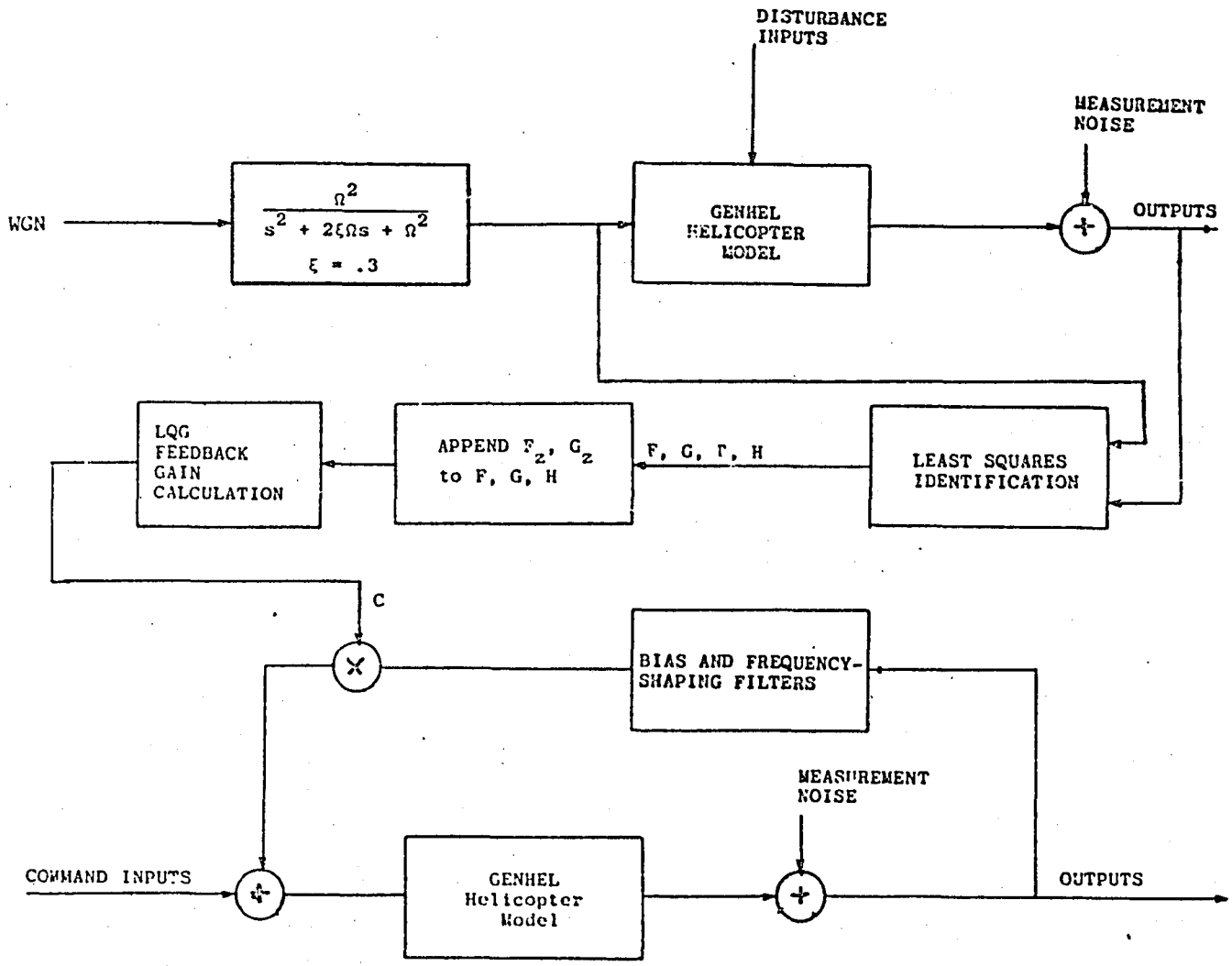

Figure 3-1. Fixed-gain Controller Design Procedure

The destabilizing effect of including the fuselage flexible modes was not unexpected, and demonstrated clearly the need for inclusion of these modes in the control design. To include the effects of the flexible modes, each mode with a significant contribution to the vibration was added to the dynamical model, and the measurement models altered to include these flexible mode contributions. Since the model order increases by two with each additional mode, the inclusion of a significant number of modes resulted in the stability derivative calculation becoming computationally burdensome and the controller implementation virtually infeasible (the number of computations at each time step for fixed-gain controllers being proportional to the square of the number of states).

3.1.2 Identification of a Low Order Linearized Model of the RSRA Simulation

To reduce the number of states in the linearized model of the RSRA, several approaches can be taken. The high order model including all the flexible modes of interest can be reduced by one of several procedures for eliminating combinations of states which are weakly observable with the measurements available and/or weakly controllable with the inputs available. This presumes, of course, that the effort to acquire such a detailed model has already been expended. However, based on the observation of the rotor frequency is fixed in most helicopters, an alternate procedure was chosen. Since most of the power in the vibrational forces is at this frequency and its harmonics, approximate second-order models adequately describe the input-output relationships required for controller design in the frequency band of interest. As discussed in Section 1, this class of models is an extension of the class of linear static models to include control lag effects as well as approximate impulse response characteristics. The parameters in these models must be identified from input-output data before a fixed-gain controller can be designed.

In almost all helicopters the rotor angular velocity (Ω_r) is kept nearly constant. Thus, the vibration is concentrated in narrow frequency ranges, and second-order systems can be employed to adequately represent the transfer function gain and phase over each interval. As previously discussed, the fuselage flexible modes are the most significant contributors to

the vibration at the pilot location. Since the objective of the analysis was to demonstrate the feasibility of various control designs, the problem was simplified to include only major contributors around Ω, resulting in insignificant power at higher harmonics. Thus, a single second-order model of the RSRA vibration dynamics, designed to be accurate over a finite frequency interval around Ω, was chosen for each accelerometer measurement.

To excite all the flexible modes around Ω for the purposes of model parameter identification, control deflections containing frequencies in a band above and below Ω (approximately $\pm$ 20%, i.e., 90 rad/sec $< \omega <$ 130 rad/sec) were input to the RSRA simulation. The resulting accelerations in the x, y, and z directions along with the four control inputs and the 'known' disturbances, $\cos\psi$ and $\sin\psi$, were then used as outputs and inputs respectively of a linear autoregressive model with exogenous inputs (ARX). Sine and cosine of the rotor azimuth angle were included in order to account for the periodic disturbance of unknown amplitude and phase. Algorithms for identification of the parameters in ARX models assume that the stochastic processes entering into the models is white and Gaussian (WGN). Colored (time-correlated) noise such as the periodic disturbances which are the sources of the vibration must be taken into account (pre-whitened), otherwise biased parameter estimates result. In this formulation then, the variables in the ARX model of the input-output dynamics were;

$$y^T = [a_x,\ a_y,\ a_z],$$

$$u^T = [B_{1s},\ \theta_c,\ A_{1s},\ \theta_{tr}],$$

and

$$w^T = [\cos\psi,\ \sin\psi]\ .$$

For these three measurements and four control inputs, a sixth order linear discrete ARX model with fully coupled modes may be written as:

$$y_{k+1} = A_1\, y_k + A_2\, y_{k-1} + B_1\, u_k + B_2\, u_{k-1} + \Gamma\, w_k \qquad (3.1)$$

where the A_i's, B_i's and Γ are matrices containing the parameters to be identified. The A_i's are 3 x 3 matrices, the B_i's are 3 x 4 matrices, and Γ is a 3 x 2 matrix. For future reference, by defining;

$$T_k = A_2\, y_{k-1} + B_2\, u_{k-1} \tag{3.2}$$

equation 3.1 can be written in state-space form as follows:

$$\begin{bmatrix} y_{k+1} \\ T_{k+1} \end{bmatrix} = \begin{bmatrix} A_1 & I \\ A_2 & 0 \end{bmatrix} \begin{bmatrix} y_k \\ T_k \end{bmatrix} + \begin{bmatrix} B_1 \\ B_2 \end{bmatrix} u_k + \begin{bmatrix} \Gamma \\ 0 \end{bmatrix} w_k \tag{3.3}$$

For the purpose of least-squares identification, equation 3.1 was expanded for the measurement a_x as follows:

$$\begin{aligned} (a_x)_{k+1} = {} & a_{11}(a_x)_k + a_{12}(a_y)_k + a_{13}(a_z)_k \\ & + a'_{11}(a_x)_{k-1} + a'_{12}(a_y)_{k-1} + a'_{13}(a_z)_{k-1} \\ & + b_{11}(B_{1s})_k + b_{12}(\theta_c) + b_{13}(A_{1s})_k + b_{14}(\theta_{tr})_k \\ & + b'_{11}(B_{1s})_{k-1} + b'_{12}(\theta_c)_{k-1} + b'_{13}(A_{1s})_{k-1} + b'_{14}(\theta_{tr})_{k-1} \\ & + \Gamma_{11}\cos\psi_k + \Gamma_{12}\sin\psi_k \,. \end{aligned} \tag{3.4}$$

where the a_{ij}, a'_{ij}, b_{ij}, b'_{ij}, and Γ_{ij} are the elements of A_1, A_2, B_1, B_2 and Γ respectively. A linear least squares solution of equation 3.4 was used to find the parameters from a data record of 2500 points (2.5 seconds of data sampled at 1000 points/second). The same technique was used for obtaining ARX model coefficients for the remaining outputs a_y and a_z. The dynamic matrices for the identified linear model for a steady-state level flight condition of 120 knots forward speed at an altitude of 100 feet are given in Appendix B.

3.2 FIXED-GAIN CONTROL LAW DESIGN

The performance objective of the fixed-gain controller was to eliminate the vibration at the pilot location which for the purposes of this study was concentrated at Ω (N/rev). Since most of the vibrational energy was concentrated at a single frequency, the control design was based on a low order

linear model which designed to be accurate near the vibration frequency. The fixed-gain frequency-shaped controller employed utilizes a state-space model of the plant and optimizes a cost function which places a large penalty on the outputs (accelerations at pilot location a_x, a_y, a_z) at the vibration frequency.

3.2.1 Derivation of the Frequency Shaped Controller

In order to place an increased cost on the outputs of a dynamical system over a specified frequency range, a modification to the standard LQR cost functional is required. In this subsection, the details of modifications required are discussed along with the implementation in the overall controller design. The continuous-time analog of the ARX model of the helicopter discussed in the previous subsection can be written in state-space form as follows:

$$\dot{x} = Fx + Gu + \Gamma w \tag{3.5}$$

$$y = Hx + Du \tag{3.6}$$

where y is the measurement vector of accelerometer outputs, u is the vector of control inputs, and w is the narrowband disturbance vector (cf. equation 3.3). Subject to these dynamical constraints, minimization of the following frequency-shaped cost functional is desired.

$$J = \frac{1}{2\pi} \int_{-\infty}^{+\infty} [y^*(j\omega)A(j\omega)y(j\omega) + u^*(j\omega)B(j\omega)u(j\omega)]d\omega \tag{3.7}$$

where

$$A(j\omega) = P_m^*(j\omega)P_m(j\omega) \quad , \tag{3.8}$$

$$P_m(j\omega) = P(j\omega)\text{diag}\{\alpha_1, \alpha_2, \ldots\}, \tag{3.9}$$

$$P(s) = \frac{h_0 s^2 + h_1 2\zeta_1 \Omega s + h_2 \Omega^2}{s^2 + 2\zeta_2 \Omega s + \Omega^2} \quad , \tag{3.10}$$

and $B = I$.

The α_i's are scalar weighting factors and Ω is the vibration frequency.

The location of the poles and the zeros of the scalar frequency-shaped penalty function, P(s), are determined by h_0, h_1, h_2, ζ_1 and ζ_2. The log-magnitude and phase plot of P(s) for two sets of h's and ζ's are shown in Figures 3-2 and 3-3. As can be seen in Figure 3-2, both the magnitude and slopes of the phase plot of the penalty function at $\omega = \Omega$ are infinite (since $\zeta_2=0$). These properties manifest a lack of robustness to modeling errors and a significant performance sensitivity to the choice of center frequency. Using a small amount of damping makes the system more robust to estimation and modeling errors at the expense of vibration reduction at the center frequency. As can be seen in Figure 3-3, the 3-dB bandwidth of the frequency response of the penalty function P (for $\zeta = 0.5\%$) is $2\zeta\Omega$. Note that setting $\zeta_1=\zeta_2=\zeta$, $h_0=h_2=0$ and $h_1=1$ results in unity gain at $\omega = \Omega$.

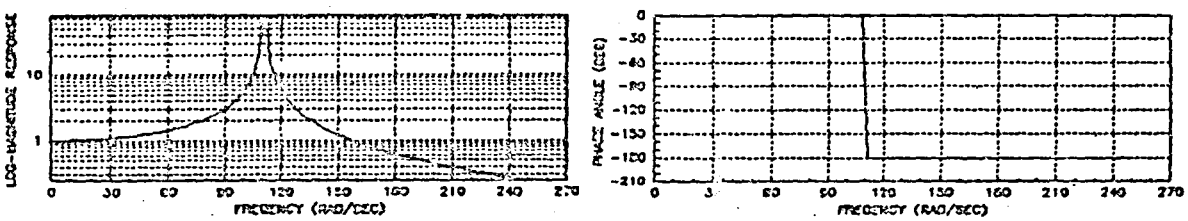

Figure 3-2. Frequency Response of the Frequency Shaped Filter for $\frac{\Omega^2}{s^2 + \Omega^2}$ $(h_0=h_1=\zeta_1=\zeta_2=0,\ h_2=1)$

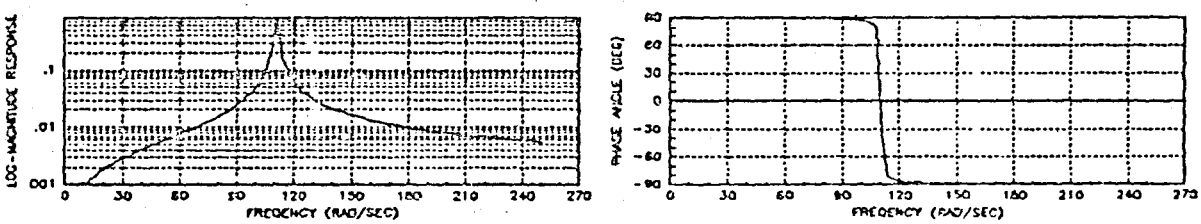

Figure 3-3. Frequency Response of the Frequency Shaped Filter for $\frac{2\zeta\Omega s}{s^2 + 2\zeta\Omega s + \Omega^2}$ $(h_0=h_2=0,\ h_1=1,\ \zeta_1=\zeta_2=0.5\%)$

In order to obtain a state-space model for the frequency shaping filters, these equations are transformed to time domain. This is accomplished by defining:

$$z_i = Py_i \; ; \qquad i = 1, 2, \ldots, N \tag{3.11}$$

where N is the number of outputs to be frequency shaped. Using (3.10) in (3.11),

$$z_i = \frac{h_0 s^2 + h_1 2\zeta\Omega s + h_2\Omega^2}{s^2 + 2\zeta\Omega s + \Omega^2}\; y_i . \tag{3.12}$$

In the time domain, (3.12) becomes

$$\ddot{z}_i + 2\zeta\Omega\dot{z}_i + \Omega^2 z_i = h_0\ddot{y}_i + 2\zeta\Omega h_1\dot{y}_i + \Omega^2 h_2 y_i \tag{3.13}$$

Equivalently, (3.13) can be written in state-space form:

$$\dot{x}_{fs_i} = F_{fs}x_{fs_i} + G_{fs}y_i \; , \tag{3.14}$$

$$z_i = H_{fs}x_{fs_i} + h_0 y_i \; , \tag{3.15}$$

where

$$F_{fs} = \begin{bmatrix} 0 & 1 \\ -\Omega^2 & -2\zeta\Omega \end{bmatrix} \; , \quad G_{fs} = \begin{bmatrix} \beta_1 \\ \beta_2 \end{bmatrix} \; , \quad H_{fs} = [1 \;\; 0]$$

$$\beta_1 = 2\zeta\Omega(h_1 - h_0)$$

and $$\beta_2 = \Omega^2[h_2 - h_0 + 4\zeta^2(h_0 - h_1)]. \tag{3.16}$$

Finally, substitution of (3.9) and (3.11) in (3.7), and using Parseval's Theorem, equation (3.6) can be rewritten:

$$J = \int_0^\infty [z^T \mathrm{diag}\,\{\alpha_1^2, \alpha_2^2, \ldots\} z + u^T B u]\, dt \; . \tag{3.17}$$

Thus, the frequency-weighted optimization problem is transformed into a standard linear-quadratic-regulator (LQR) design problem.

As discussed in previous sections, the control law design employed a large cost on the outputs at the vibration frequency. As discussed above, the frequency-shaped cost functional can be rewritten in the standard LQR form by augmenting the state-space dynamical model with additional states corresponding to those of a state-space time-domain realization of the frequency weighting function. The LQR design for the augmented system then considers cost on the frequency-shaping filter states and controls only.

The frequency-shaping filter used in the fixed-gain control design was:

$$H(s) = \frac{\Omega^2}{s^2 + \Omega^2} \quad . \tag{3.17}$$

and is shown in Figure 3-1. Transformation into the discrete-time domain is required and was accomplished using the bilinear transformation (trapezoidal integration):

$$s = \frac{2(z-1)}{T(z+1)} \, , \tag{3.18}$$

where T is the sampling interval. Substituting equation 3.18 into 3.17, the frequency-shaping filter in the discrete domain can be written:

$$H(z) = \frac{b_0 z^2 + b_1 z + b_2}{z^2 + a_1 z + a_2} \, , \tag{3.19}$$

where: $b_0 = b_2 = [1 + \frac{4}{T^2\Omega^2}]^{-1}$,

$b_1 = 2b_0$,

$a_1 = \frac{T^2\Omega^2 - 4}{T^2\Omega^2 + 4}$,

and $a_2 = 1$.

Transforming this transfer function into a state-space description is readily accomplished:

$$x_{fs_i}(k+1) = F_{fs}x_{fs_i}(k) + G_{fs}y_i(k) ,$$

$$z_i(k) = H_{fs}x_{fs_i} + D_{fs}y_i(k) . \qquad (3.20)$$

If F_{fs} is chosen in observer canonical form,

$$F_{fs} = \begin{bmatrix} -a_1 & 1 \\ -a_2 & 0 \end{bmatrix} .$$

Then,

$$G_{fs} = \begin{bmatrix} b_1 - a_1 b_0 \\ b_2 - a_2 b_0 \end{bmatrix} ,$$

$$H_{fs} = [1 \quad 0] ,$$

and $$D_{fs} = b_0 .$$

In the discrete domain, the helicopter linear model of the vibration dynamics (cf. equations 3.3, 3.5 and 3.6) may be written as follows

$$x(k+1) = F_p x(k) + \Gamma_p u(k) + \Gamma_p w(k)$$

$$y(k) = H_p x(k) + D_p u(k) , \qquad (3.21)$$

where y is the measurement vector of accelerations at the pilot location. The subscript 'p' is used in equation 3.21 to denote helicopter vibration dynamics plant matrices which are hereafter assumed to be in the discrete domain. Appending frequency shaping filter states to the plant states yields the following combined state-space description of the system which can be used to design the control law. For the purposes of illustrating the form of the system matrices, two measurements and two inputs are assumed.

$$F = \left[\begin{array}{cc|cc} & F_p & & 0 \\ \hline G_{fs}H_{p1} & 0 & F_{fs} & 0 \\ 0 & G_{fs}H_{p2} & 0 & F_{fs} \end{array}\right],$$

$$G = \left[\begin{array}{c} G_p \\ \hline G_{fs}D_{p1} \\ G_{fs}D_{p2} \end{array}\right], \quad D = \left[\begin{array}{c} D_{p1} \\ D_{p2} \end{array}\right], \tag{3.22}$$

and $$Y = \left[\begin{array}{c} y \\ z \end{array}\right] = \left[\begin{array}{c} H_p\, x_p \\ H_{fs}x_{fs} \end{array}\right] + \left[\begin{array}{c} D_p u \\ D_{fs} y \end{array}\right].$$

The measurement equation is not in standard from, but can be reorganized to yield:

$$Y = \left[\begin{array}{cc} H_p & 0 \\ D_{fs}H_p & H_{fs} \end{array}\right]\left[\begin{array}{c} x_p \\ x_{fs} \end{array}\right] + \left[\begin{array}{c} D_p \\ D_{fs}D_p \end{array}\right] u . \tag{3.23}$$

The cost function now can be written in terms of Y's and u's, or X's and U's, where $X^T = [x_p^T, x_{fs}^T]$.

$$J = \sum_{k=0}^{\infty} [Y^T(k)A_Y Y(k) + u^T(k)Bu(k)] \tag{3.24}$$

where $$A_Y = \left[\begin{array}{c|cc} 0 & 0 & \\ \hline 0 & \alpha_1 & \\ & & \alpha_2 \end{array}\right] \tag{3.25}$$

Equivalently,

$$J = \sum_{k=1}^{\infty} [X^T(k)A_X X(k) + X^T(k)A_{Xu}u(k) + u^T(k)A_{Xu}^T X(k) + u^T B_u u] . \tag{3.26}$$

where $$A_X = H^T A_Y H ,$$

and $$A_{Xu} = H^T A_Y D .$$

Because of the feedforward terms present in the outputs Y, there is cross-coupling between state costs and control costs. This is evident in the

latter description. Instead of optimizing (3.26), an equivalent cost function ($\bar{J}$) can be minimized which contains no cross-coupling between states and controls.

$$\bar{J} = \sum_{k=1}^{\infty} [X^T(k)\bar{A}_X X(k) + u^T(k)\bar{B}u(k)] \qquad (3.27)$$

where

$$\bar{B} = B + D^T A_X D$$

$$\bar{A}_X = A_X - A_X D \bar{B}^{-1} D A_X$$

$$\bar{F} = F - G \bar{B}^{-1} D A_X H .$$

The control gain is also modified to give:

$$C = \bar{C} + \bar{B}^{-1} D^T A_X H .$$

A derivation of these modifications is presented in Appendix C.

Using the plant identified by the least-squares identification method described in the previous section, optimal closed-loop regulator gains were obtained via solutions to the steady-state algebraic Riccati equations resulting from the minimization of the cost function J. Cost matrices A_Y and B_u were determined such that the closed-loop eigenvalues of the model had damping between 1% and 5%. This restriction on damping was empirically found to balance the controller performance in all three axes. Open-loop eigenvalues of the augmented system, cost matrices used, and closed-loop eigenvalues and feedback gains calculated for a 120 knot speed and 100 ft altitude flight condition are given in Appendix B. The performance of the controller at this design point as well as the performance at various flight conditions and disc loadings away from the design point are discussed in the next subsection.

3.3 FIXED-GAIN CONTROLLER PERFORMANCE

This section presents the results of the fixed-gain controller design and implementation. The robustness of the design to modeling errors is also discussed. In order to maintain continuity in the discussions, the figures are presented at the end of the section.

3.3.1 Controller Performance at the Design Point

Having identified a simplified linear model of the RSRA vibration dynamics and designed a fixed-gain 'optimal' controller as discussed in the previous subsections, the GENHEL simulation was augmented with the feedback control design and the controller performance investigated. Figure 3-4 presents time histories of the three accelerometer outputs and the four feedback command control inputs for four (4) seconds of simulated flight at 120 knots and 100 feet altitude. No process or measurement noise was included in the fixed-gain controller simulation.

During the first second of the simulation, no control authority was exercised in order to allow the simulation time to reach a steady-state vibration level in all three axes. The transients are clearly manifest in the accelerometer outputs in Figure 3-4. These accelerometer outputs were also filtered to remove the center-of-mass specific force components which were of little interest in the vibration control problem. Similarly, the control deflections shown do not include the control deflections required to trim the RSRA at the indicated flight condition.

As expected, the controller performance is excellent at the design point as indicated by the rapid convergence and magnitude of vibration suppression. The vibration levels in all three axes are reduced to approximately 10% of their original levels. The root-sum-square (RSS) acceleration output in Figure 3-4 indicates the overall performance of the controller.

3.3.2 Control Law Robustness

To investigate the robustness of the controller designed at the 120 knot speed and 100 feet altitude flight condition, the same control gains

were used and the simulation run at different velocities, altitudes, and disc loading. The results are shown in Figures 3-5 through 3-14.

Figures 3-5 through 3-8 show the vibration reduction achieved at different helicopter altitudes at the same 120 knot speed. Little degradation in performance of the controller is seen for altitudes below 5,000 ft. A significant degradation is noted at 7,000 feet altitude (Figure 3-8), but still the overall vibration level is reduced to about 25% of uncontrolled level. It should be noted that the low frequency low amplitude modulation of the measurement and control time histories shown in Figure 3-8 is not an instability in the controller, but rather an artifact due to the subsampling of the program outputs required to reduce the number of points to be plotted, and represents an excellent example of the phenomenon of 'aliasing' in sampled data systems.

As evidenced by the control time histories in Figures 3-4 through 3-8, the major effect of operating the controller at increasing distances from its design point for this RSRA simulation is a significant increase in the control authority required to achieve the vibration reduction. A probable cause for the increased control deflection requirements is the decrease in control effectiveness as the air density decreases. The air density 1/e altitude is approximately 6000 feet, so the density is approximately a factor of three smaller at 7000 feet than at 1000 feet!

Figures 3-9 and 3-10 show the time histories of controls and the accelerations at the pilot location for 40 knots and 5 knots forward speed at 100 feet altitude. There is not much degradation in performance of the controller for 40 knot condition. There is, however, a slight degradation in performance of the controller at the 5 knot flight condition, but still the vibration is reduced to about 25% of the uncontrolled level.

Variations in disc loading (helicopter weight) on the order of 20% did not significantly degrade the fixed-gain controller performance as indicated in Figures 3-11 and 3-12. Though the steady-state controlled vibration level is roughly twice that of the controlled vibration at the design point, the performance is still acceptable.

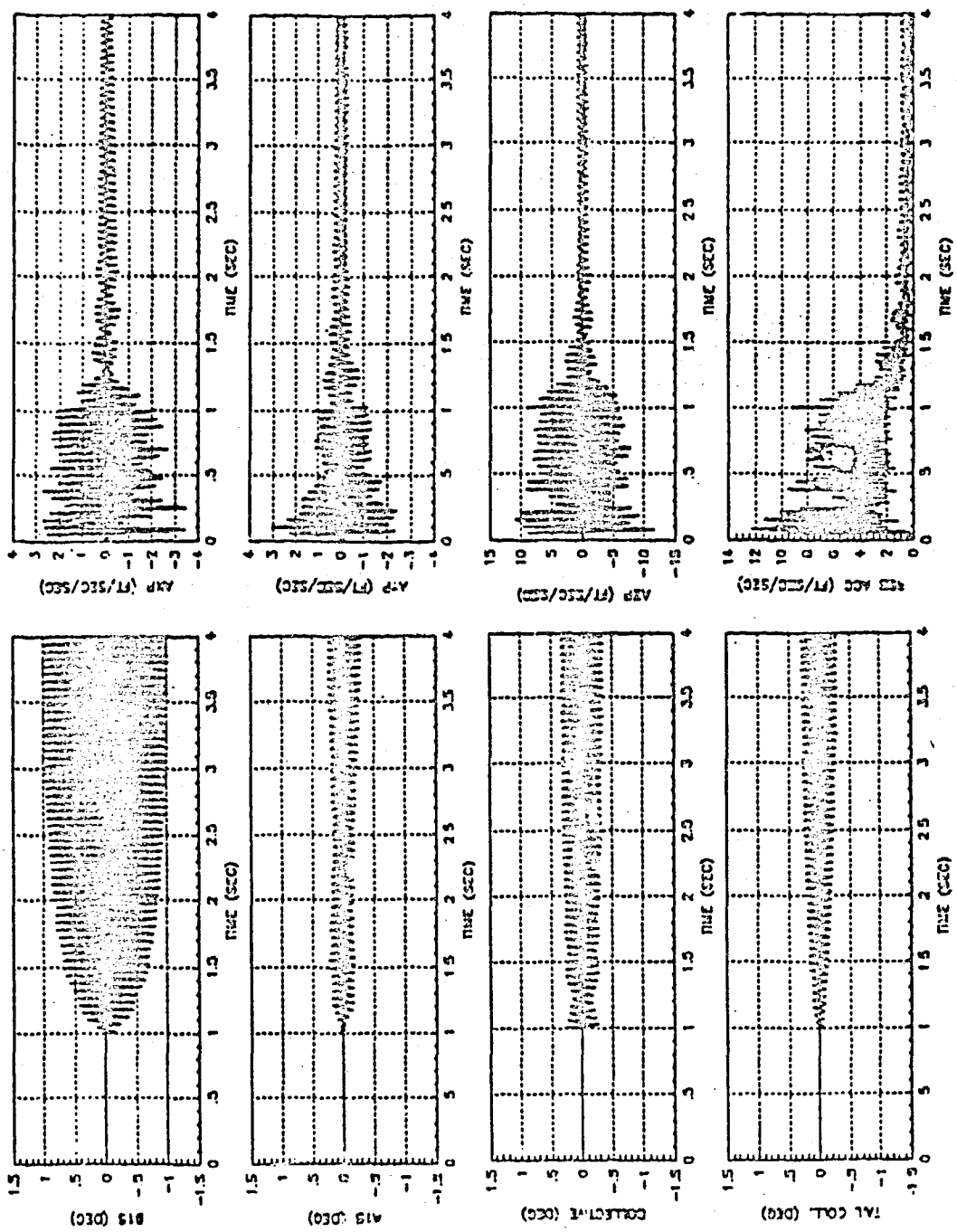

Figure 3-4. Control Inputs and Accelerometer Outputs for Fixed-Gain Control at 120 kts/100 ft - Design Point 120 kts/100 ft

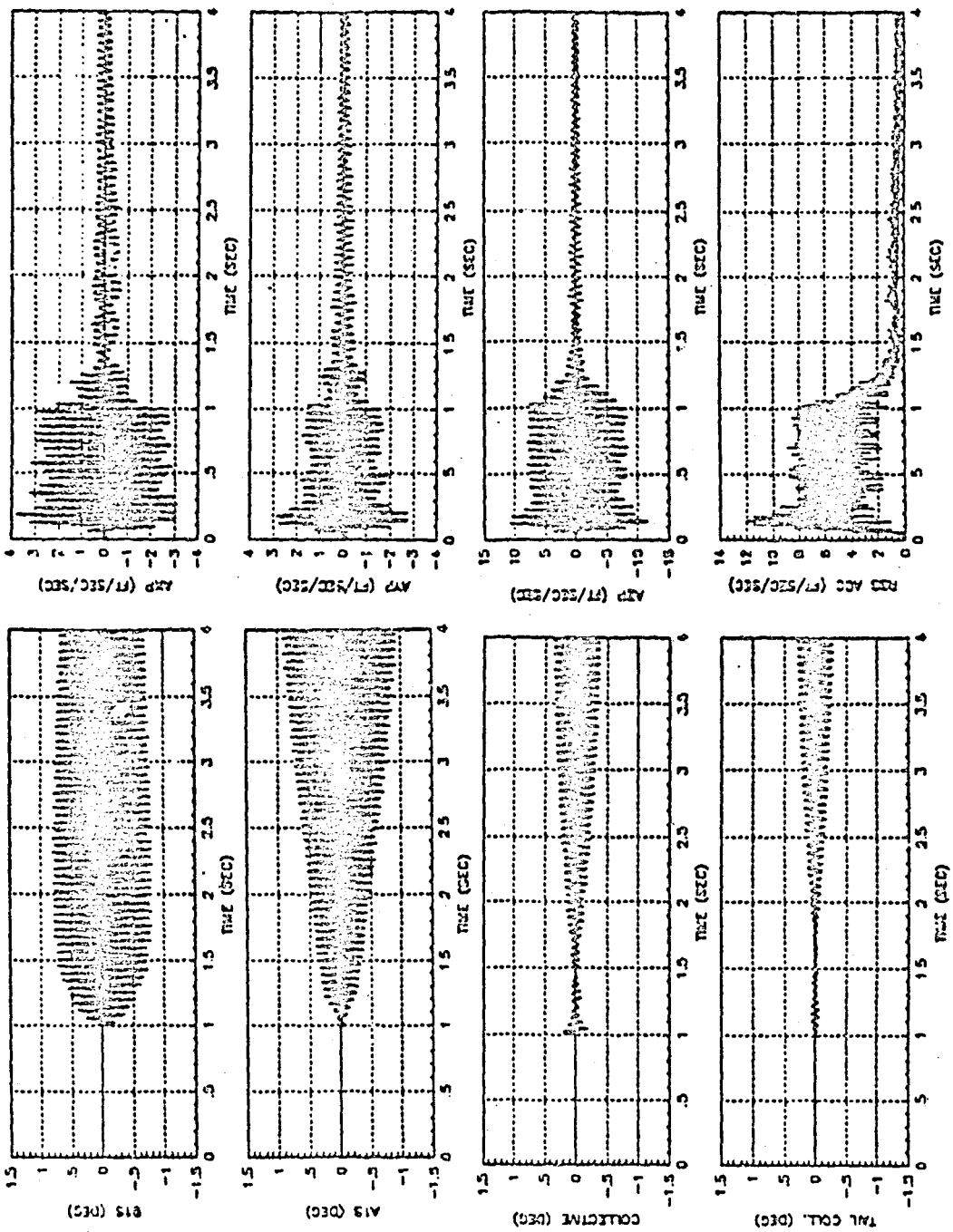

Figure 3-5. Control Inputs and Accelerometer Outputs for Fixed-Gain Control at 120 kts/1000 ft - Design Point 120 kts/100 ft

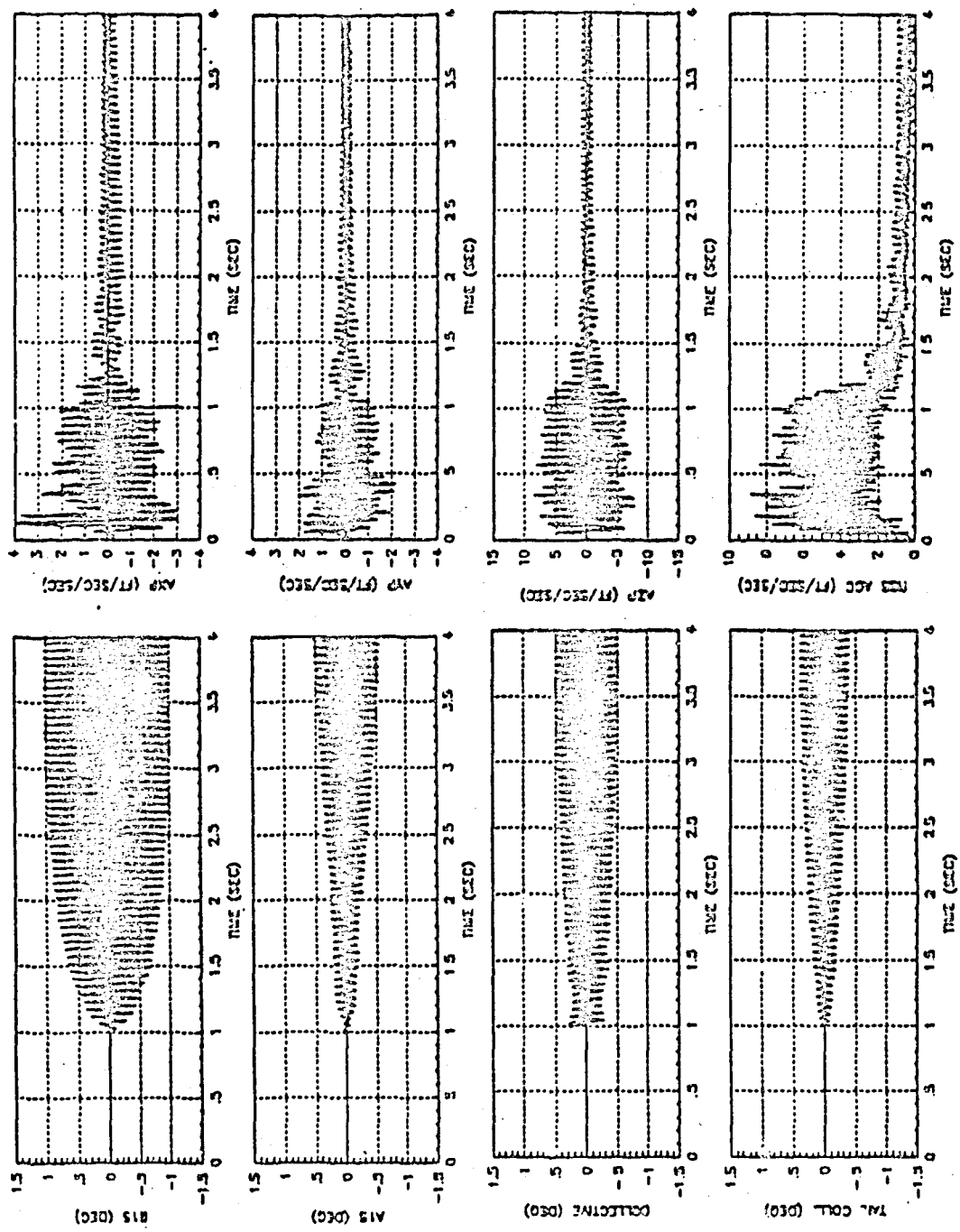

Figure 3-6. Control Inputs and Accelerometer Outputs for Fixed-gain Control at 120 kts/2000 ft - Design Point 120 kts/100 ft

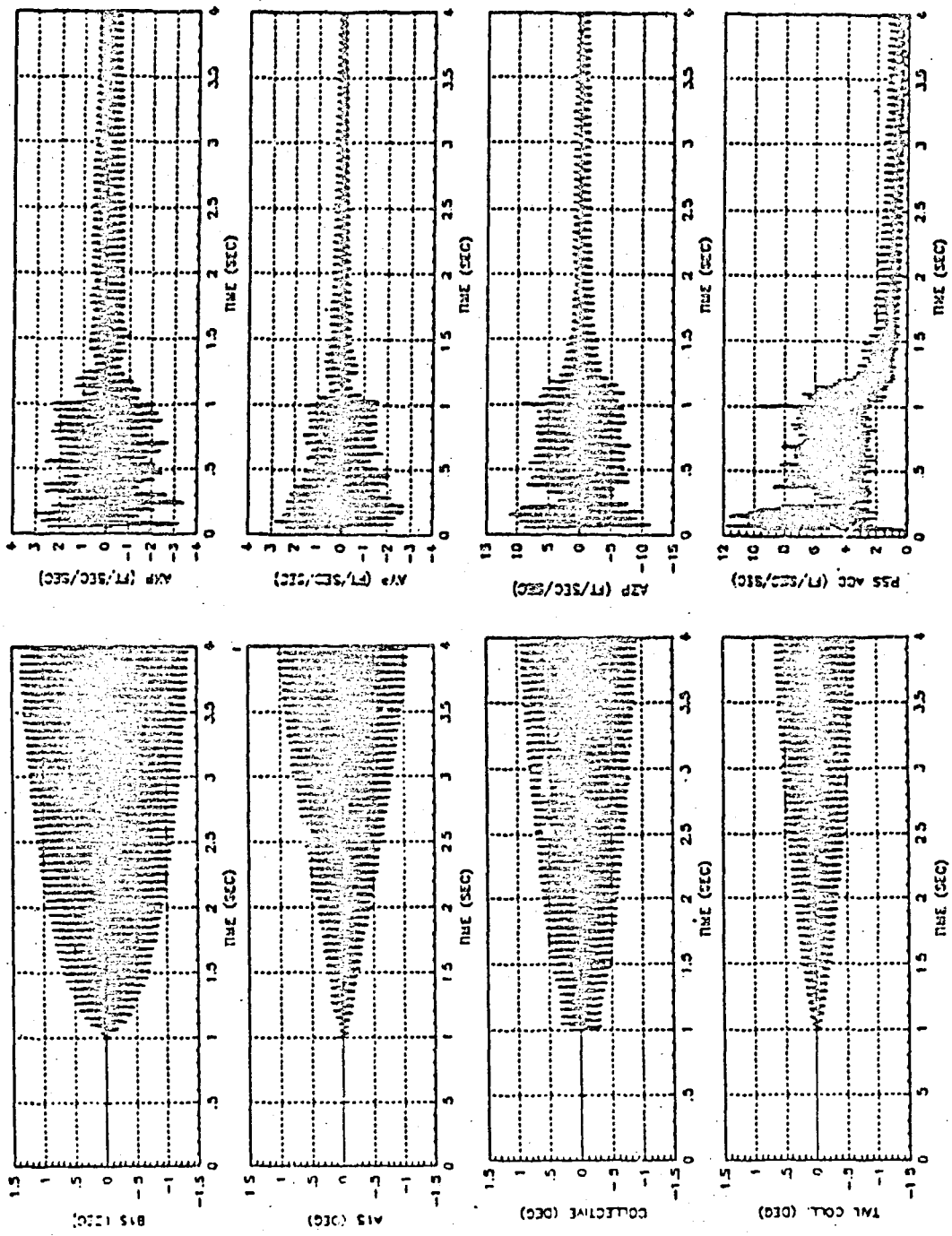

Figure 3-7. Control Inputs and Accelerometer Outputs for Fixed-gain Control at 120 kts/5000 ft - Desi.. Point 120 kts/100 ft

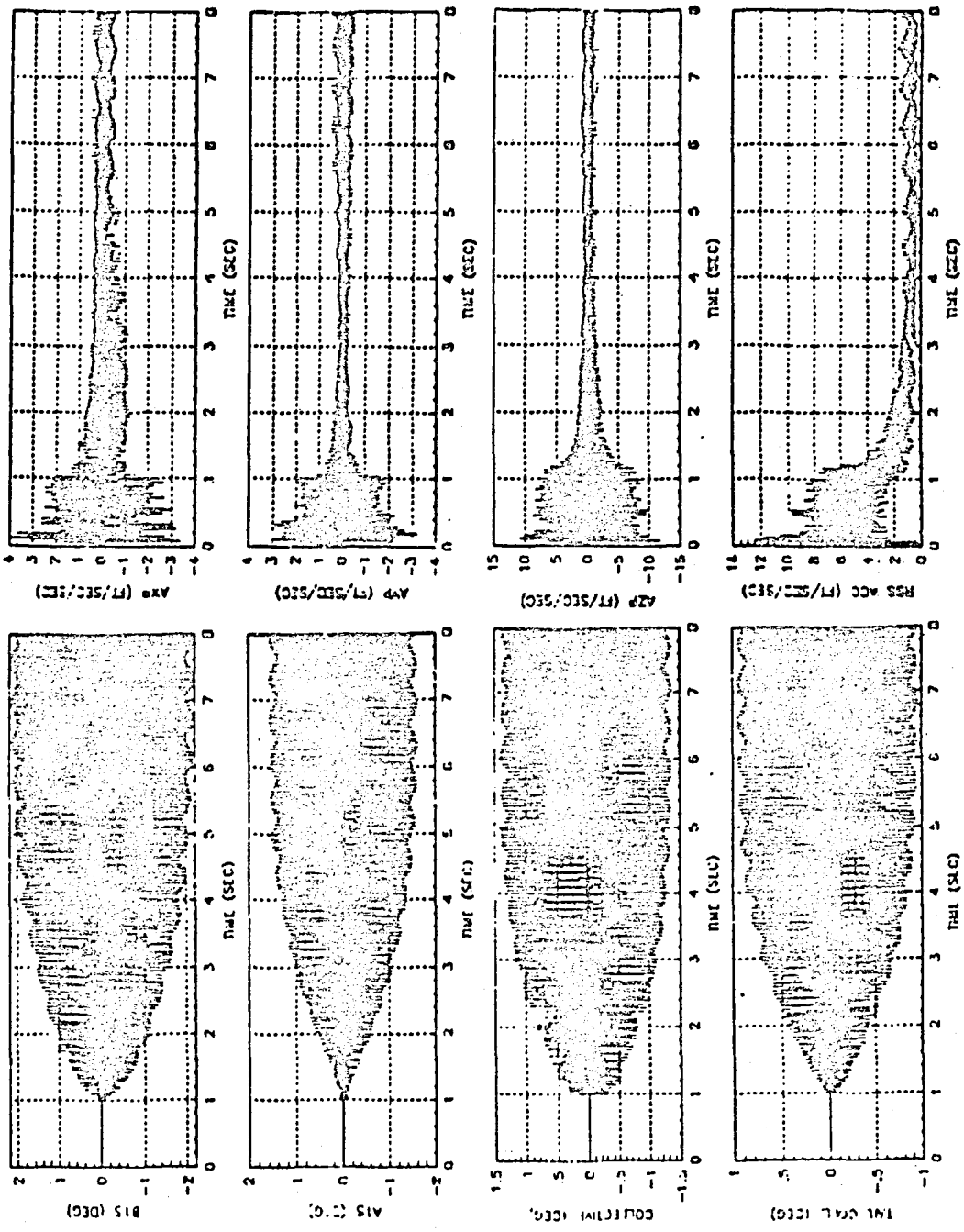

Figure 3-8. Control Inputs and Accelerometer Outputs for Fixed-gain Control at 120 kts/7000 ft - Design Point 120 kts/100 ft

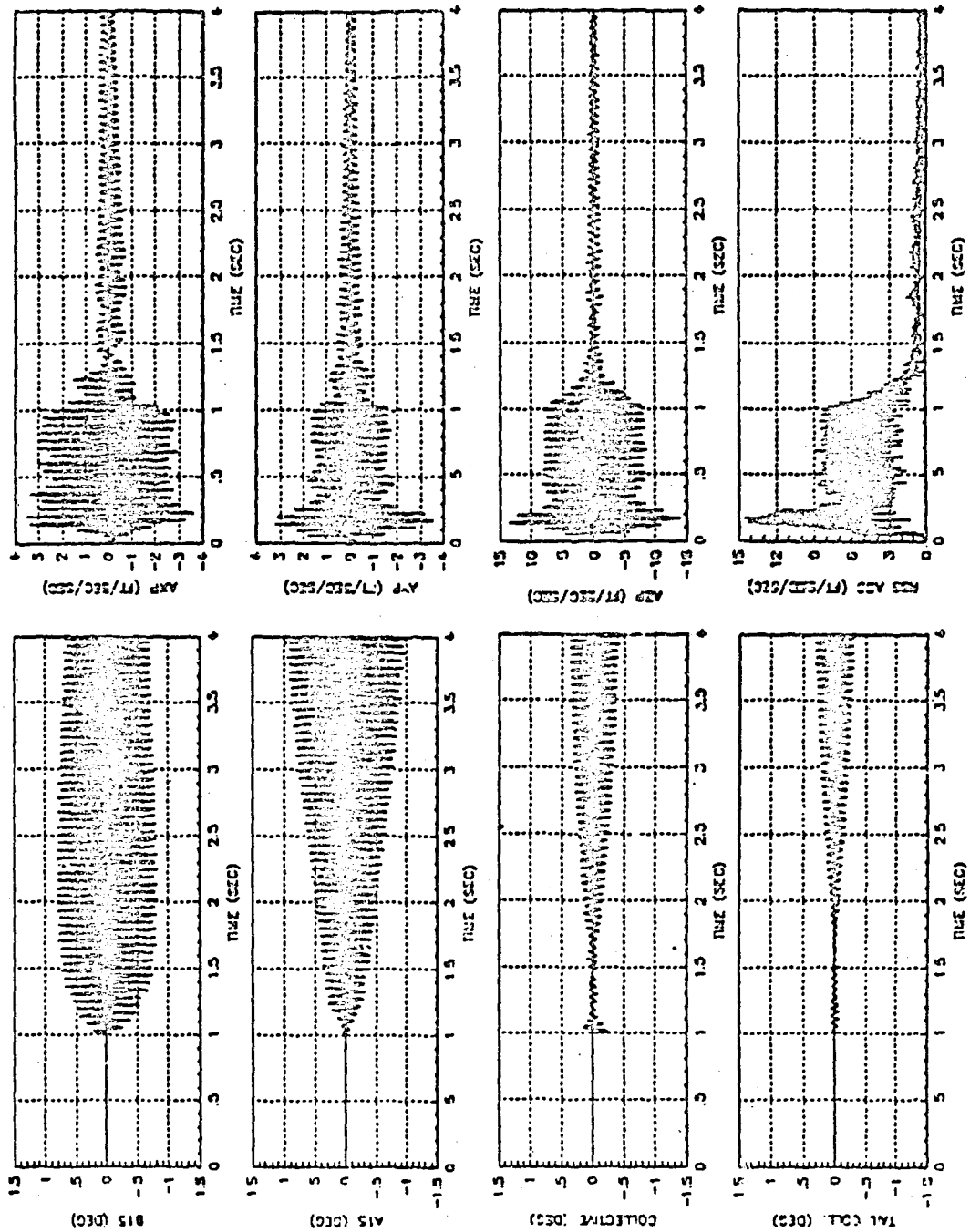

Figure 3-9. Control Inputs and Accelerometer Outputs for Fixed-gain Control at 40 kts/100 ft - Design Point 120 kts/100 ft

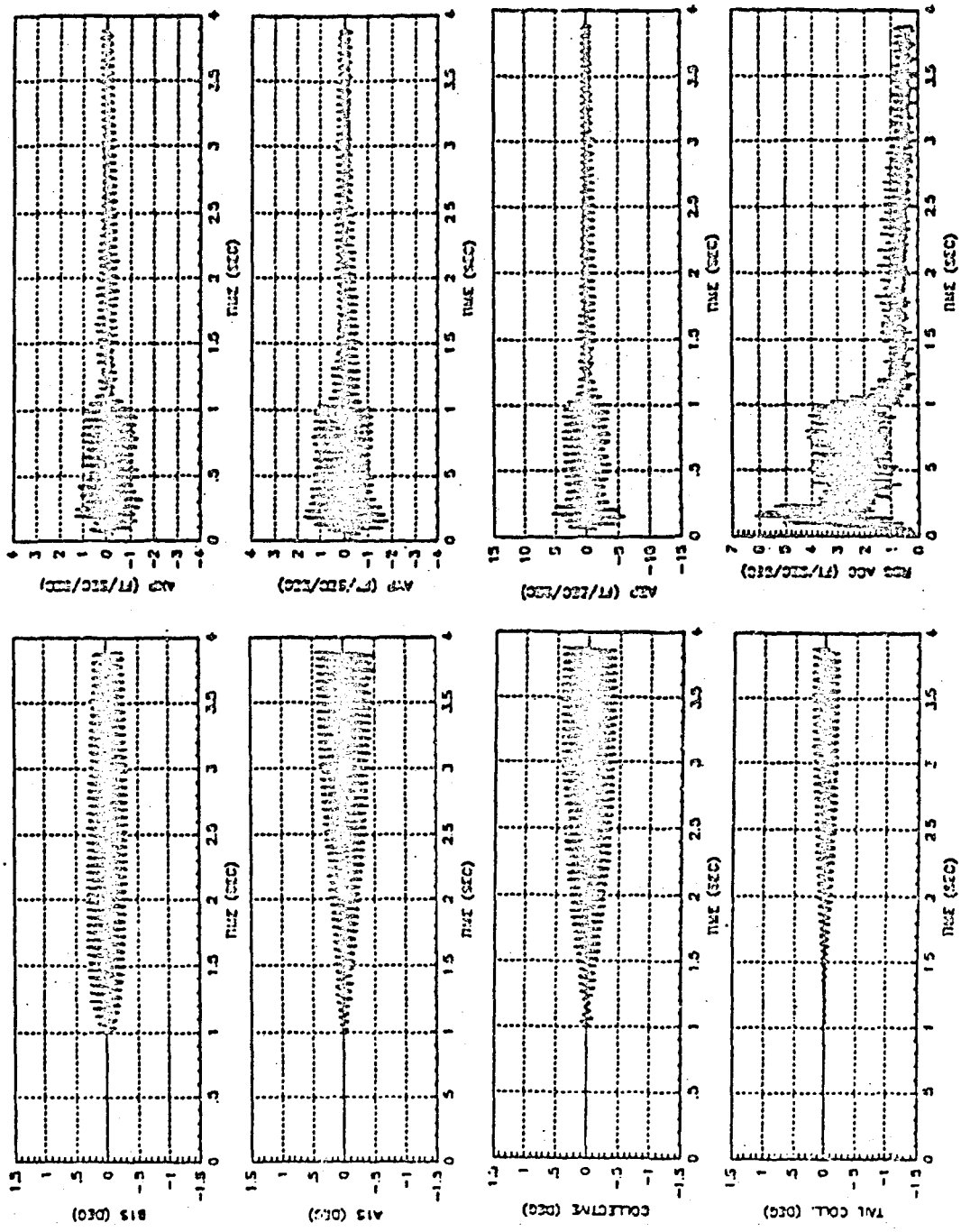

Figure 3-10. Control Inputs and Accelerometer Outputs for Fixed-gain Control at 5 kts/100 ft - Design Point 120 kts/100 ft

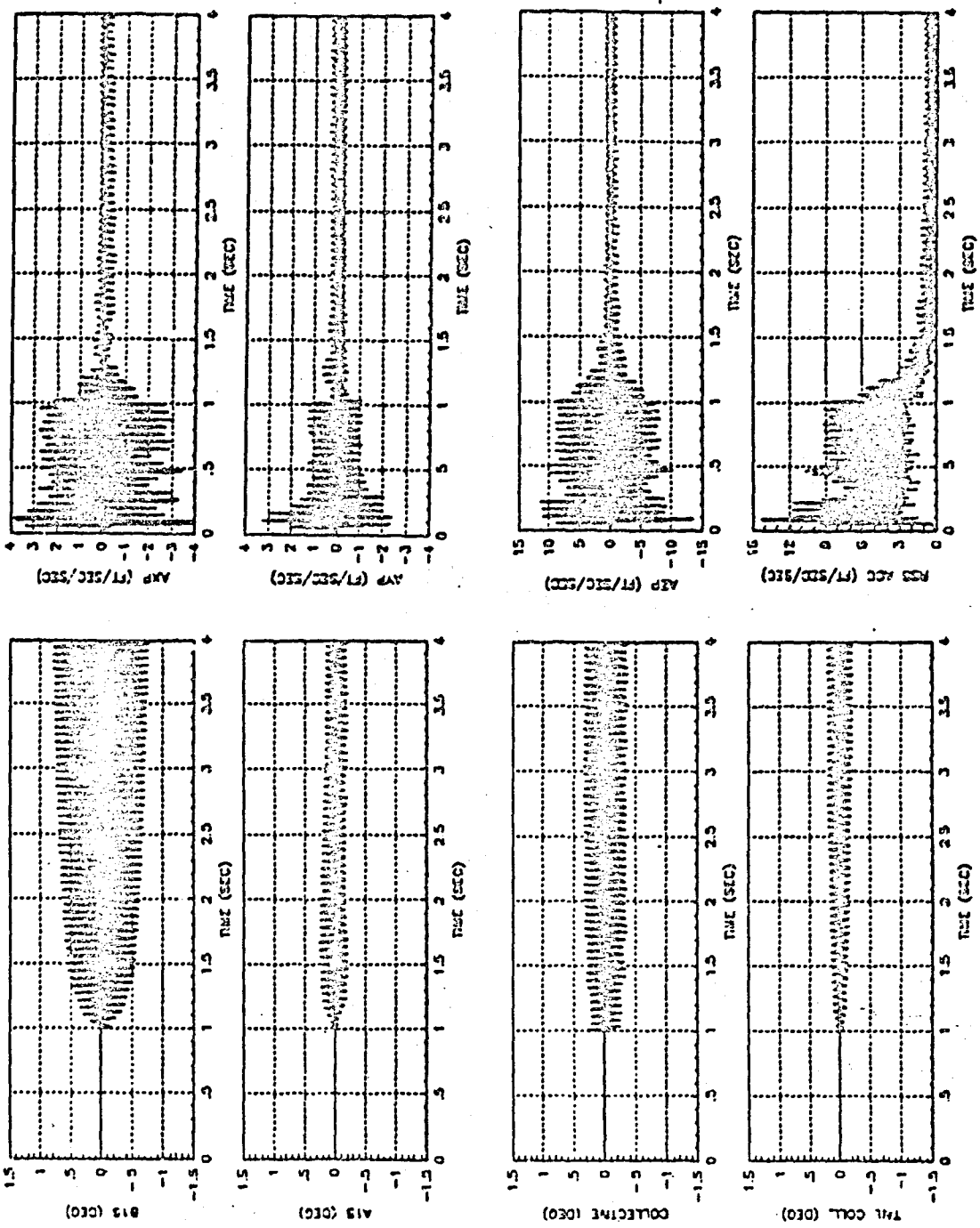

Figure 3-11. Control Inputs and Accelerometer Outputs for Fixed-gain Control at 120 kts/100 ft/ΔW = +20% (W=23520 lbs) Design Point 120 kts/100 ft

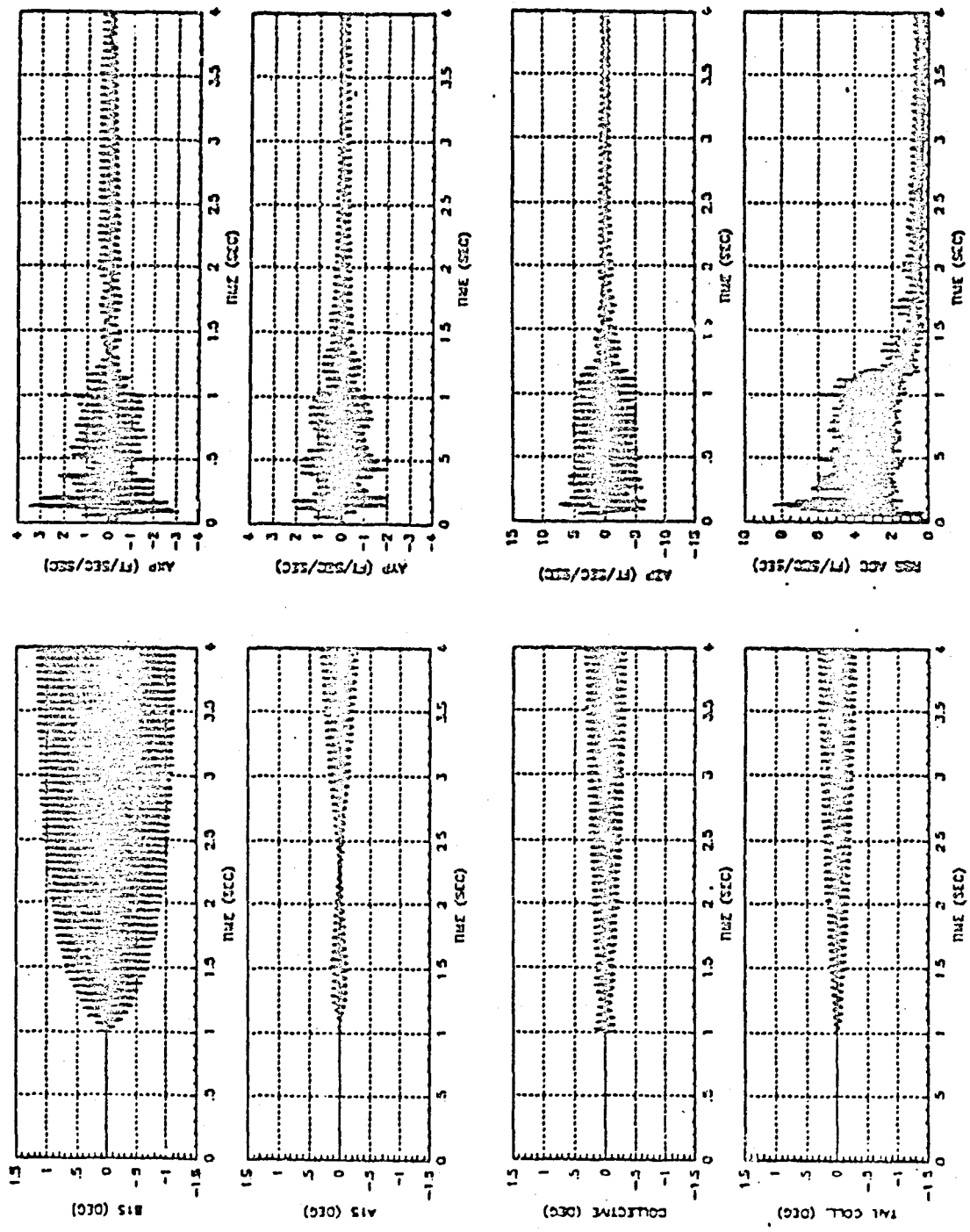

Figure 3-12. Control Inputs and Accelerometer Outputs for Fixed-gain Control at 120 kts/100 ft/ΔW = -20% (W=15680 lbs) Design Point 120 kts/100 ft

3.3.3 Simulation of Transient Flight Conditions

The fixed-gain controller for the RSRA simulation manifested considerable robustness with respect to variation in flight condition and aircraft configuration (disc loading). In an attempt to demonstrate the robustness of the controller during non-steady-state flight conditions, the GENHEL simulation was set up to allow alteration of the trim control surface deflections. Since the SAS was not operative in the available GENHEL simulation program, the transient flight was performed by interactive 'manipulation of the stick', using ramp and step inputs for short periods of time while continually monitoring flight conditions. The command inputs used to accelerate from 80 knots to 125 knots forward speed and selected flight parameters are shown in Figure 3-13. Though the intent was to maintain altitude at 1000 feet, this proved an exceedingly difficult task. The altitude time history indicates a loss of about 400 feet. The control feedback commands and the vibrations for all three axes are presented in Figure 3-14.

In these figures, no control is applied until 1 second. At 1 second the fixed-gain controller is turned on. From 3 seconds on, the input command is applied. From 1.5 to 3 seconds the vibration level is reduced to less than 10% of its original level as is expected. During the transient flight, except during periods of radical command input, the vibration is reduced to about 15% of the uncontrolled level. Between 3 and 6.5 seconds, large control commands are being applied resulting in an increase in the RSS vibration level. Similar behavior is observed from 13 to 14 seconds during a period of increased swash plate deflection During these periods however, the RSS vibration level does not exceed its unforced level.

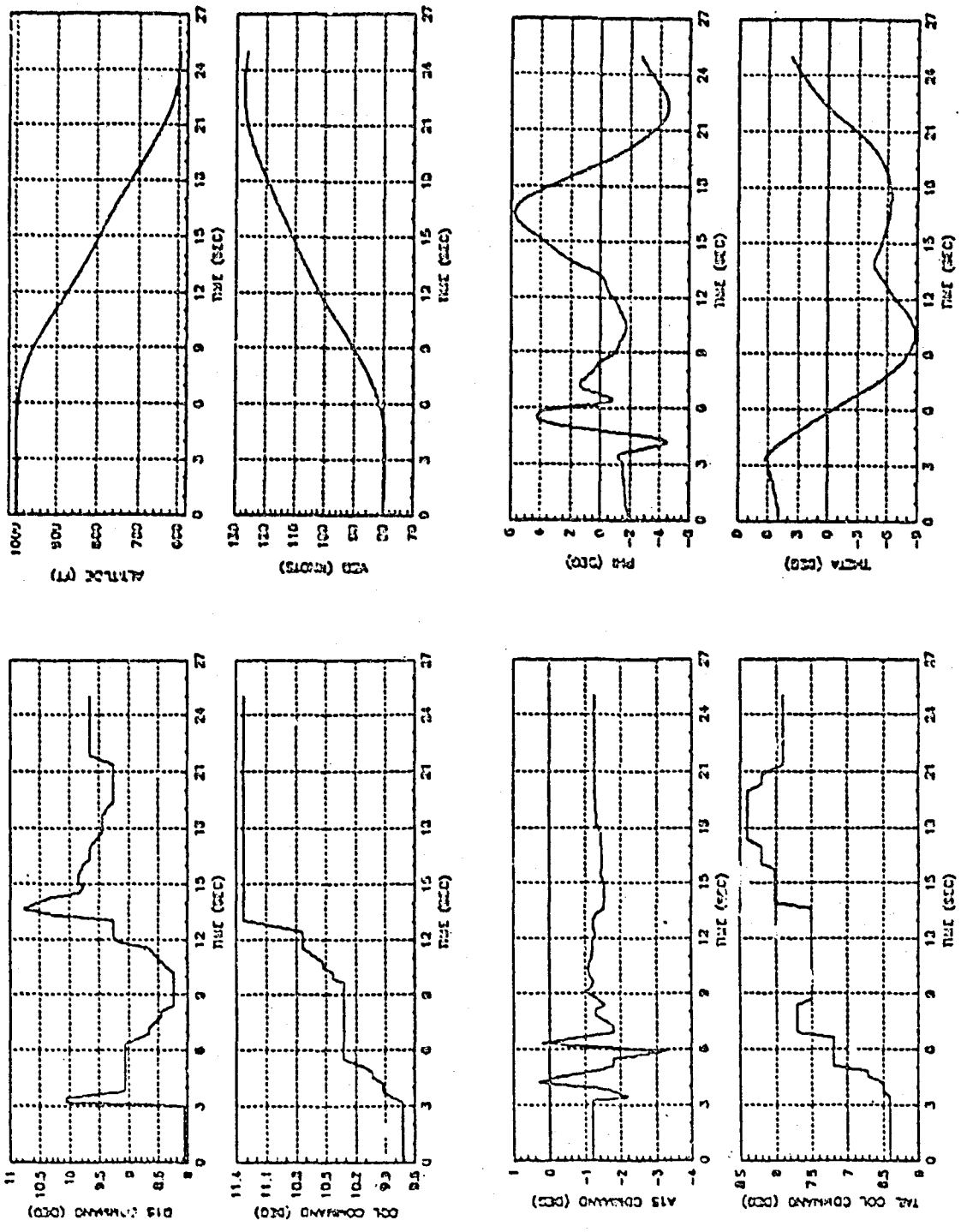

Figure 3-13. Command Inputs and Selected Flight Parameters for Fixed-gain Control during Transient Flight from 80 kts/1000 ft to 127 knot/595 ft

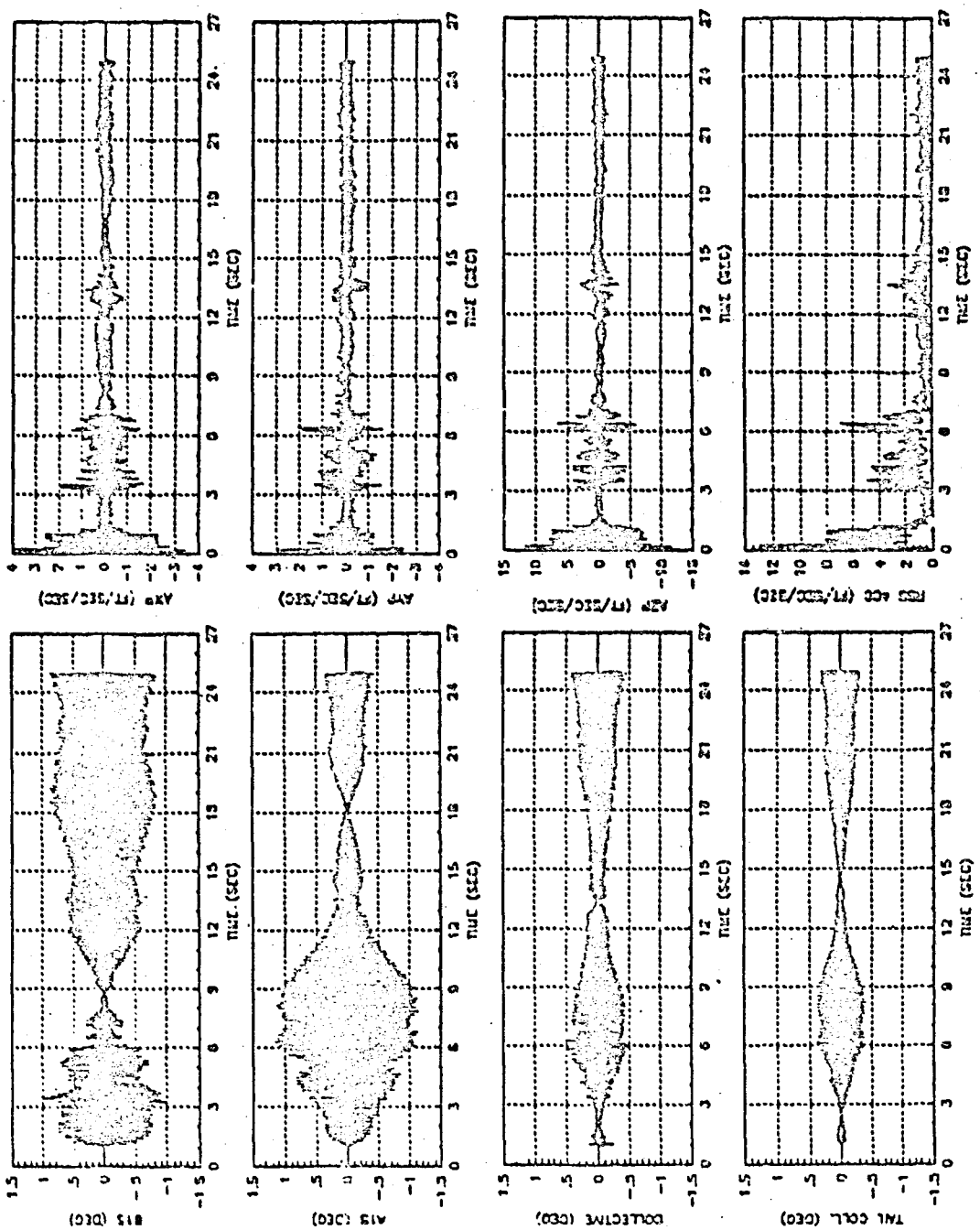

Figure 3-14. Control Inputs and Accelerometer Outputs for Fixed-gain Control during Transient Flight from 80 kts/1000 ft to 127 kts/595 ft

3.3.4 Discussion of Fixed-gain Controller Simulation Results

Table 3-1 summarizes the results of the fixed-gain control applied to the GENHEL simulation of the RSRA. As indicated earlier, their is a significant increase in the control authority required to achieve similar vibration reduction as the various flight conditions move farther from the design point of 120 knots forward speed and 100 feet altitude. The fixed-gain controller performs quite well overall when applied to the simulation however.

Table 3-1. SUMMARY OF FIXED-GAIN CONTROLLER STEADY-STATE ACCELERATION AND CONTROL AMPLITUDES FOR STEADY-STATE FLIGHT CONDITIONS

Flight Condition		Steady-State RSS ACC	Steady-State Amplitude Feedback Control (Peak-to-Peak)			
VEQ (knots)	Altitude (ft)	(ft/sec^2)	B_{1s}(deg)	θ_c(deg)	A_{1s}(deg)	θ_{tr}(deg)
5	100	1.0	0.3	0.4	0.4	0.2
40	100	0.9	0.7	0.4	1.0	0.3
120	100	0.8	1.0	0.4	0.3	0.3
	1000	0.9	0.8	0.4	0.8	0.3
	2000	1.0	1.0	0.5	0.5	0.4
	5000	1.5	1.3	0.9	1.0	0.6
	7000	1.8	2.0	1.4	1.5	1.0
80-127	1000-600	1.5	0.8	0.4	0.5	0.3

SECTION 4

ADAPTIVE CONTROLLER FOR RSRA ROTORCRAFT VIBRATION SUPPRESSION

This section discusses the issues involved in the design of an adaptive controller for the RSRA helicopter. The primary reason for considering an adaptive controller for vehicles of this type is the wide range of input-output dynamic characteristics the helicopter is expected to assume as the flight conditions and/or structural configurations change. Rather than designing off-line, fixed-point control strategies, i.e. control strategies designed for a specific operating condition, and attempting to choose the appropriate strategy to meet the current conditions, the basic idea is to perform on-line system identification and control design simultaneously. As the operating conditions change, so does the system being identified and appropriate changes are made in the control law. Thus, the control system is adapting to the changing operating environment.

Adaptive control systems have two basic components: an estimation and identification 'subsystem', and a feedback control 'subsystem'. The estimation and identification subsystem uses the inputs and outputs of the system in order to identify an equivalent input-output model of the system. In addition, estimation of states in an internal description of the system to be controlled may be performed in order to provide sufficient information to the controller subsystem. The distinction being made here is between full-state feedback versus output feedback control strategies.

The controller subsystem uses the outputs from the estimation and identification subsystem to compute feedback control commands. In a full-state feedback control design, an estimator is then used to obtain 'optimal' estimates of the states in the dynamical model of the system based on past and present inputs and outputs of the system. Figure 4-1 gives a block diagram of the basic subsystems of an adaptive controller. The remainder of this section describes the design of the two basic subsystems and their interconnections. The state estimation is performed utilizing a time-varying Kalman filter whose system parameters are the outputs of a multi-input, multi-output parameter identification algorithm based on recursive prediction error methods. The controller is implemented via the time-varying LQR optimal control law which is dual to the Kalman filter estimator.

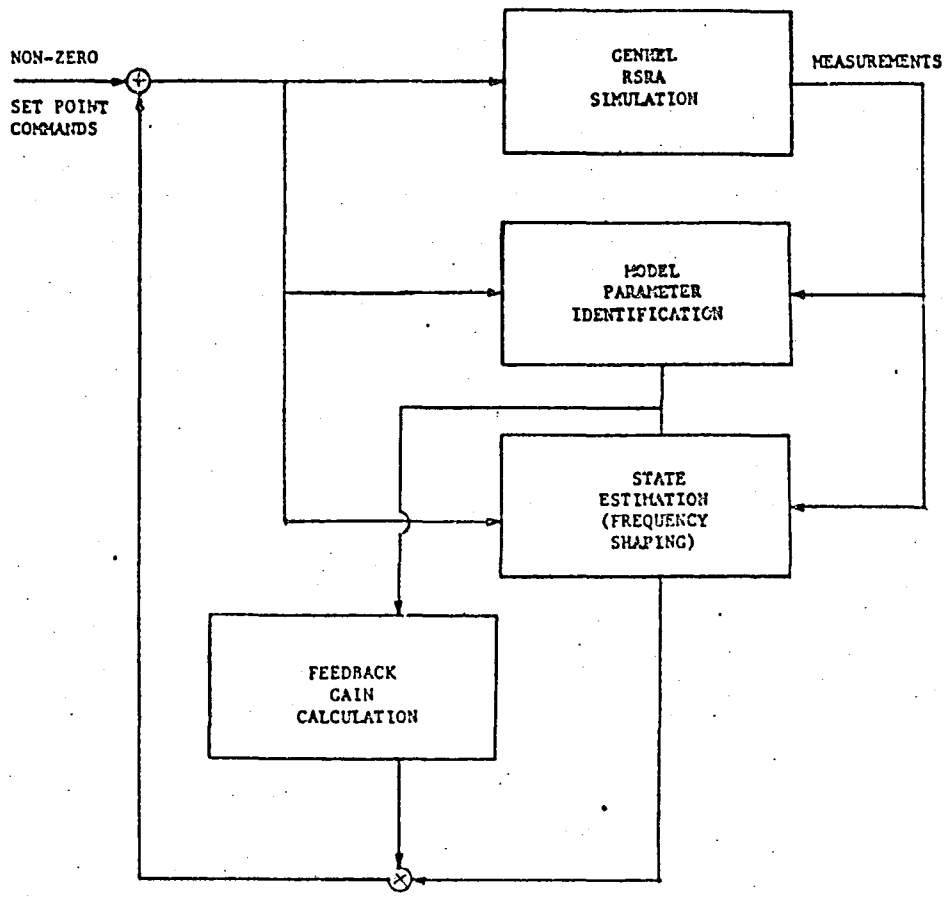

Figure 4-1. Block Diagram of an Adaptive Controller

4.1 PARAMETER IDENTIFICATION AND STATE ESTIMATION

State estimation and parameter identification is performed to provide to the control subsystem necessary information for the implementation of an effective control law. This is certainly not a simple task in the case of the RSRA helicopter due to the extremely nonlinear nature of the vehicle. In this study, the state estimation and parameter identification were implemented sequentially rather than simultaneously. The option of augmenting the state estimation algorithm with states which are the parameters to be identified was considered, but not implemented due primarily to computational considerations. This decoupling of state estimation and model parameter identification is 'suboptimal' however, and the possible performance degradation warrants further analysis.

In this subsection, the parameter identification algorithm which was employed is discussed in detail. The approximate model of the vibration dynamics is discussed, and the modeling and rejection of the periodic disturbances for identification purposes is detailed. Finally, discussions of practical issues such as implementation and tuning of the algorithm are given.

4.1.1 Parameter Identification Algorithm

The basic objective of parameter identification is to select from a class of models, a model of the dynamics of the system under investigation which does the best job, according to a given criterion, of predicting the future given the past. Implicit in the statement of the objective are three main tasks to be accomplished; selection of a class of models (model form), choosing appropriate criteria for discrimination between models in the class, and finally determination of the 'optimal' solution. The most difficult of these tasks in general, is the selection of the model form. Models which are overly complex unnecessarily increase the computation load, and are more prone to suffering from input-output identifiability problems. On the other hand, models which are overly simplified may not retain sufficient information for adequate control. In designing the identification

subsystem, the goal is to find the simplest model which results in an adequate closed-loop controller. Knowledge of the underlying physics of the problem, i.e. helicopter vibration, is used wherever possible.

4.1.1.1 Dynamic Model for Parameter Identification

As discussed in the previous section, the majority of the power in the vibration is due to the excitation of the flexible modes of the RSRA helicopter by the periodic disturbances at Ω (N/rev) and its harmonics. A controller designed to suppress vibration at Ω and its harmonics will eliminate most of the vibration and could very well satisfy the objectives in terms of overall vibration reduction.

The extremely narrowband nature of the vibration permits major reductions in the complexity of the model of the vibration dynamics. The majority of the vibration at the pilot location results from transmission of periodic disturbances at the rotor through the hub, amplified (or attenuated) and phase-shifted by the fuselage flexible modes. Therefore, models which can correctly account for the phase shift and attenuation from each of the inputs to each of the outputs in intervals of frequency around Ω and its harmonics should be sufficient. Linear second-order systems satisfy these requirements for linear forced response. Thus, the model for approximating the vibration dynamics amounts to a direct sum of underdamped second-order linear systems whose center frequencies are the dominant vibration frequencies, Ω and its harmonics. As discussed in the previous sections, the inclusion of only the RSRA flexible fuselage modes near Ω was intentionally designed to restrict the number of vibration frequencies to one (Ω).

Given a multi-input, multi-output system such as the RSRA helicopter, there are many model structures which incorporate the second-order single input to single output relationships desired. Noting that the flexible modes in the simulation were uncoupled by construction (cf. Section 2); and reasoning that for small vibrations the three orthogonal acceleration components would be nearly decoupled in an actual helicopter as well, three uncoupled multi-input single-output (MISO) models were used. With reference to equation 3.3, the equations for one of the axes can be written (in observer canonical state-space form) as follows:

$$x(k+1) = \begin{bmatrix} F_{p11} & 1 \\ F_{p21} & 0 \end{bmatrix} x(k) + \begin{bmatrix} G_{p11} & G_{p12} & G_{p13} \\ G_{p21} & G_{p22} & G_{p23} \end{bmatrix} u(k) + \Gamma w(k) \qquad (4.1)$$

$$y(k) = [1\ 0]x(k) + D_p u(k) + v(k)$$

where x is a two-vector $[x_1, x_2]'$ of dynamic states, u is the vector of control inputs, Γ is the process noise/disturbance distribution matrix, and w is a vector of process noise/disturbance terms. The subscript 'p' is used to denote the 'plant.

It should be noted that for performing vibration control, there are actually four control degrees of freedom (inputs) assumed to be available, including the swashplate (two degrees of freedom), the main rotor collective, and the tail collective. However, due primarily to its distance from the pilot location and its limited thrust capabilities in the lateral direction, the tail rotor effectiveness in vibration reduction at the pilot location was found to be minimal. For the majority of the flight conditions investigated, the vertical, or z-component of uncontrolled vibration acceleration was the dominant component, and the lateral, or y-component was the smallest. Thus, in order to reduce the computation load and control effort requirements, the tail rotor collective was subsequently ignored in the adaptive controller design.

4.1.1.2 Disturbance Modeling and Rejection

The vector w(k) in equation 4.1 is assumed to be composed of a broadband, low power component modeling disturbances at frequencies other the Ω and its harmonics (as well as accounting for dynamical model uncertainties to some extent), and a relatively high power narrowband disturbance at Ω. In order to obtain meaningful estimates of the parameters in the approximate second-order model of the input-output relationship, the effect of the narrowband disturbance term which is present must be taken into account. An important difference between the fixed-gain and adaptive control algorithms lies in the different approaches taken in addressing this important issue.

In the off-line identification procedure used in the fixed-gain controller design, these disturbances were modeled as purely periodic with unknown amplitude and phase. The amplitude and phase were estimated by explicitly including terms proportional to $\cos\psi_k$ and $\sin\psi_k$ in the ARX models. Similar parameters could also be estimated in the on-line identification algorithm by employing model extensions similar to those used in the off-line identification procedure. A further extension would allow for estimation of narrowband disturbances by including a damping coefficient in the model. This would seem appropriate in light of potential helicopter nonlinearities 'broadening' the disturbance spectrum at Ω. The key point is that these approaches require augmenting the helicopter vibrations dynamics model with a model of the narrowband disturbance process.

The main objective in estimation of these periodic disturbance terms, however, is basically to eliminate the disturbance ('colored noise') component from the measurements. This is done prior to updating the parameters in the identification algorithm, otherwise biased parameter estimates result (leading to potential problems in the controller). Realizing the objective is to eliminate a narrowband disturbance of known center frequency, a computationally more attractive, but suboptimal approach was taken. The elimination of the frequency components at N/rev was accomplished with a digital notch filter. The continuous domain transfer function equivalent of the digital filter employed has two zeroes on the imaginary axis at N/rev, and two poles just inside the left half-plane:

$$F_{BP}(s) = \frac{s^2 + \Omega^2}{s^2 + 2\zeta\Omega s + \Omega^2} \quad .$$

As a practical issue, in order to improve the transient performance of the notch filter for parameter identification and retain the narrow bandwidth required during the identification process, a time-varying damping coefficient was implemented. During the transient region of the simulation start-up, a relatively wide bandwidth notch (ζ~2%) is used. The damping coefficient is decreased exponentially when parameter identification is initiated, narrowing the notch filter bandwidth significantly (ζ~0.2%). Note both the inputs and outputs are notch filtered before they are passed to the parameter identification algorithm so as not to introduce an distortion of one relative to the other.

To conclude the discussion of the model of the vibration dynamics and the disturbance modeling (rejection), several important points concerning the number of identifiable parameters (to be estimated) in the model in equation 4.1 are noted. Without loss of generality, the state component of the output was chosen to be the first state x_1 (i.e. observer canonical form). Since a second-order system is completely specified by its natural frequency and damping coefficient, only two parameters are required in the system dynamics matrix. The remaining elements in the control distribution matrix are unconstrained. By notch filtering the measurements and inputs, identification of parameters in the disturbance distribution matrix as well as possible parameters in a dynamical model of the narrowband disturbances is not required.

4.1.1.3 MISO RPEM Parameter Identification Algorithm

Decoupling of the model into three separate axes led to considerable simplifications in the design of the parameter identification scheme. The MISO state-space model in equation 4.1 is readily transformed into an equivalent MISO ARX (autoregressive model with exogenous inputs) model, which is a standard form used in several recursive prediction error parameter identification (RPEM) algorithms. Transforming equation 4.1 into an ARX form gives:

$$y(k+1) = A_1 y(k)+A_2 y(k-1)+B_0 u(k+1)+B_1 u(k)+B_2 u(k-1) + v(k) \quad (4.2)$$

where in an obvious notation, the arguments are time indices and y is a scalar output with u the vector of control inputs. The coefficients are matrices of the appropriate dimensions, and bear the following simple relationships to the parameters in the state space model:

$$\begin{aligned} F_{11} &= A_1 \\ F_{21} &= A_2 \\ G_{ij} &= B_{ij} + A_i B_{0j} \\ D_i &= B_{0i}. \end{aligned} \quad (4.3)$$

By stacking the outputs and inputs on the right-hand side of equation 4.2, and collecting all the parameters in a single vector, the equation can be written in regression form as indicated in equation 4.4:

$$y(k) = \theta^T \phi(k) + v(k). \tag{4.4}$$

A derivation of the classical recursive least-squares identification algorithm is outlined below, leaving detailed derivations to the references. The least-squares cost criterion on the parameter vector estimate is:

$$J = \sum_{k=0}^{N} [y(k) - \theta^T \phi(k)]^2.$$

Minimization of this cost function is accomplished by differentiating with respect to the parameter vector (θ) and setting the gradient to zero. Taking care to preserve the recursive nature of the equations, the recursive least-squares identification algorithm is obtained.

$$\begin{aligned} R(k) &= R(k-1) + \frac{1}{k}[\phi(k)\phi^T(k) - R(k-1)] \\ \theta(k) &= \theta(k-1) + \frac{1}{k} R(k)^{-1}\phi(k)\varepsilon(k), \\ \varepsilon(k) &= y(k) - \theta^T(k-1)\phi(k). \end{aligned} \tag{4.5}$$

Though these equations are recursive, they are not well suited for on-line implementation since at each step a matrix inverse is required. However, taking advantage of the fact that the update to the information matrix (R) is of rank one, the matrix inversion lemma can be used to exchange the matrix inverse for a scalar division in the propagation of the parameter covariance matrix as shown in equation 4.6.

$$P(k) = P(k-1) - \frac{P(k-1)\phi(k)\phi^T(k)P(k-1)}{1 + \phi^T(k)P(k-1)\phi(k)} \tag{4.6}$$

The parameter update equation becomes:

$$K(k) = P(k-1)\phi(k)[1 + \phi^T(k)P(k-1)\phi(k)]^{-1}$$
$$\theta(k) = \theta(k-1) + K(k)\varepsilon(k). \tag{4.7}$$

The above equations assume that the parameters are constant over time, though the estimate $\theta(k)$ is certainly a time-varying quantity. The interpretation to be given is that $\theta(k)$ is the best estimate of the constant parameter vector given all the past information. In order to allow for time-variation of the parameters, past information must somehow be deweighted and greater emphasis placed on more recent information.

There are several methods for modifying the above equations to accomplish this goal. The first, and computationally less intensive method is to insert a 'forgetting factor' into the cost function such that more weight is placed on recent errors than past errors. If the weighting is exponential, then above equations are simply modified:

$$P(k) = \frac{1}{\lambda(k)} P(k-1) - \frac{P(k-1)\phi(k)\phi^T(k)P(k-1)}{\lambda(k) + \phi(k)P(k-1)\phi^T(k)}$$
$$K(k) = P(k-1)\phi(k)/(\lambda(k) + \phi(k)P(k-1)\phi^T(k)), \tag{4.8}$$

where $\lambda(k) < 1$ is the 'forgetting factor', a scalar variable (usually set to some fixed value). These equations effectively include a time update along with the measurement update by scaling up the parameter covariance matrix P by the factor $1/\lambda(k)$.

There is a certain amount of redundancy in equations 4.8, and this fact can be taken advantage of in designing a fast algorithm for computing the necessary quantities. The fast implementations rely on the fact that a positive definite matrix (all covariance matrices are positive definite) can be factored into a product of three matrices; an upper (lower) triangular matrix with unit diagonal elements, a diagonal matrix with positive ele-

ments, and the transpose of the upper (lower) triangular matrix, the so-called U-D algorithm. These equations propagate an upper triangular factor (U) and a diagonal matrix (D) such that

$$P = UDU^T.$$

The U-D update equations are basically a modified version of the Gram-Schmidt orthogonalization procedure, the details of which are left to the references (cf. Bierman, [9]).

Returning to the problem of the time update of the parameter covariance, the fact that only a scalar forgetting factor is allowed is quite restrictive in the sense that all parameters are assumed in some sense to have the same time-varying time constant. In most practical situations, excellent arguments based on physical laws can be made to suggest that some parameters have larger expected time-variation than others. An identification algorithm which does not take this information into account must certainly suffer performance degradation in comparison to an algorithm which does.

The discussion in the preceding paragraph suggests that an implementation of the covariance time update which allows for the inclusion of more (stochastic) information is more appropriate. This second method of deweighting past information is more appropriately thought of as propagation of the filtered parameter covariance in the presence of additive disturbances (process noise or model uncertainty). The time update equation is now separate from the measurement update and is given by:

$$P(k+1|k) = P(k|k) + Q(k) \qquad (4.9)$$

where the notation has changed to reflect the fact that at each time k there are predicted and filtered covariances. Though the computation load is increased, there is a modified weighted Gram-Schmidt procedure (cf. Bierman, [9]) for performing this time update in the U-D factorization formalism. For the reasons already cited, this method of covariance time update was chosen over the 'forgetting factor' approach. Tests of both approaches indicated that the choice was well-founded on the basis of robustness and overall vibration suppression performance.

4.1.1.4 Practical Considerations for ID Algorithm Implementation

An important consideration in parameter identification is that of input design. Identification of parameters in a closed-loop system without persistently exciting external inputs is a singular problem in the sense that parameters in the open loop transfer function are not identifiable. In order to insure a well-posed identification problem, a sufficiently wide bandwidth external input is required to excite all the modes of the system. For identification of the parameters in the narrowband model of the RSRA helicopter dynamics near N/rev, such an input was constructed by passing random noise through a cascade of two second-order filters whose damping coefficients were 30% and whose center frequencies were Ω. Figure 4-2 gives a two-second sample of this excitation as well as a plot of its power spectrum.

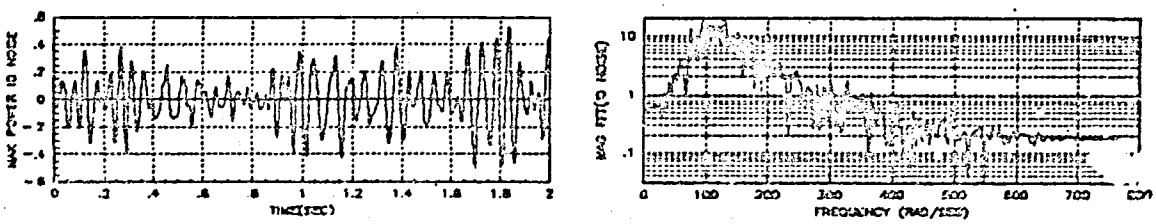

Figure 4-2. Sample Time History and Power Spectrum of Wideband Excitation for Identification.

The issue of how much noise to add for identification basically involves a trade-off between the requirement for persistent excitation at a signal-to-noise ratio (SNR) sufficient to provide reliable parameter estimates and the desire to keep the control effort and induced vibration outside the controller bandwidth below acceptable levels. In the case of the RSRA helicopter, acceptable control surface deflections for vibration control (at N/rev) were assumed to be on the order of two degrees for all the controls.

In the implementation, the noise amplitude was made a function of the performance of the controller. The controller performance measure used was a sum of low-pass filter outputs whose inputs were the rectified accelerometer outputs from each axis. Between preset upper and lower limits, the input

noise amplitude was a linear function of the difference between the performance measure and a preset ID-OFF threshold (discussed in the next paragraph). This had the effect of increasing the input amplitude when the performance measure indicated a need for improved parameter identification, and reducing the control deflection required to suppress vibration resulting from this noise when the identified parameters were sufficient for control purposes.

The performance measure was used not only to regulate the wideband external input amplitude, but also to turn on and off the identification algorithm. Using hysteresis logic, ID was turned off as the performance measure fell below a preset threshold (3 ft/sec^2 is used for most of the results presented in this section), and was turned on if the performance measure exceeded a second preset threshold which was larger than the first (3.6 ft/sec^2 was used for most of the results presented in this section).

This switching logic is primarily used to prevent the identification algorithm from diverging during periods when identifiability of the parameters is low. Parameter identifiability decreases as the amplitude of the external wide bandwidth noise input decreases, and the parameter identification algorithm becomes singular when the exogenous wide bandwidth input is removed. Since the controller bandwidth is narrow, it is desirable to eliminate the wide bandwidth noise when a steady-state is reached. This enabling/disabling logic prevents the burst-type of instabilities reported in the literature for adaptive controllers.

4.1.2 State Estimation Algorithm

The state estimation algorithm uses the model of the system to be controlled which, as discussed in the previous section, is comprised of three decoupled second-order systems. The parameters in these second-order models are functions of the outputs of the parameter identification subsystem, and are given by the relationships in equation 4.3. The states of these second-order models are estimated using the measurements, and these estimates are used in the feedback control law. In the limit of zero measurement noise on the accelerometer outputs and control surface deflections, state estimation

reduces to bandpass filtering of the outputs as was employed in the fixed-gain algorithm. The inclusion of a state estimator in the adaptive algorithm makes the feedback controller less susceptible to input process noise, input measurement noise and output measurement noise at the cost of an increase in the computational load.

4.1.2.1 Dynamic Model/Frequency Shaping Filters for State Estimation

The second-order model which approximates the dynamics of the RSRA helicopter around N/rev has been discussed in detail in the previous sections. The state estimation algorithm augments this model with the frequency shaping filter states as discussed in detail in Section 3.2.1. The parameters associated with these artificial states are calculated based on the frequency shaped filter requirements and are not parameters to be identified. These frequency shaping filters effectively penalize the bandwidth of interest in the cost functional in the LQR problem formulation, and can be thought of as simply providing dynamically compensated outputs for feedback control. Only that frequency which is dominant in the vibration spectrum is fed back through the controller so as not to excite any other vibration modes via helicopter nonlinearities.

The dominant frequency in the RSRA helicopter (simulation) vibration spectrum is N/rev and is nearly constant. Variations in angular velocity are expected only under severe, or rapid, control demands, possible regulator failure (a rotor speed regulator was included in the simulation), and random disturbances. The random disturbances are expected to be small, but important in the sense that the phase of the disturbance terms is altered. These observations formed the guidelines for the design of the frequency shaping filters.

The frequency shaping filters used in the control design have conflicting design requirements. Less control effort will be used in suppressing the N/rev vibration as the filter bandwidth is decreased. However, infinite Q (or zero bandwidth) filters are not desirable from the standpoint of either robustness or speed of response of the adaptive system. On the other hand, relatively large bandwidths (e.g. 5% of N/rev) excite modes which are outside the region of validity of the second-order model used, and consequently may not be controllable. Values of the damping coefficient from 0.1% to 0.5%

gave satisfactory response times while sufficiently suppressing frequencies other than N/rev.

In an attempt to employ a strategy similar to that used in the notch filter design (cf. Section 4.1.1.2), the capability to vary the damping coefficients as a function of time and controller performance was also implemented. A wider bandwidth is used during the transient region to improve the response time, followed by a period of decreasing bandwidth to improve the steady-state vibration suppression performance. Damping coefficients on the order of 0.5% were used during the transient region, exponentially decreasing to 0.05% after sufficient vibration suppression was achieved. This resulted in improvement in the steady-state performance, however it was not significant enough to warrant the increased computational load (improvement was on the order of 3dB over fixed damping coefficient filters).

Several other filter design issues were also addressed. Zero phase shift at N/rev effectively eliminated any estimator lags that the controller would have to compensate for with leads (differentiation). Care was taken in the digital mechanization to accurately determine the center frequency of the filters. Finally, normalization of the filter gain at the center frequency reduced round-off error propagation in the estimator and controller equations.

Based on the frequency shaping filter design requirements, a filter with a zero at the origin, unity gain at Ω, and complex pair of poles determined by the desired damping coefficient and a natural frequency of Ω was constructed. Assuming a measurement of the rotor angular velocity was available, the filters were continuously tuned to a center frequency of N/rev, tracking any variations in the rotor frequency. The bilinear transformation from continuous to discrete domain with prewarping was used, giving the desired digital filter. The critical frequency for prewarping was Ω.

In the continuous-time domain, the frequency shaping filters have the following Laplace transfer function;

$$H(s) = \frac{2\zeta\Omega s}{s^2 + 2\zeta\Omega s + \Omega^2}$$

The transformation to discrete-time domain first involves substitution of Ω with Ω_p, the prewarped critical frequency:

$$\Omega_p = \frac{2}{T} \tan(\frac{\Omega T}{2})$$

Then the Laplace variable s is replaced with;

$$s = \frac{2(z - 1)}{T(z + 1)}$$

where T is the sampling interval. Expanding the resulting numerator and denominator expressions results in the following discrete equivalent transfer function:

$$H(z) = \frac{b_0 z^2 + b_1 z + b_2}{a_0 z^2 + a_1 z + a_2} .$$

where

$$b_0 = \zeta \Omega_p T$$
$$b_1 = 0$$
$$b_2 = -b_0$$
$$a_0 = 1 + \zeta \Omega_p T + \frac{\Omega_p^2 T^2}{4}$$
$$a_1 = \Omega_p^2 T^2/2 - 2$$
$$a_2 = 1 - \zeta \Omega_p T + \frac{\Omega_p^2 T^2}{4}$$

Note that this transformation results in a filter with direct feedthrough since the numerator and denominator polynomials are of the same order. This results in a requirement to modify the standard control gain calculations as was discussed in Section 3.2. Realizing this transfer function in observer canonical state-space form gives the following second-order system for the frequency shaped filters:

$$x(k+1) = \begin{bmatrix} F_{fs11} & 1 \\ F_{fs21} & 0 \end{bmatrix} x(k) + \begin{bmatrix} G_{fs11} \\ G_{fs21} \end{bmatrix} y(k) ,$$

$$z(k) = [1\ 0]\ x(k) + D_{fs} y(k),$$

where
$$F_{fs11} = -a_1/a_0$$
$$F_{fs21} = -a_2/a_0$$
$$G_{fs11} = (b_1 - a_1 b_0/a_0)/a_0$$
$$G_{fs21} = (b_2 - a_2 b_0/a_0)/a_0$$
and
$$D_{fs} = b_0/a_0.$$

The output of the frequency shaped filters (z) is assumed with loss of generality to be the first state plus a direct feedthrough term. However, since the controller feeds back the states of the model only, the filter output need never be constructed. The effect of the direct feedthrough term is to modify the costs in the performance function for the controller design (cf. Section 3.2 and Appendix C).

4.1.2.2 Measurement Models for State Estimation

The accelerometer outputs can be modeled without loss of generality as the first of the two states in the second-order models for the input-output relationships in each axis. A direct feedthrough term is also estimated in the ARX form of the transfer function, but since significant cost is placed only on the frequency shaped filter states, the sole effect of the direct feedthrough term is to modify the elements in the augmented control distribution matrix G.

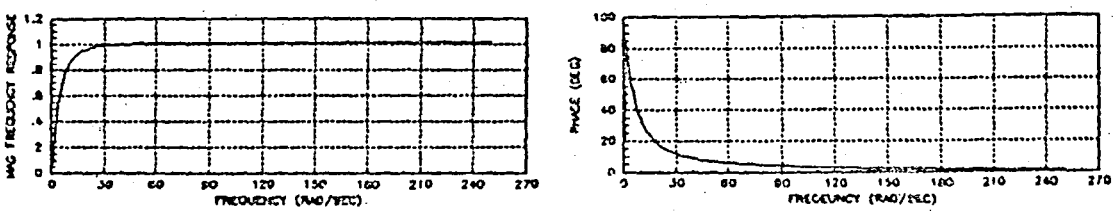

Figure 4-3. Frequency Response of Bias Rejection Filter

The issue of biases in the accelerometer outputs must be addressed. Biases can either be estimated (identified along with the other parameters in the model) so there effect can be removed, or more directly, removed from the measurements before entering the estimation and identification subsystem. Since the frequency range of interest for vibration control is well

above DC, a first-order lead-lag filter with a zero at DC and a pole at 1 Hz is sufficient. Transforming this filter into the discrete domain using the zero-order hold equivalence transformation gives the following discrete transfer function:

$$F(z) = \frac{z - 1}{z + 0.9752} ,$$

assuming a sample rate of 250 Hz. A frequency response plot of the bias rejection filter is shown in Figure 4-3.

4.1.2.3 Kalman Filtering for State Estimation

Having a set of three decoupled fourth-order systems (a second-order approximate dynamics model with a second-order frequency shaping filter) with parameters predetermined as well as identified in the parameter identification subsystem, state estimation is performed using a Kalman filter. The dynamical model of one of the fourth-order subsystems is given by:

$$x(k+1) = \begin{bmatrix} F_p & 0 \\ G_{fs}H_p & F_{fs} \end{bmatrix} x(k) + \begin{bmatrix} G_p \\ G_{fs}D_p \end{bmatrix} u(k) + w(k) ,$$

$$y(k) = [1\ 0\ 0\ 0]x(k) + D_p u(k) + v(k) ,$$

where the elements of the system matrices have been previously defined. Denoting by F the entire 12 by 12 system matrix, and by G the entire 12 by 3 control distribution matrix, the Kalman filter equations can be written:

$$\hat{x}(k+1|k) = F\hat{x}(k|k) + Gu(k) ,$$

$$\nu(k+1) = y(k+1) - H\hat{x}(k+1|k) ,$$

$$\hat{x}(k+1|k+1) = \hat{x}(k+1|k) + K(k+1)\nu(k+1) ,$$

$$P(k+1|k) = FP(k|k)F^T + Q(k) ,$$

$$R_\nu(k+1) = HP(k+1|k)H^T + R \ ,$$

$$K(k+1) = P(k+1|k)H^T R_\nu(k+1)^{-1} \ ,$$

$$P(k+1|k+1) = [I - K(k+1)H]P(k+1|k),$$

where $H = [1\ 0\ 0\ 0]$ is the measurement distribution matrix, R is the covariance of the measurement noise (v), and Q is the covariance matrix of the process noise (w). The process noise is included in the estimator to model the source of the periodic disturbances (the process noise is filtered through the bandpass filters) as well as to account for the approximate nature of the dynamical model. P is the covariance matrix of the state estimation error, and K is the Kalman gain matrix which corrects the state estimates ($\hat{x}$) based on the prediction error, or innovations (v).

To conclude this subsection on state estimation, a few algorithm implementation issues are addressed. The Kalman filter equations were implemented in square-root form to decrease storage requirements and computational load, as well as to ensure the positive definiteness of the covariance matrix. The details of the square-root formulation can be found in the references (cf. Bierman, [9]).

The filtered state estimates are the estimates actually passed to the controller for feedback control computation. If this estimator/controller combination is mechanized in a real-time environment, the control law computation by a flight computer will result in a delay in the control actuation. Further study to determine the effects of the delay on the stability of the controller will be required.

4.2 CONTROLLER SUBSYSTEM

4.2.1 Adaptive Controller Gain Calculation

The design of the controller subsystem utilizes basically the same linear quadratic regulator (LQR) design procedure discussed in detail in the previous section. The main difference is that the dynamical model of the

system is time-varying, thus requiring on-line gain computation. Also as discussed in the previous section, the standard LQR problem formulation must be modified to include the effects of a component of the inputs in the outputs. This modification is described in detail in Appendix C.

Using the dual formulation of the estimation problem discussed in the previous subsection, the same equations in square-root form can be used (with appropriate variable substitutions) to obtain the optimal time-varying controller gains. Basically, the measurement distribution matrix is replaced with the control distribution matrix, and the process and measurement noise covariance matrices are replaced with state and control cost matrices respectively. The appropriate substitutions can be found in the references (cf. Bryson and Ho, [8], Franklin and Powell, [9]). Using the time-varying 'optimal' gains gives the following control feedback law:

$$u(k) = C(k)x(k|k) \ ,$$

where $C(k)$ is the optimal Ricatti controller gain, the dual of the Kalman filter estimator gain $K(k)$, suitably modified to account for the direct feedthrough term as discussed in Appendix C.

4.2.2 Determination of State and Control Cost Matrices

The parameters which must be predetermined for control gain calculation other than the frequency shaping filter parameters are the state and control cost matrices. Following the heuristic rules of thumb proposed by Bryson and Ho, the control costs are set to the inverse of the square of the maximum RMS control authority desired.

$$1^\circ \text{ peak-to-peak deflection} \Rightarrow 0.707^\circ \text{ RMS} \Rightarrow \text{cost of } 2 \ (\text{deg}^{-2})$$

The state costs are similarly set to the inverse of the square of the maximum steady-state RMS vibration level acceptable. Cost is placed only on the frequency shaping filter output states to insure that the majority of the feedback control authority is at Ω.

In order to prevent transients in the controller, the state costs are time-varying as well. When the controller is first turned on, the initial Ricatti matrix (the dual to the state estimate error covariance matrix) is set nearly to zero and the state costs are set to zero. The costs are then exponentially increased to their final predetermined level. The exponential time constant was iteratively determined to give satisfactory transient controller performance, the primary objective being prevention of large control deflections from exciting the nonlinearities of the RSRA helicopter simulation. Since the Ricatti equation is nonlinear, the transient performance is a function of the magnitude of the state costs as well as their time dependence.

To summarize this discussion of the adaptive control design, a more detailed block diagram of the controller is given in Figure 4-4.

4.3 ADAPTIVE CONTROLLER TUNING AND SIMULATION RESULTS

The adaptive controller discussed in detail in this section was programmed and added to the GENHEL simulation of the RSRA helicopter. In this subsection, he results of simulations run at various operating conditions are presented. The initial conditions for the runs at each operating condition are the same as is the tuning of the various process noise covariance matrices and regulator cost matrices. Since these matrices represent in a stochastic sense the uncertainty in the dynamical model and relative costs of control and acceleration at N/rev respectively, they could easily be scheduled on dynamic pressure, rotor angular velocity, altitude, or some other appropriate parameter if further study showed that there is a corresponding change in the model uncertainty or control and state costs. However, no attempt to optimize the performance at each operating condition over the various weighting matrices (process noise and cost matrices) was made in the analysis presented here.

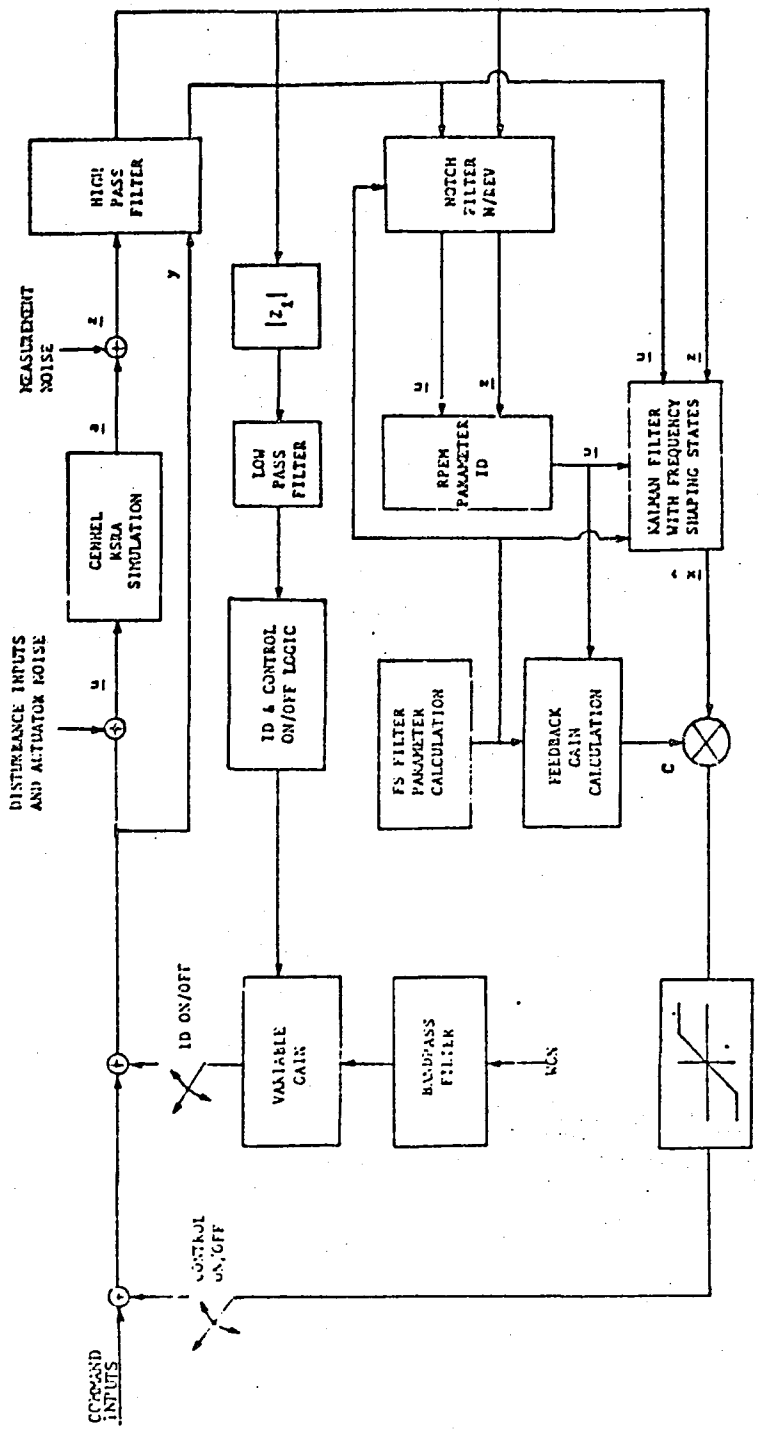

Figure 4-4. Detailed Block Diagram of the Adaptive Controller for the RSRA Helicopter

4.3.1 Initial Conditions and Algorithm Tuning

The initial conditions were the same for each of the runs at the various operating conditions. The initial parameters for the three decoupled oscillators which modeled the dynamics of the helicopter around N/rev were the same:

$$A_1 = 1.7 ,$$
$$A_2 = -0.9 .$$

Recall for a pair of discrete poles at $\rho e^{j\theta}$ and $\rho e^{-j\theta}$,

$$A_1 = 2\rho\cos\theta ,$$
$$A_2 = -\rho^2 .$$

Thus, these initial conditions represent stable poles (inside the unit circle) near Ω (at a sampling rate of 250 Hz) and lightly damped. The initial values of the entries in the control distribution matrices (B) are all zero. The initial covariance of these parameters is diagonal with a value of 10 for each parameter variance in the parameter identification algorithm. Moderate changes in the initial covariance do not affect the final results significantly for two reasons. First, after allowing the GENHEL simulation internal states one second to reach steady state, the identification algorithm is given another second to accumulate information before the controller is turned on. Secondly, process noise is included in the model which deweights the contributions of initial conditions as data are processed.

The initial values of all the states in the estimator are zero, and their corresponding covariance matrix is the identity matrix. Since the estimator is turned on even before the identification is enabled, and since process noise is included in the model for these states, large changes in the initial state covariance will not affect the final results significantly.

The process noise variances on the parameters and the states in the estimator were determined iteratively. At 40 knots and 1000 feet altitude, these variances were iteratively changed until satisfactory performance was

achieved. (As an aside, only two iterations were required, since excellent initial values could be calculated based on expected parameter variations over time. A priori information such as this can be used to schedule these variances in the future if desired.) The process noise variance associated with the parameters was required to allow the parameters to vary with time. The equivalent dynamical model for the parameters is:

$$\dot{\theta} = w$$

where w is white Gaussian noise of variance density corresponding to the discrete excitation noise variance (a factor of the sampling interval is involved). For the oscillator parameters (A_1,A_2), the variance used was 0.001, and for the remaining parameters (B), the variance was 0.01. The variance of the oscillator parameters is unitless, while that of the parameters in the control distribution matrices is in units of degrees squared. (The continuous variance density would have units degrees squared per second.)

The process noise variance used for the estimator states was the identity matrix. This value, though somewhat arbitrary, is reasonable based on the fact that the states in the estimator are in effect normalized so that their magnitudes remain near unity. Though the magnitude of the process noise variance is important in determining the covariance of the state estimation error, its value relative to the measurement noise variance is the key factor in determining the optimal Kalman estimator gains. A value of 0.01 ft/sec^2 for the standard deviation of the accelerometer noise was used for the results presented in this report in which measurement and process noise were absent. In cases where measurement noise was added, an appropriate measurement noise sigma was used in the estimation algorithm.

The cost matrices for the regulator gain calculations were also determined iteratively. Initial values were calculated by the Bryson method mentioned earlier, and fine tuning to obtain acceptable performance was performed at 40 knots and 1000 feet altitude. The final values for the state and control costs used for the results presented herein are 5 for the states representing the frequency shaping filter outputs, zero for the remaining states, and a cost of 2 on all three controls; A_{1s}, B_{1s}, and θ_c.

As mentioned earlier, the controller is turned on after two seconds to allow transients in the GENHEL simulation and the estimation and identification algorithms to settle. The rate at which the control gains approach their steady-state values (assuming for the moment that the parameter variations are insignificant) is determined by two factors; the initial value of the Ricatti matrix (the control dual to the state estimate error covariance matrix), and the time history of the state and control cost matrices. The Ricatti matrix is initialized to an extremely small factor times the identity matrix. This results in essentially zero initial control gains (yet avoids numerical difficulties which would arise if zero were input instead!), a desirable feature in preventing possible transients. The exponential growth of the state costs from zero to their final fixed value also helps prevent undesirable transients in the control demand. The time constant of this exponential growth is approximately two seconds for the results presented in this report.

It should be emphasized that these intial parameter values are required for the most part to overcome the phenomenon of algorithm start-up, not helicopter start-up. Once the RSRA helicopter and the adaptive controller are past the initial transients, if the algorithm is properly tuned, it will track the system variations and should not require reinitialization. However, should it become necessary to reinitialize the algorithm as the result of a detected instability, the same initialization procedure is engaged.

As discussed in the previous subsection, once the algorithm has achieved an acceptable steady-state performance as determined by a cumulative acceleration magnitude threshold, the parameter identification algorithm is disabled in order to alleviate the need to add noise to the control inputs (for identifiability) and to reduce the computation load. The performance is continually monitored, however, and should it degrade past a second cumulative acceleration threshold, the identification algorithm is re-enabled. When the identification algorithm is re-engaged, the parameter covariance is augmented by adding 0.1 to all the diagonal elements. Since the models of parameter dynamics include process noise, this increase in the covariance serves merely to speed up the adaptation time constant. The overall tracking performance is still determined by the process noise variance, not by the initial parameter covariance.

4.3.2 Adaptive Controller Simulation Results

This subsection presents graphically the results of the adaptively controlled GENHEL simulation runs of the RSRA helicopter at various flight conditions. The plots of accelerometer outputs are the outputs of the GENHEL simulation program, filtered through a high-pass filter as discussed in section 4.1.2.2 to remove any low frequency components. Removal of most of the rigid body accelerations yields plots which are conveniently nearly zero-mean. Also, unless otherwise indicated, the plots of control surface deflections are plots of the feedback correction components only, and do not include any non-zero set point commands from a stability augmentation sys . (SAS) or the trim conditions. Thus, the plots of control deflections are also nearly zero-mean.

The time histories plotted clearly manifest the controller time constants as envelopes of the N/rev modulation and its harmonics. Also, as discussed previously, the first one second of output is unsuppressed vibration of the RSRA helicopter. Thus, the first second of the accelerometer outputs gives an indication of the unforced vibration levels (at the pilot location) for each flight condition. Furthermore, during the second one-second interval of the output time histories, the effect of the additive noise can be seen by comparing the vibration levels during the first and second one-second intervals. The control deflections during the second one-second interval indicate the amplitude of the additive excitation clearly.

The RSS acceleration output presented in each figure is the root-sum-square of the three orthogonal accelerometer outputs shown. Low frequency rigid body acceleration has been filtered out, so the RSS acceleration is a direct measure of the total vibration power at the pilot location.

Figures 4-5 through 4-9 give selected results of the adaptive controller for velocities of 5 knots, 40 knots, and 120 knots at an altitude of 100 feet. Plots of the time histories of selected parameters and their associated estimate error sigmas for the 40 knot/100 feet altitude flight condition are included as well. The notation used for the labeling of the ordinates in the parameter time histories indicates the input-output pair (eg. AZ/B1S) in the case of control distribution parameters (B0,B1), and the output only (eg. AZ) in the case of the dynamic model parameters (A^1,A2).

Table 4-1 gives the correlation matrices for the three decoupled MISO parameter covariance matrices for the 40 knots/100 feet flight condition. The correlation between the A_1 and A_2 terms in each axis is approximately -0.9 as is the correlation between the B_0 and B_1 terms in each of the input-output pairs (cf. [3,6], [4,7], and [5,8] elements of the correlation matrices). This is a consequence of the strong identifiability of the input-output amplitude ratio, and the comparatively weak identifiability of the relative phase at Ω.

Figures 4-10 through 4-12 present selected results of the adaptive controller at 5 knots, 40 knots, and 120 knots at 1000 feet. Power spectra of the controlled and uncontrolled steady-state vibrations in each axis at 120 knots and 1000 feet altitude are shown in Figure 4-13. These spectra indicate the the vibration at Ω has been suppressed to levels below the contribution of the higher harmonics and indicates the adaptive controller is performing as expected. Figures 4-14 through 4-17 present the results of the adaptive controller for a speed of 120 knots and altitudes of 2000, 5000 and 7000 feet.

The results in figures 4-5 through 4-17 indicate that from the same algorithm initial conditions, the adaptive controller converges at each flight condition, yielding excellent performance in terms of RSS vibration suppression and control effort expended. To investigate the performance of the adaptive controller under changing flight conditions, two cases were run. Figures 4-18 through 4-20 show the results for a case in which the Ω (N/rev) was changed abruptly by decreasing it 10 rad/sec in 0.2 seconds, held constant for the next 1.8 seconds, and then returned to its original value linearly over the next 4 seconds. The objective of this test was to investigate the ability of the adaptive algorithm to track variations in rotor angular velocity and resulting changes in the helicopter dynamics.

The objective of the second case was to investigate the performance of the adaptive algorithm during a transition from one flight condition to another. The initial flight condition used for this test was 80 knots at 1000 feet. Control commands were given to increase the velocity to 125 knots. Figures 4-21 through 4-23 present selected results for this case, including plots of trajectory parameters.

Table 4-1. IDENTIFIED PARAMETER CORRELATION MATRICES FOR ADAPTIVE CONTROL AT 40 KNOTS/100 FT

X-axis Parameter Correlation Matrix

A1	A2	B1S/B0	A1S/B0	COL/B0	B1S/B1	A1S/B1	COL/B1
1.0000	-0.9235	-0.2132	-0.4823	0.1084	0.0582	0.0123	-0.2859
-0.9235	1.0000	0.2791	0.3187	0.0282	-0.2012	-0.0820	0.1834
-0.2132	0.2791	1.0000	0.2044	-0.2674	-0.0586	-0.3906	0.0157
-0.4823	0.3187	0.2044	1.0000	-0.1681	-0.0423	-0.0844	0.1427
0.1084	0.0282	-0.2674	-0.1681	1.0000	0.4589	0.2021	-0.0837
0.0582	-0.2012	-0.0586	-0.0423	0.4589	1.0000	0.1949	-0.2577
0.0123	-0.0820	-0.3906	-0.0844	0.2021	0.1949	1.0000	-0.2333
-0.2859	0.1834	0.0157	0.1427	-0.0837	-0.2577	-0.2333	1.0000

Y-axis Parameter Correlation Matrix

A1	A2	B1S/B0	A1S/B0	COL/B0	B1S/B1	A1S/B1	COL/B1
1.0000	-0.0870	-0.0405	0.1327	-0.3089	-0.0681	0.0703	0.1414
-0.0870	1.0000	0.0289	-0.2506	0.3359	-0.0404	0.1437	-0.3045
-0.0405	0.0289	1.0000	0.1707	-0.2657	-0.0360	-0.2089	-0.0394
0.1327	-0.2506	0.1707	1.0000	-0.1105	-0.0252	-0.0731	0.0339
-0.3089	0.3359	-0.2657	-0.1105	1.0000	0.5403	0.1905	-0.0827
-0.0681	-0.0404	-0.0360	-0.0252	0.5403	1.0000	0.1702	-0.2726
0.0703	0.1437	-0.2089	-0.0731	0.1905	0.1702	1.0000	-0.1592
0.1414	-0.3045	-0.0394	0.0339	-0.0827	-0.2726	-0.1592	1.0000

Z-axis Parameter Correlation Matrix

A1	A2	B1S/B0	A1S/B0	COL/B0	B1S/B1	A1S/B1	COL/B1
1.0000	-0.0722	-0.2776	0.0826	-0.1309	0.2490	-0.2072	-0.0827
-0.0722	1.0000	0.2229	0.0400	0.2625	-0.2952	0.0825	-0.1102
-0.2776	0.2229	1.0000	0.1710	-0.2952	-0.0859	-0.1093	0.0334
0.0826	0.0400	0.1710	1.0000	0.0559	-0.1467	-0.0766	-0.1010
-0.1309	0.2625	-0.2952	0.0559	1.0000	0.4811	0.0949	-0.0902
0.2490	-0.2952	-0.0859	-0.1467	0.4811	1.0000	0.1967	-0.2734
-0.2072	0.0825	-0.1093	-0.0766	0.0949	0.1967	1.0000	0.0436
-0.0827	-0.1102	0.0334	-0.1010	-0.0902	-0.2734	0.0436	1.0000

Finally, to investigate the effects of process and measurement noise on the algorithm performance, two cases were run. The first case included white Gaussian noise (WGN) with a sigma of 0.1 (ft/sec^2) on the outputs only. The results are shown in Figure 4-24. Little performance degradation was noted, so the sigma was increased to 0.25 (ft/sec^2) and process noise with sigma 0.1° was added to the control feedback commands. The results of this test are shown in Figures 4-25 and 4-26. The 'measured' outputs on the right in Figure 4-25 contain the measurement noise, while the outputs on the left are the actual vibrations prior to the addition of the measurement noise. Similarly, in Figure 4-26, the control time histories on the left are the feedback commands, and those on the right are the controls actually applied to the simulation, i.e. with the process noise added.

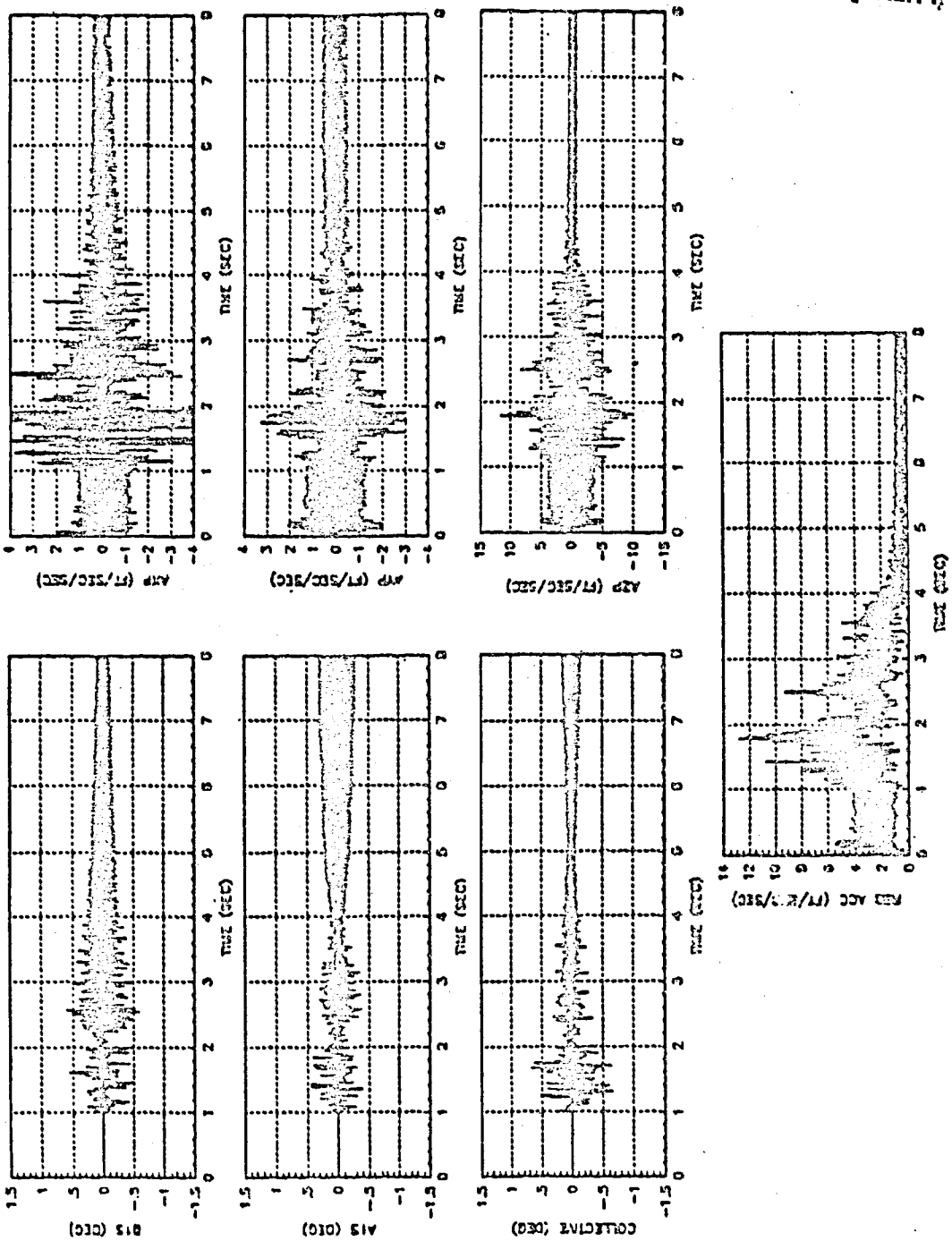

Figure 4-5. Control Inputs and Accelerometer Outputs for Adaptive Control at 5 kts/100 ft.

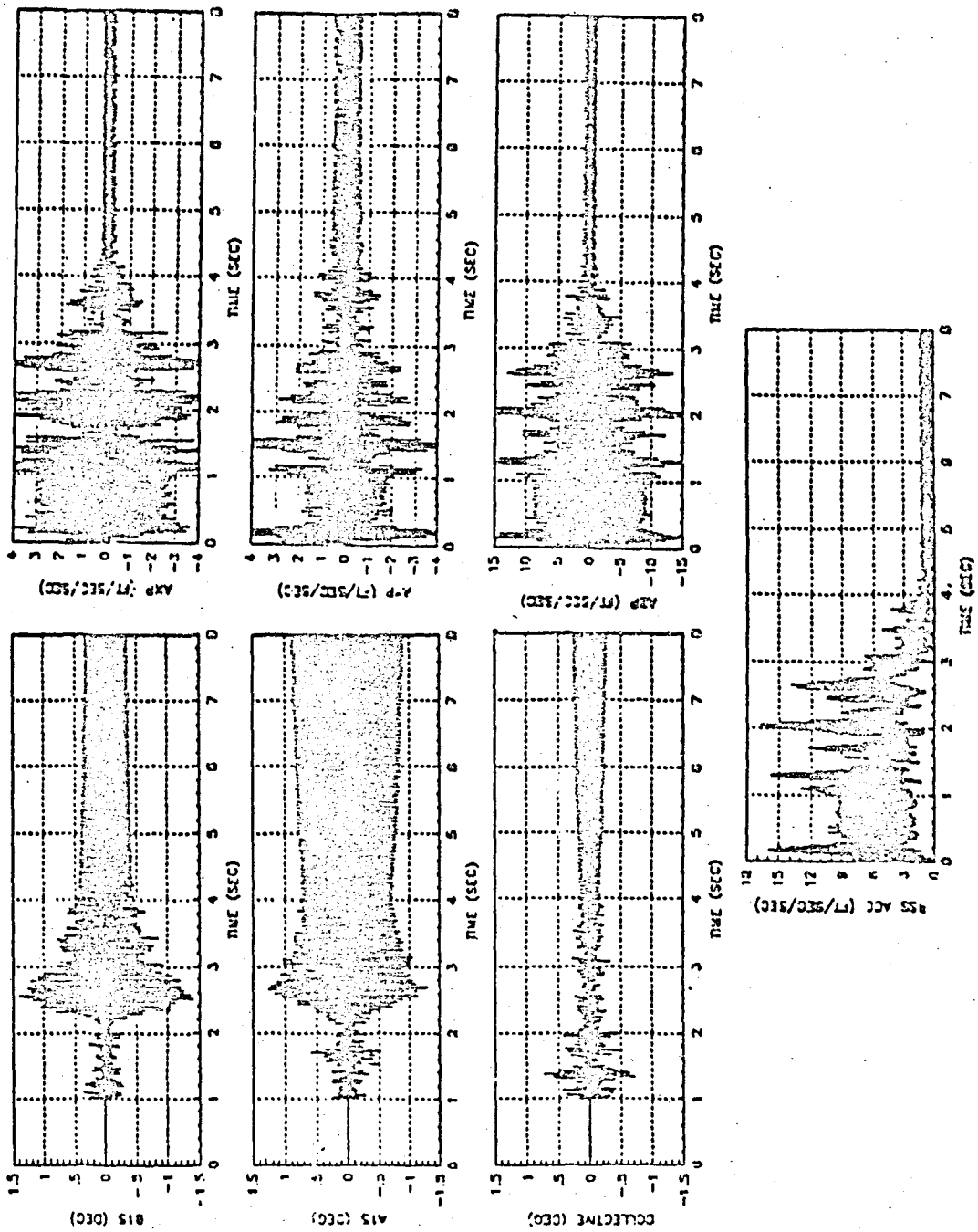

Figure 4-6. Control Inputs and Accelerometer Outputs for Adaptive Control at 40 kts/100 ft.

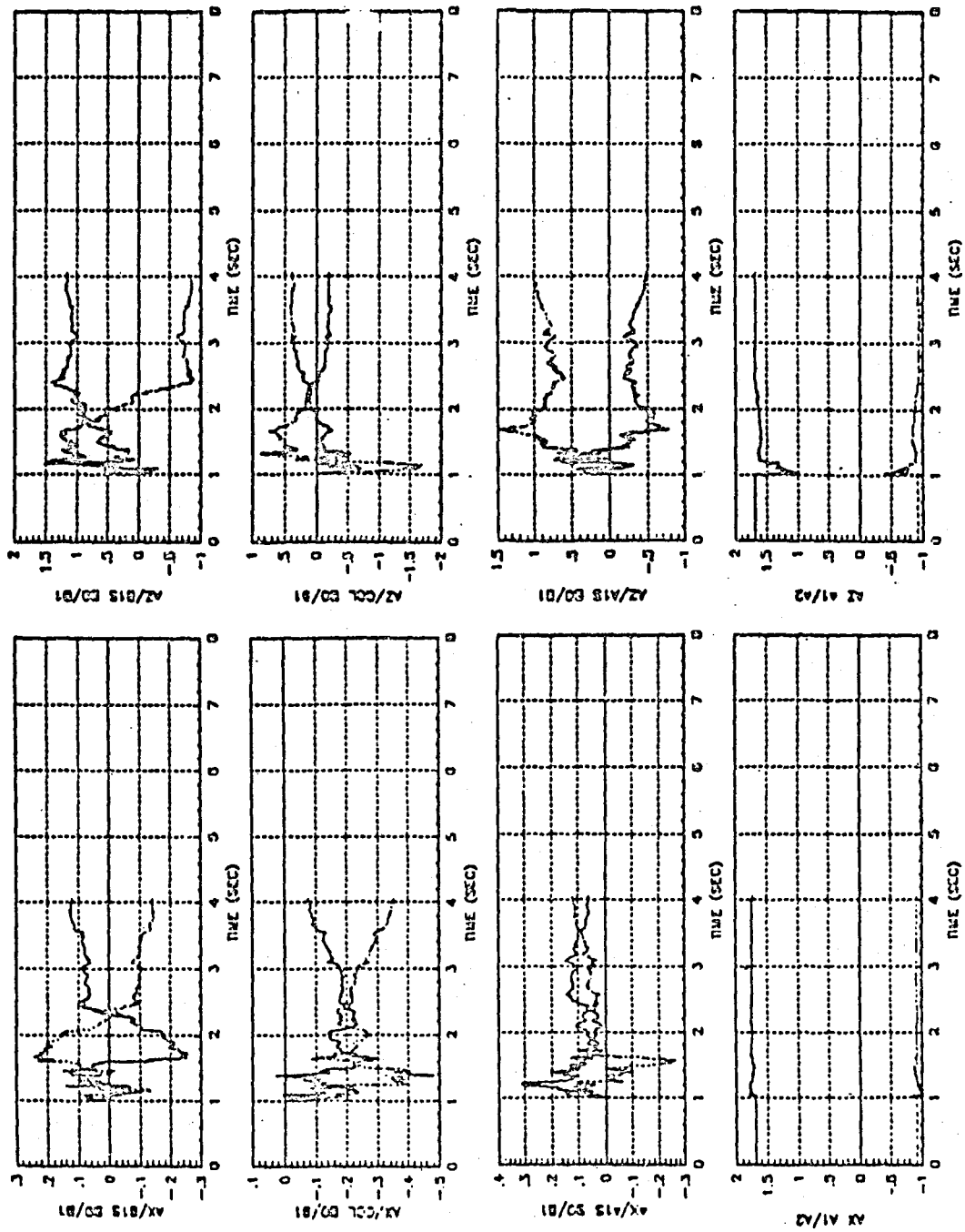

Figure 4-7. Selected Parameter Estimate Time Histories for Adaptive Control at 40 kts/100 ft.

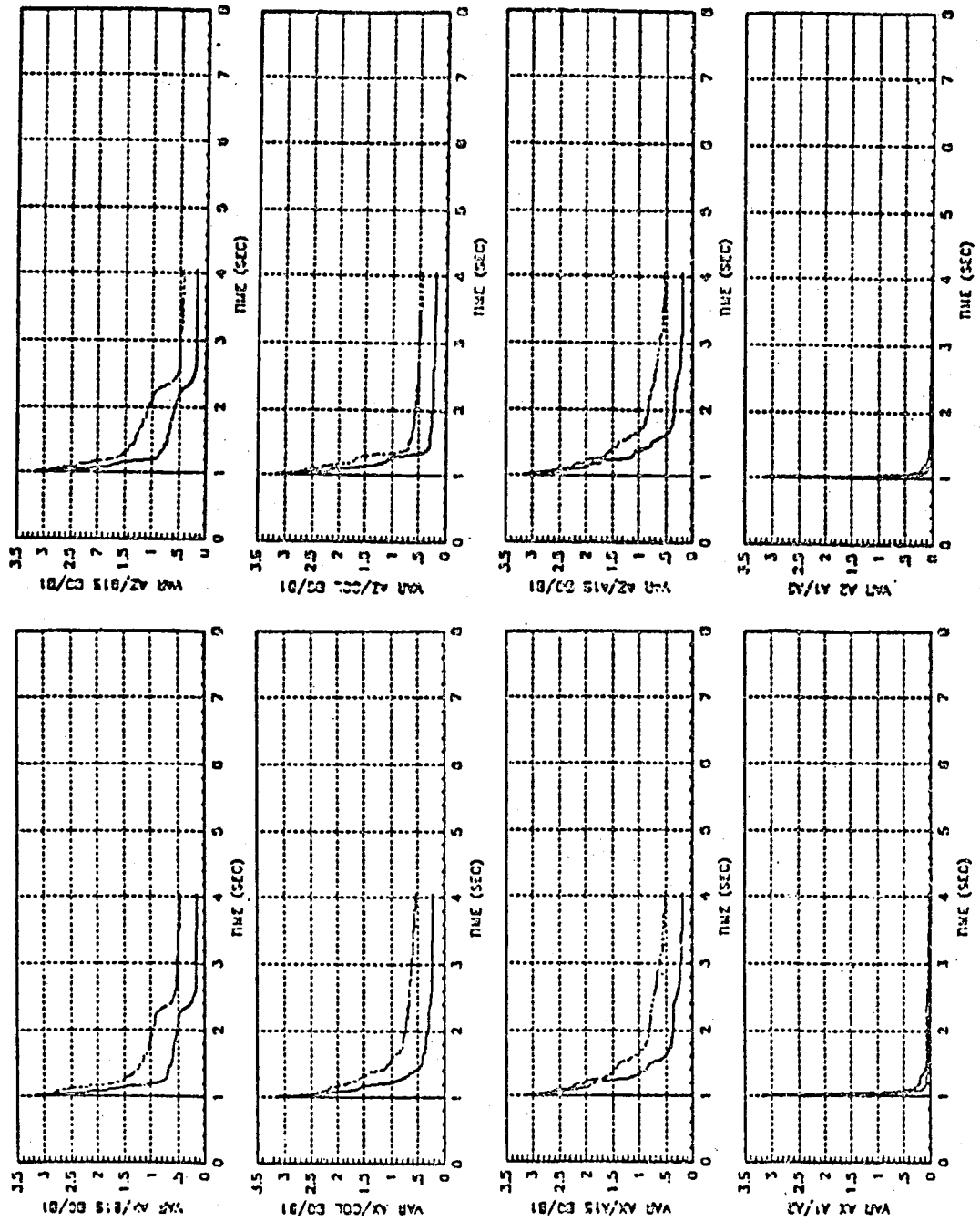

Figure 4-8. Selected Parameter Estimate Variance Time Histories for Adaptive Control at 40 kts/100 ft.

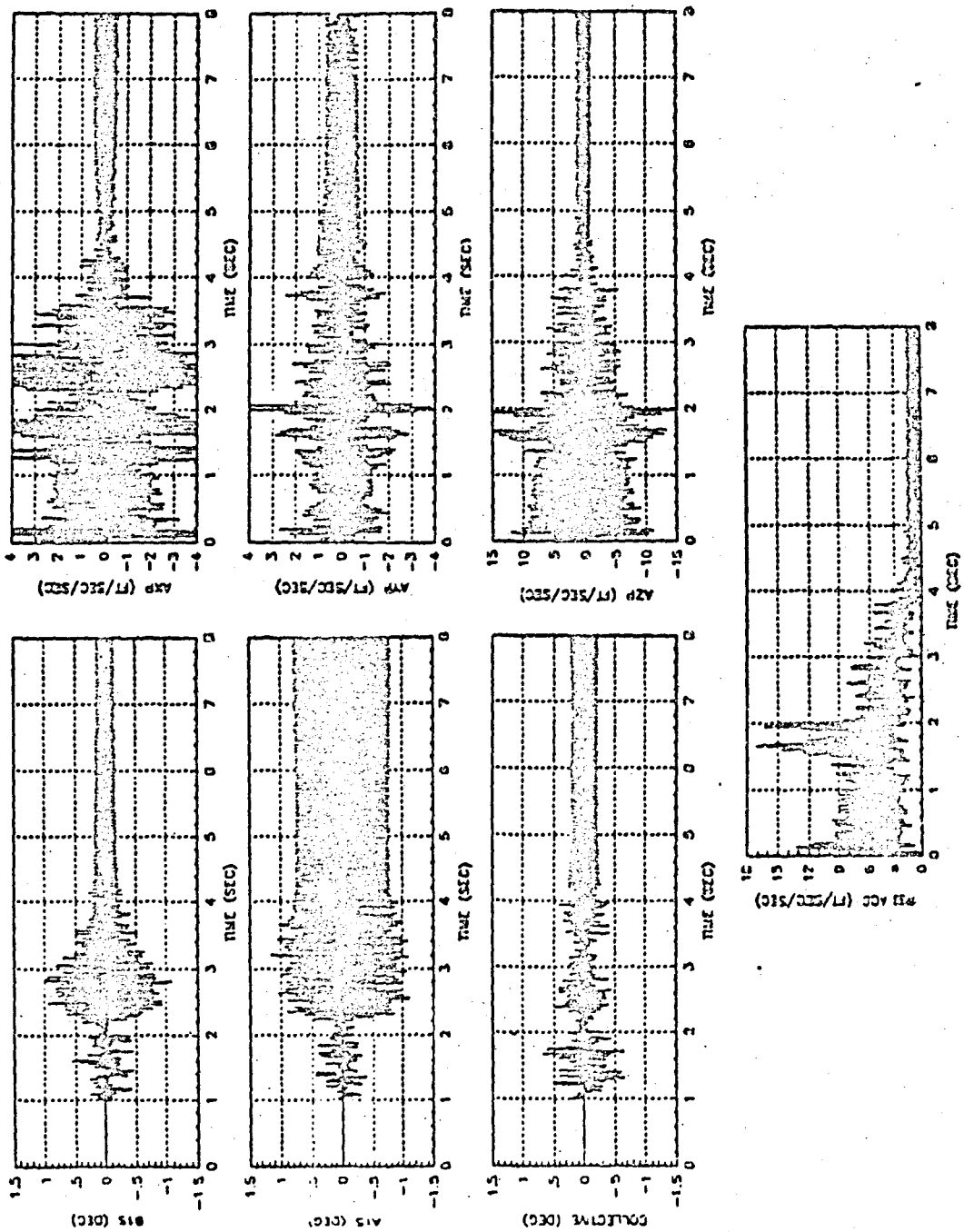

Figure 4-9. Control Inputs and Accelerometer Outputs for Adaptive Control at 120 kts/100ft.

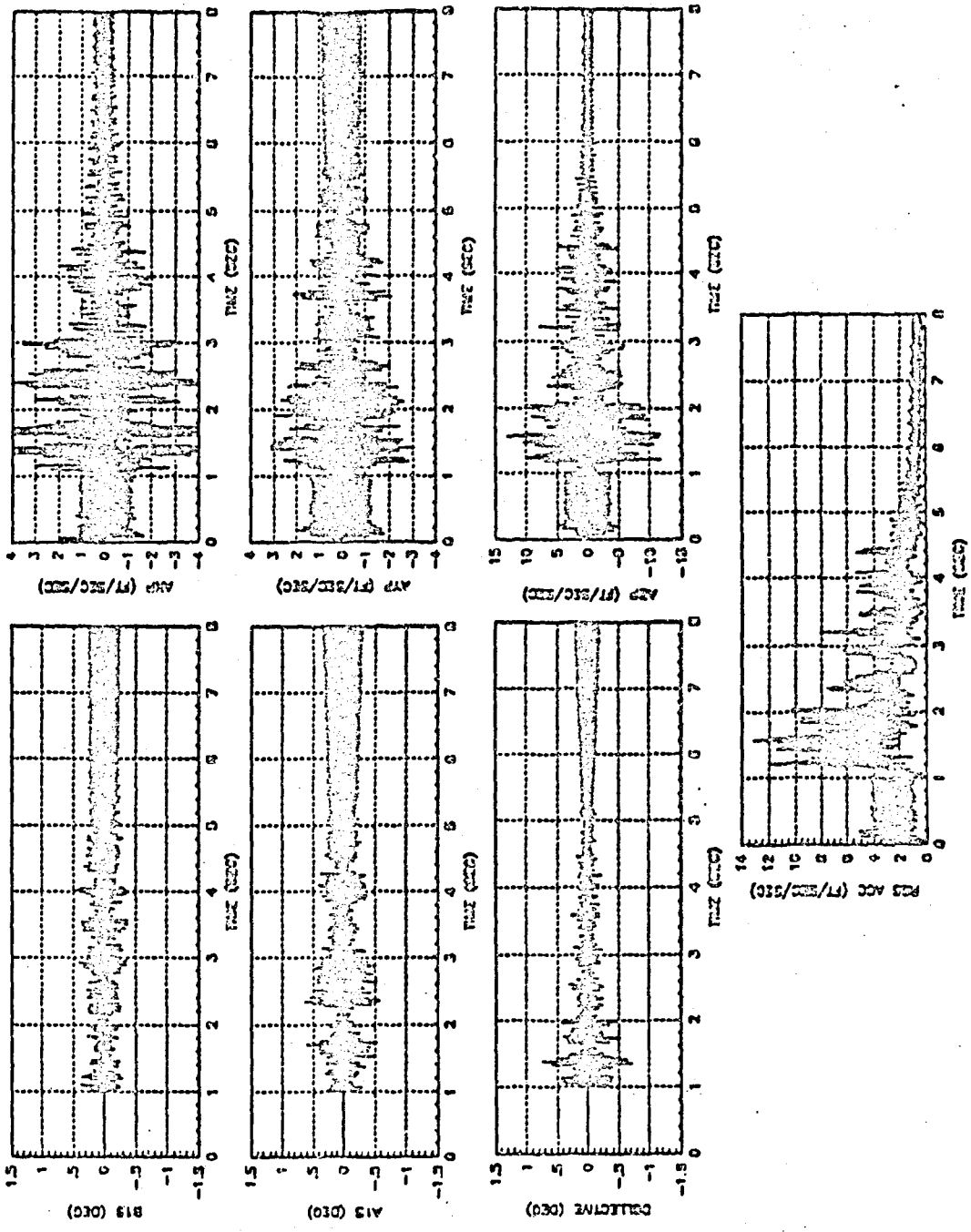

Figure 4-10. Control Inputs and Accelerometer Outputs for Adaptive Control at 5 kts/1000 ft.

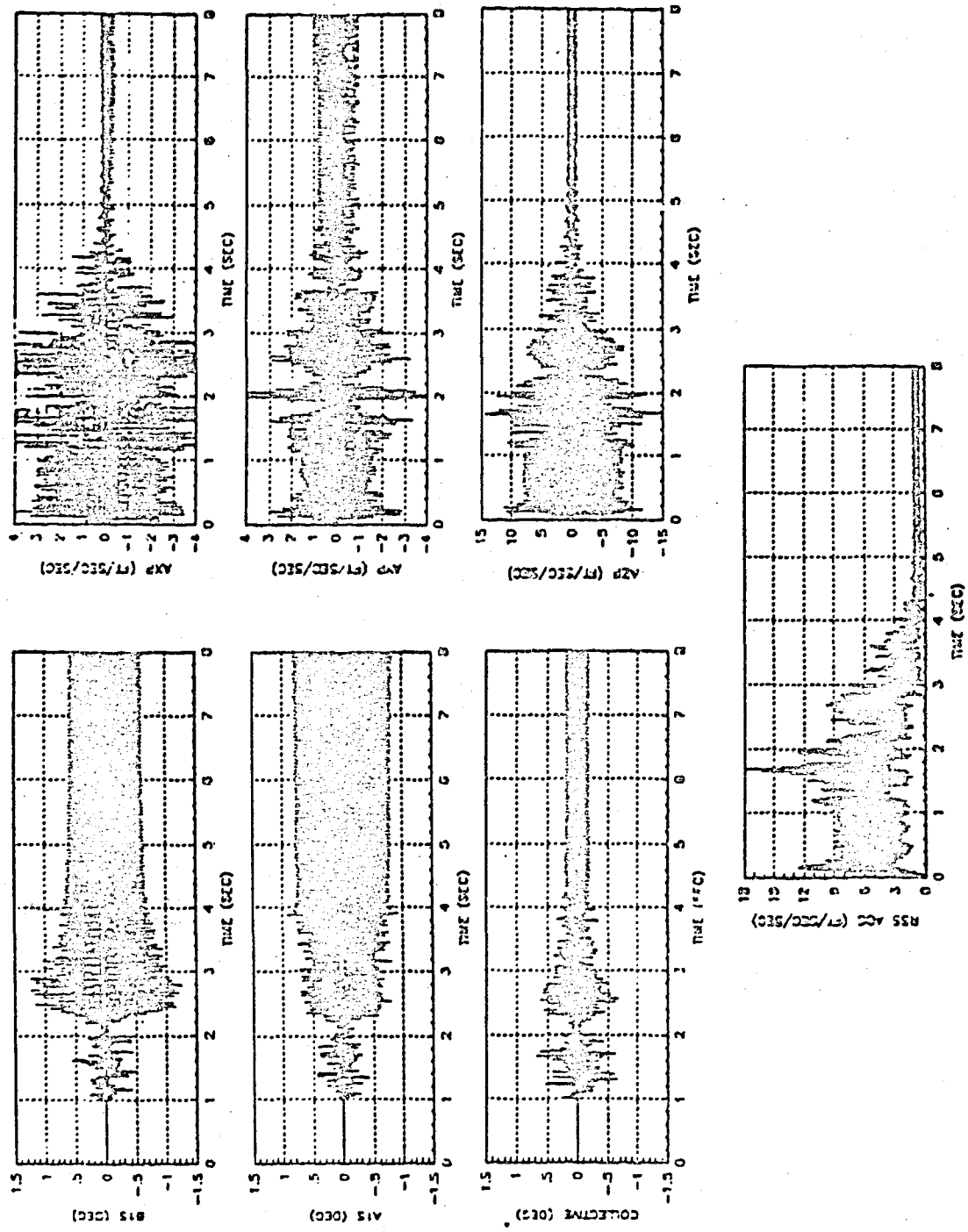

Figure 4-11. Control Inputs and Accelerometer Outputs for Adaptive Control at 40 kts/1000 ft.

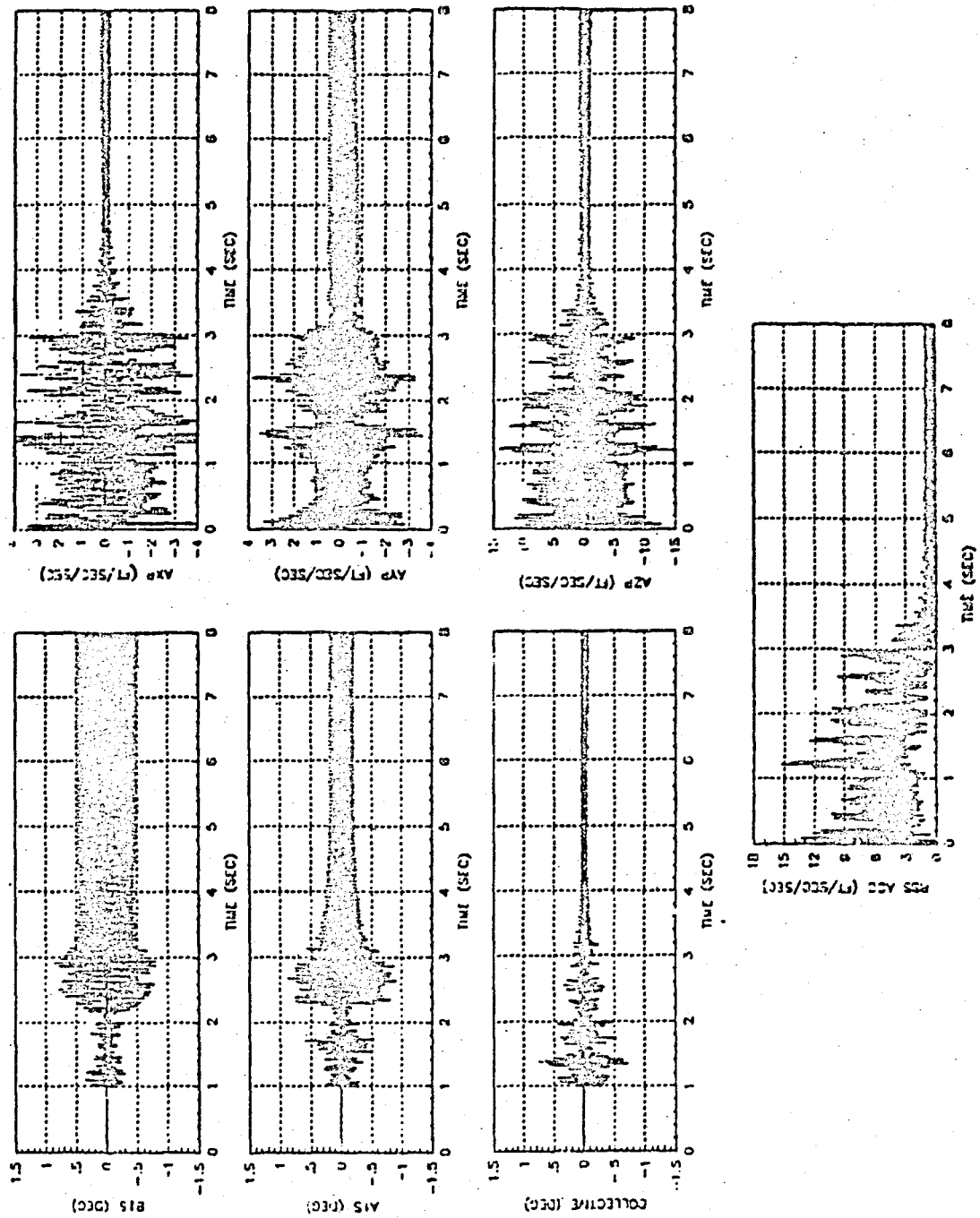

Figure 4-12. Control Inputs and Accelerometer Outputs for Adaptive Control at 120 kts/1000ft.

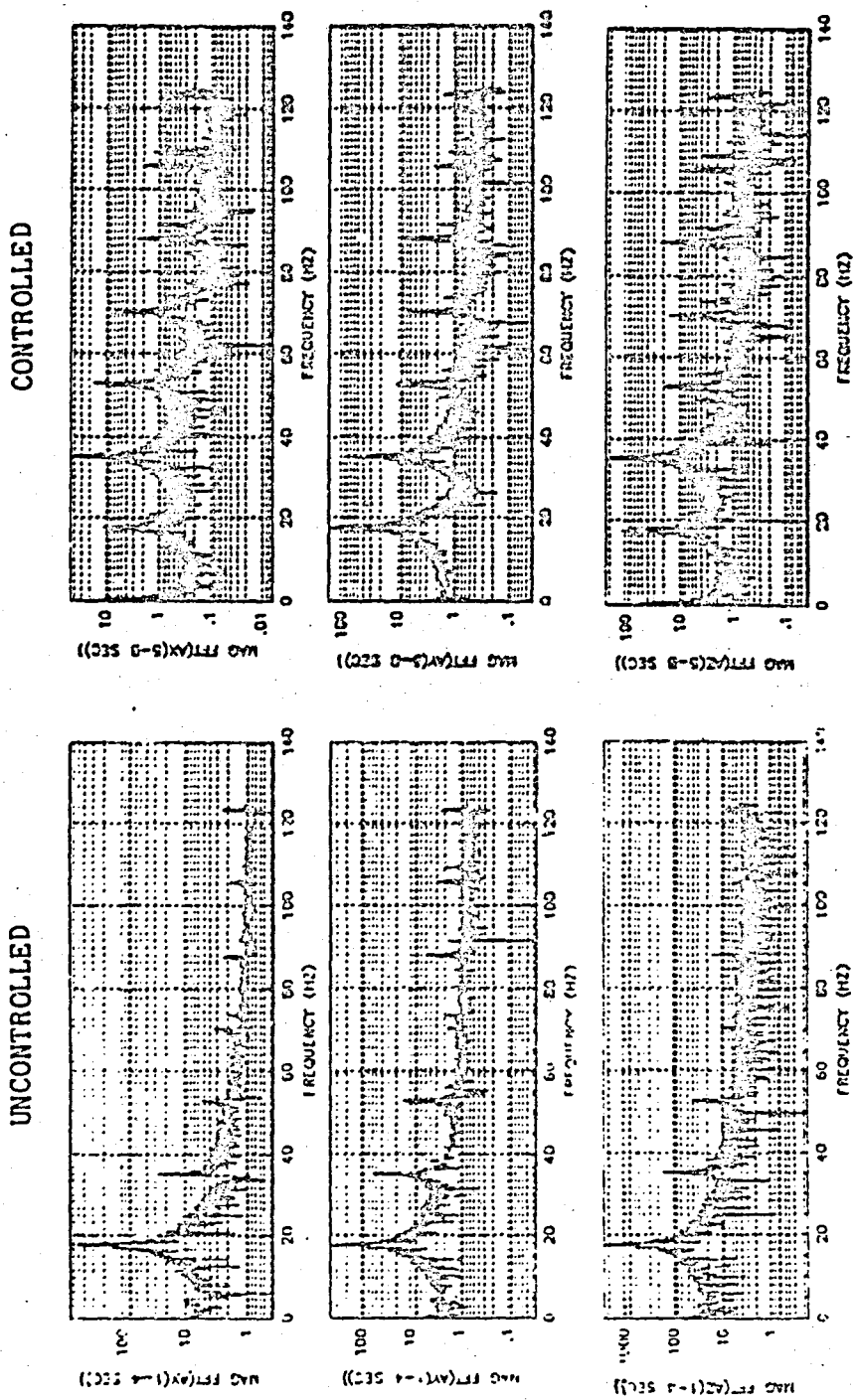

Figure 4-13. Power Spectra of the Steady-State Uncontrolled and Adaptively Controlled Accelerometer Outputs at 120 kts/1000 ft.

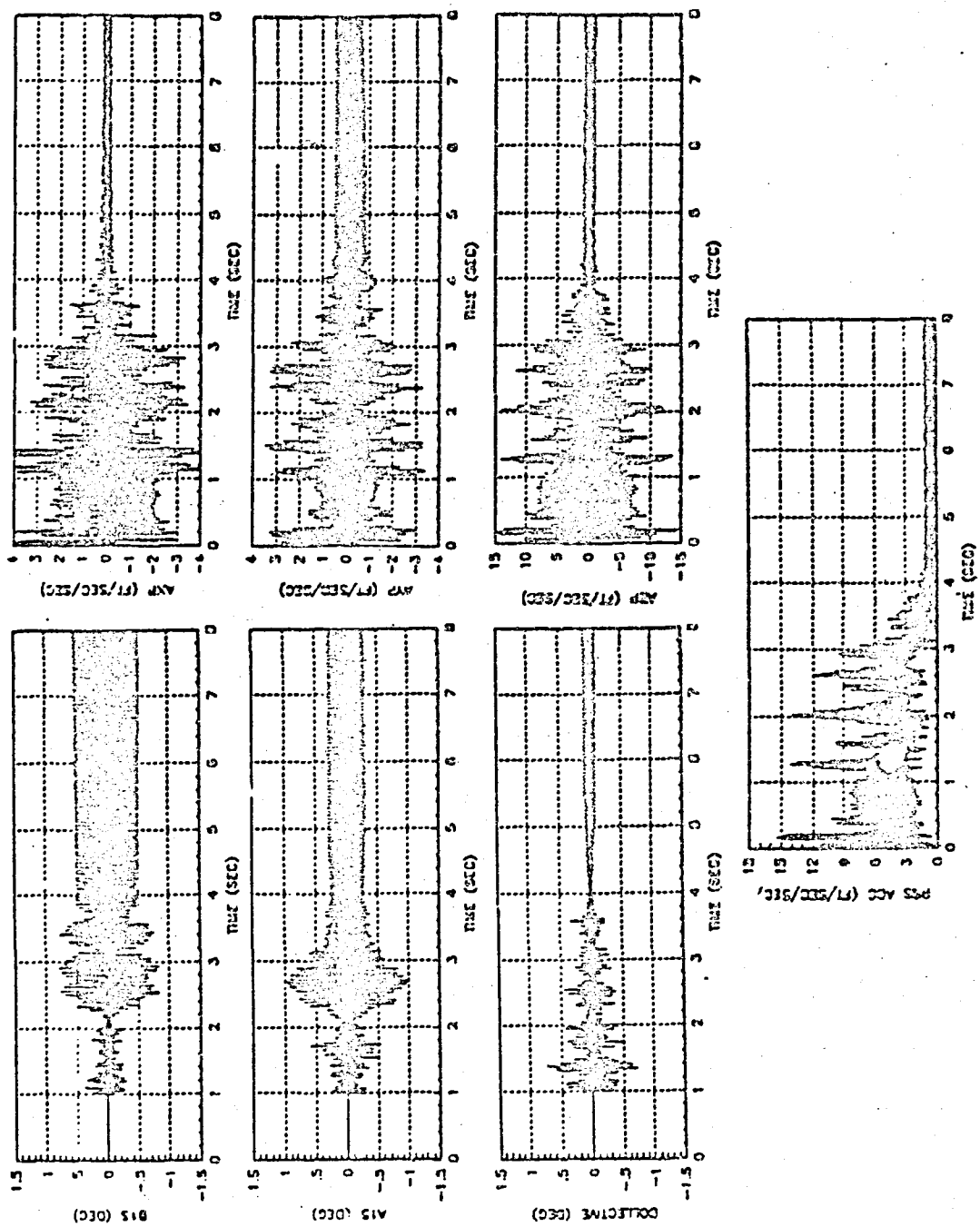

Figure 4-14. Control Inputs and Accelerometer Outputs for Adaptive Control at 120 kts/2000 ft.

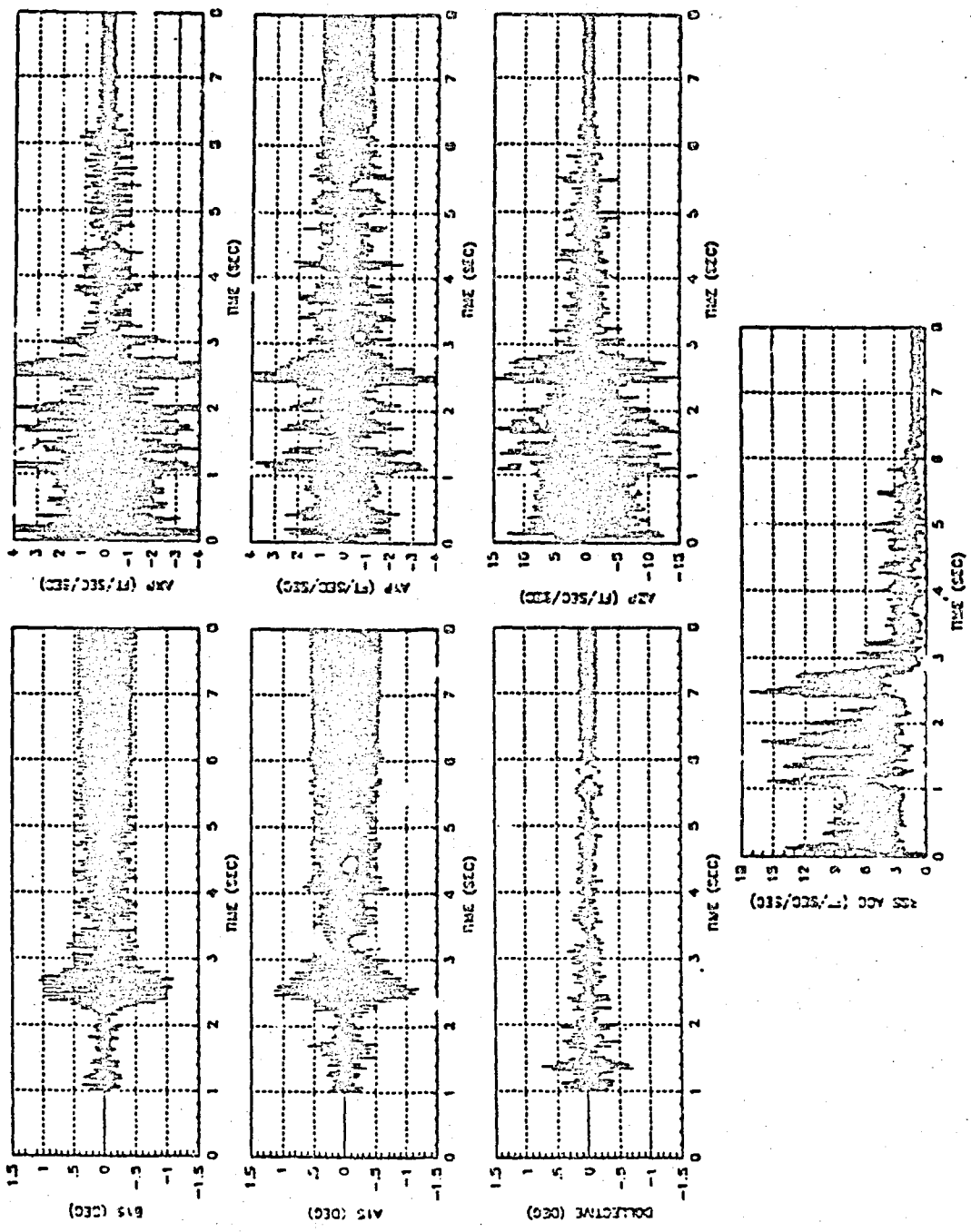

Figure 4-15. Control Inputs and Accelerometer Outputs for Adaptive Control at 120 knots/5000 ft.

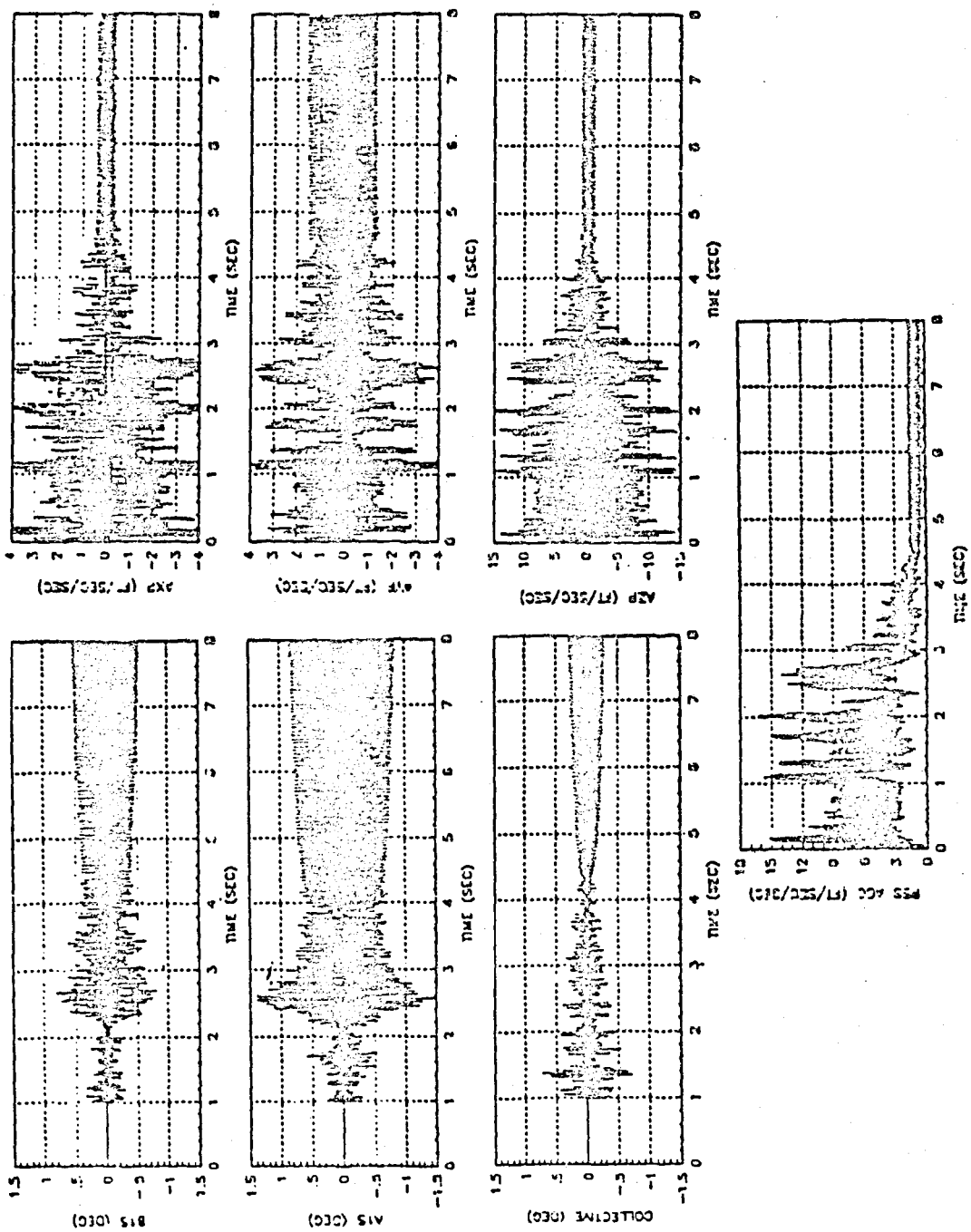

Figure 4-16. Control Inputs and Accelerometer Outputs for Adaptive Control at 120 knots/7000 ft.

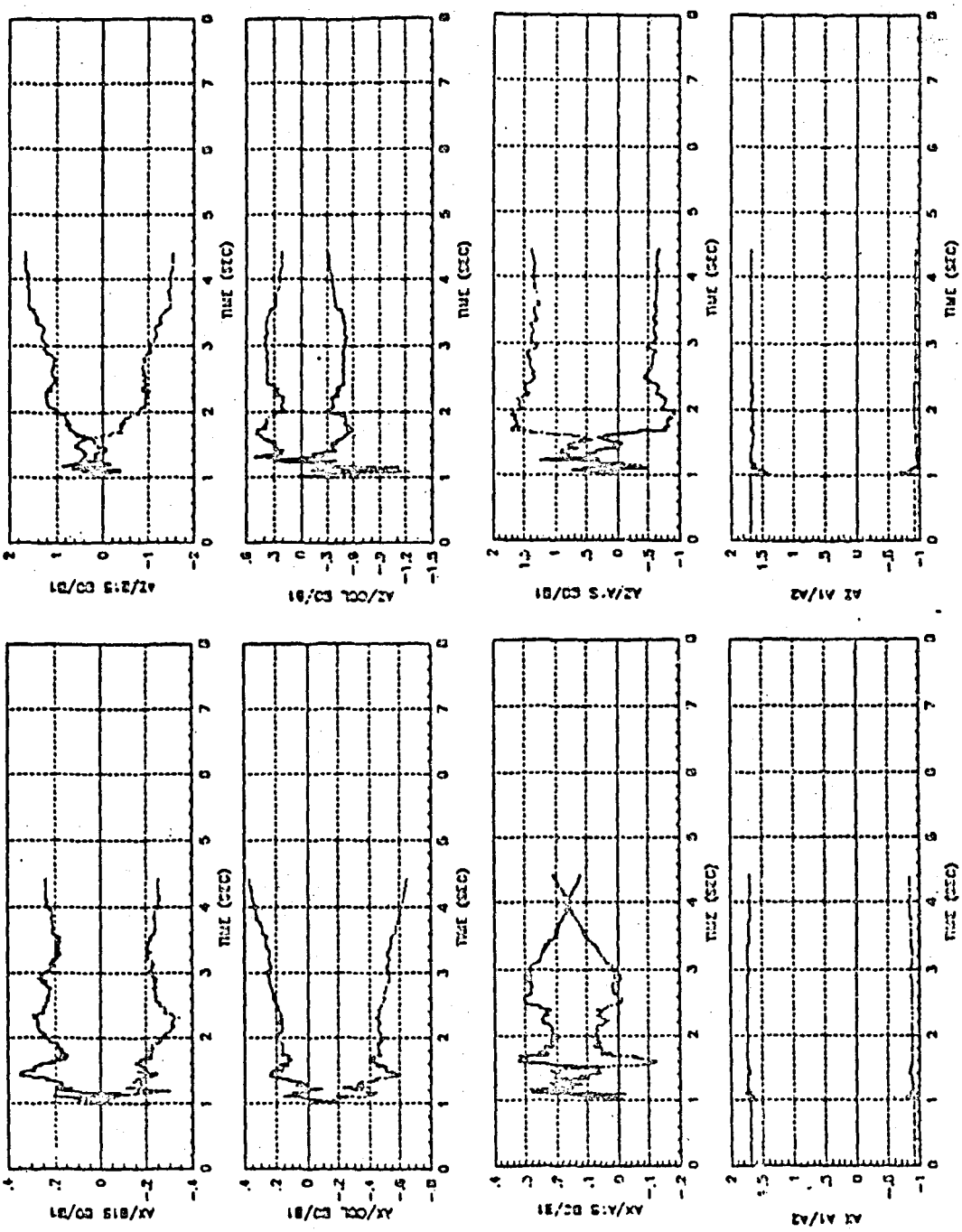

Figure 4-17. Selected Parameter Estimate Time Histories for Adaptive Control at 120 knots/7000 ft.

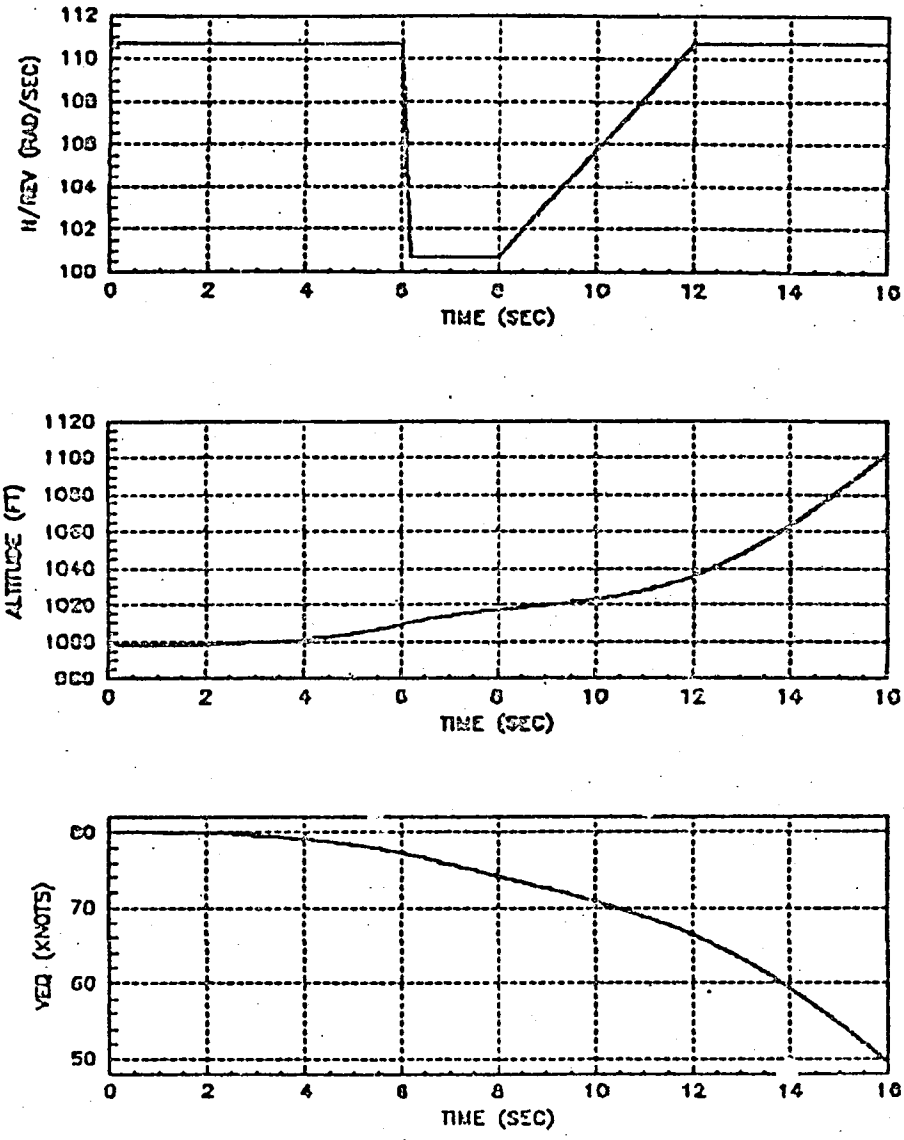

Figure 4-18. Selected Trajectory Parameter Time Histories for Adaptive Control at 80 kts/1000 ft with Time-varying Rotor Angular Velocity

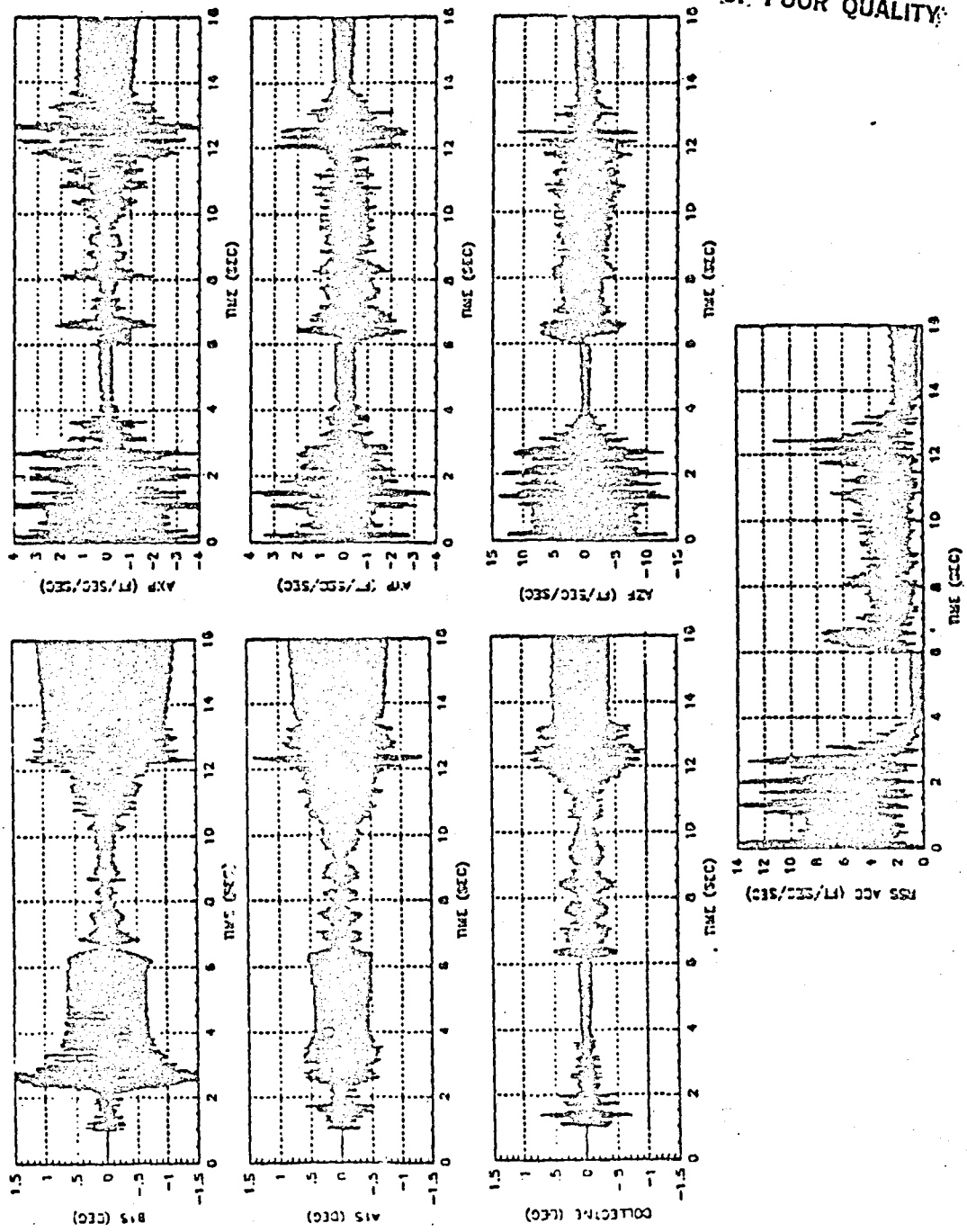

Figure 4-19. Control Inputs and Accelerometer Outputs for Adaptive Control at 80 kts/1000 ft with Time-varying Rotor Angular Velocity

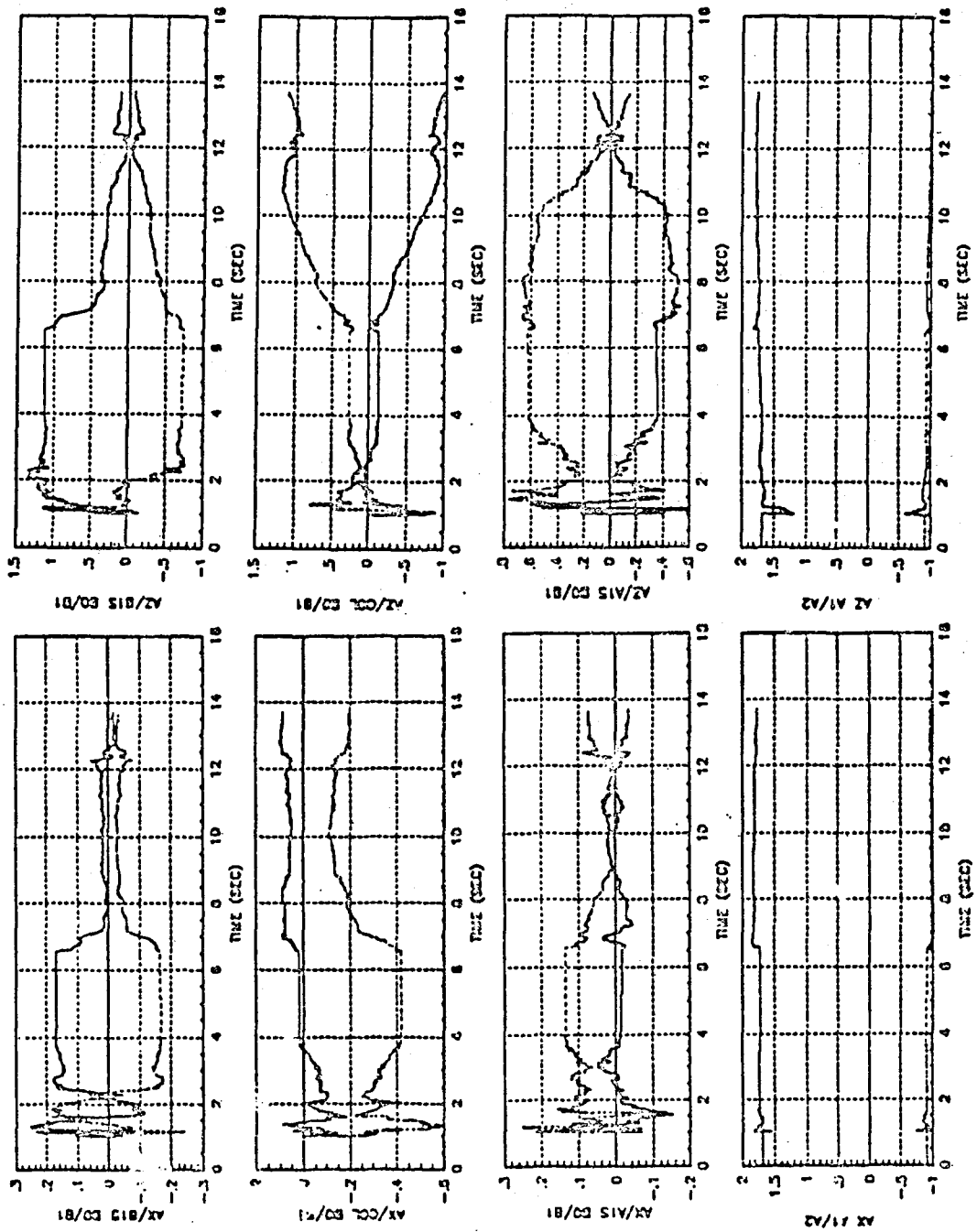

Figure 4-20. Selected Parameter Estimate Time Histories for Adaptive Control at 80 kts/1000 ft with Time-varying Rotor Angular Velocity

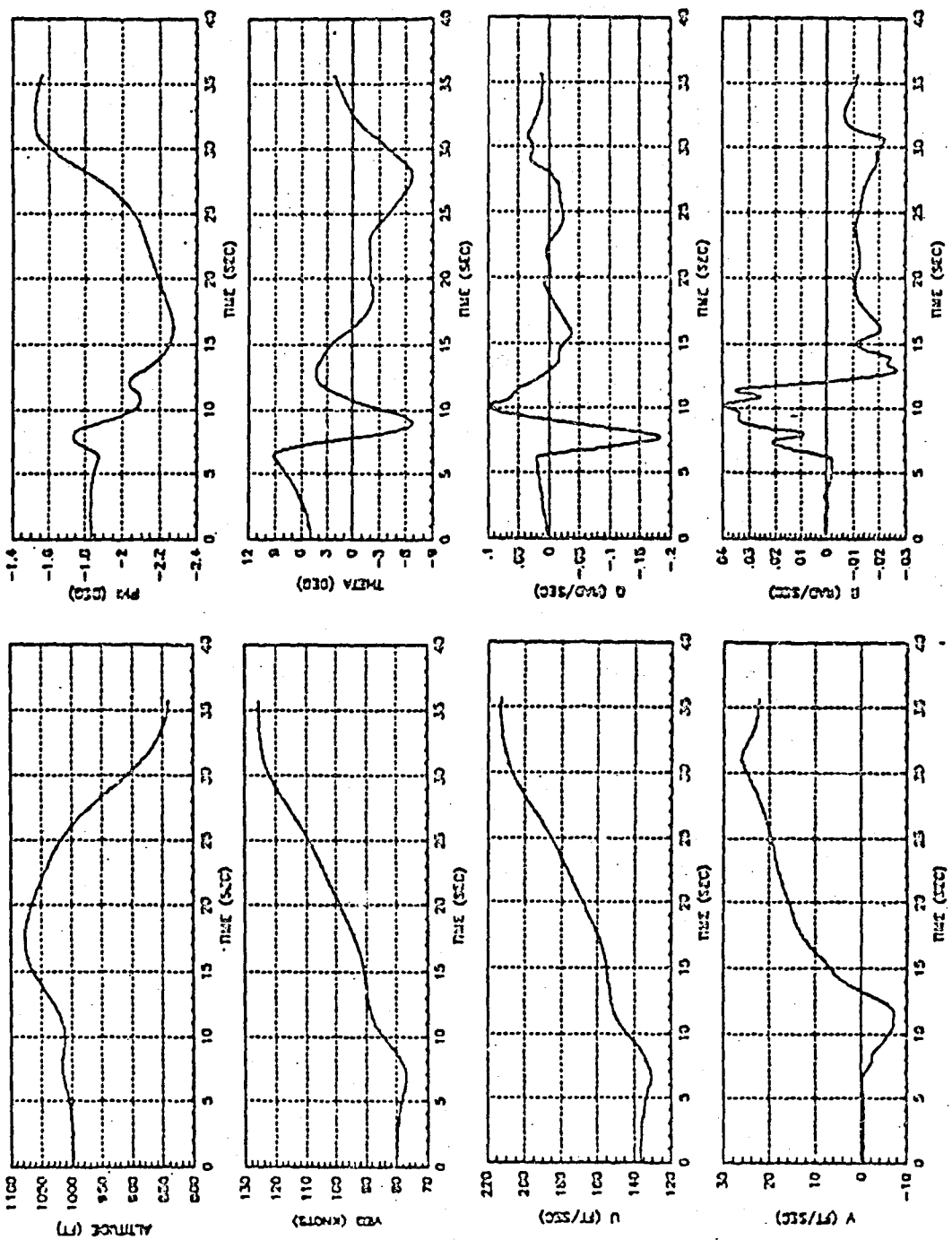

Figure 4-21. Selected Trajectory Parameter Time Histories for Adaptive Control During Transition from 80 kts/1000 ft to 125 kts/850 ft.

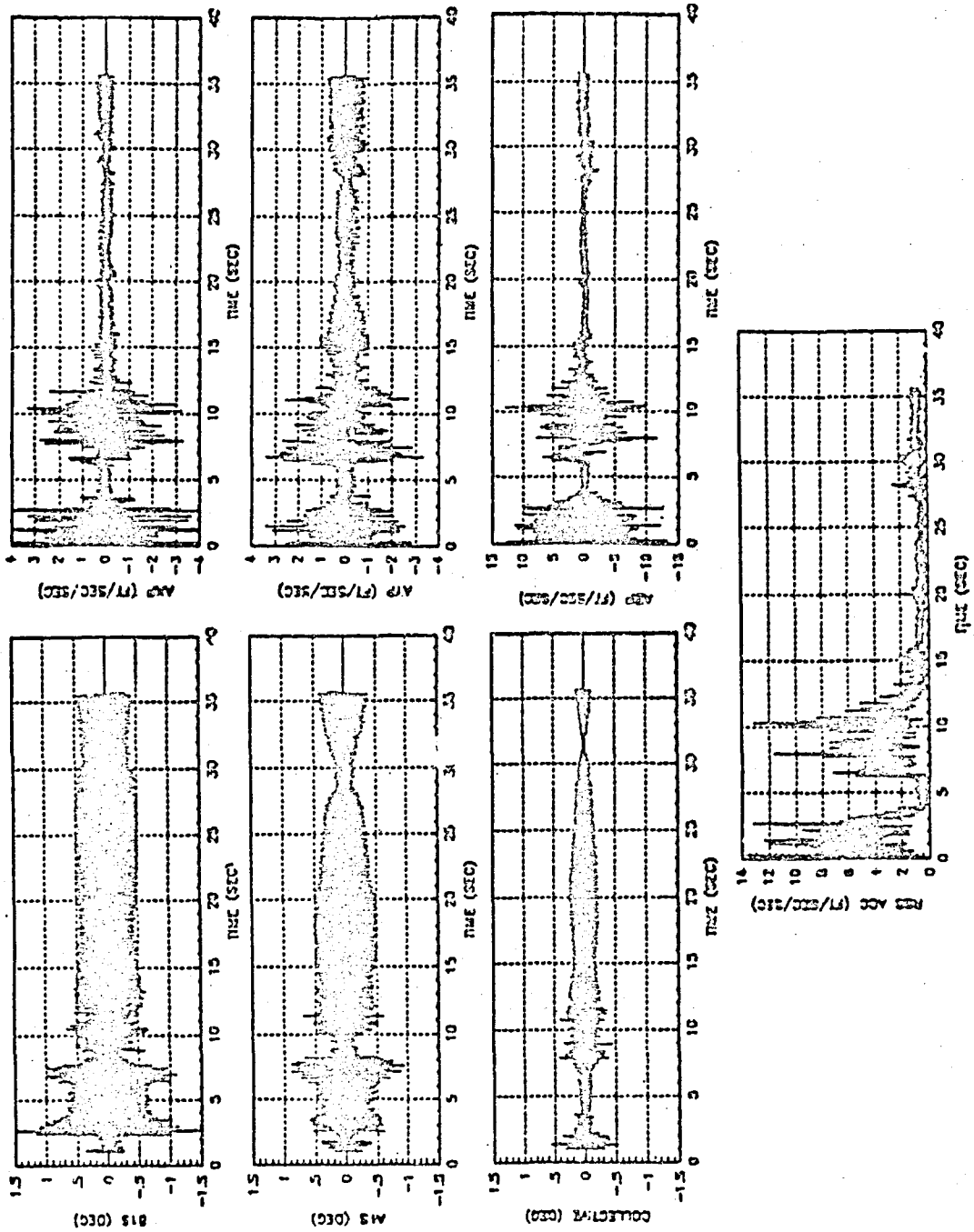

Figure 4-22. Control Inputs and Accelerometer Outputs for Adaptive Control During Transition from 80 kts/1000 ft to 125 kts/850 ft.

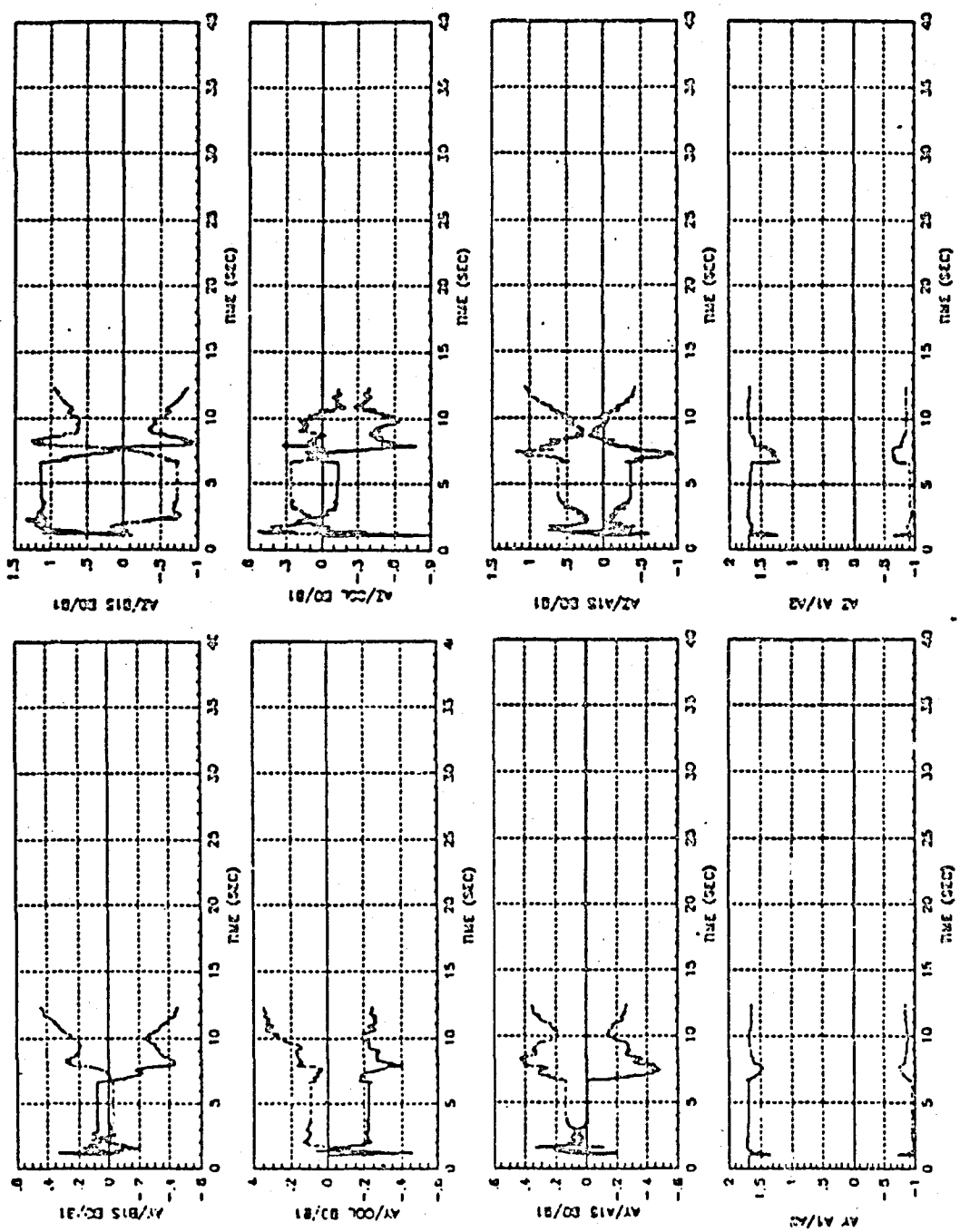

Figure 4-23. Selected Parameter Estimate Time Histories for Adaptive Control During Transition from 80 kts/1000 ft to 125 kts/850 ft.

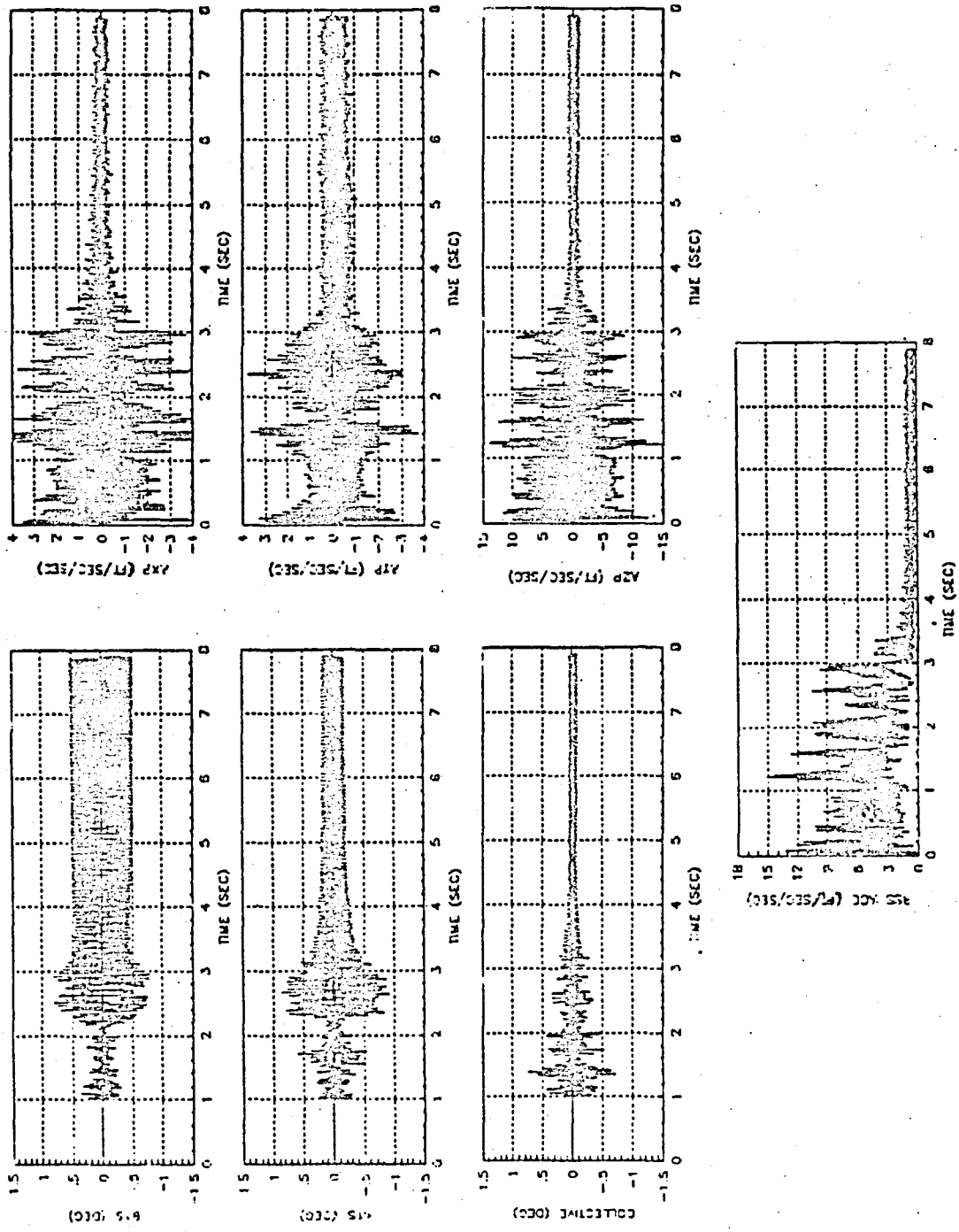

Figure 4-24. Control Inputs and Accelerometer Outputs for Adaptive Control at 120 kts/1000 ft with Measurement Noise Only (σ = 0.1 ft/sec^2)

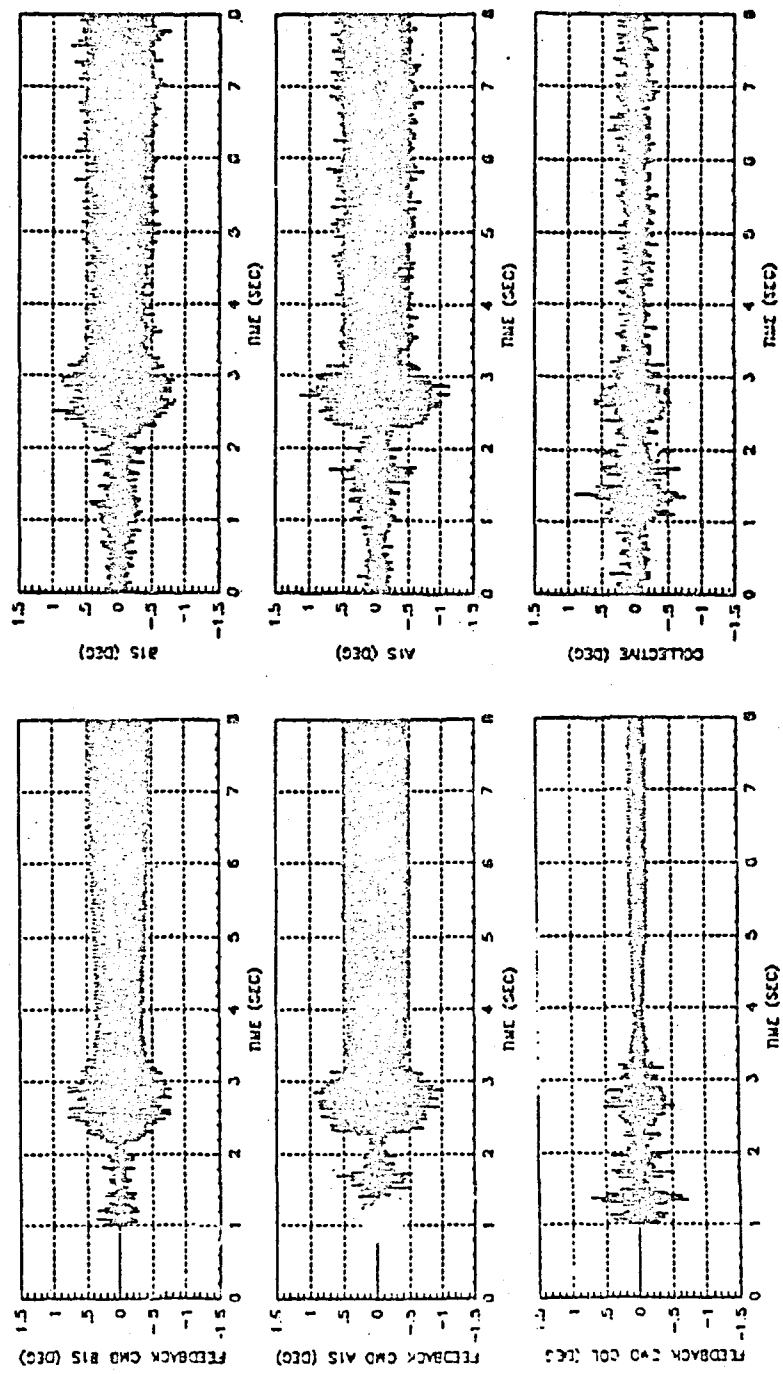

Figure 4-25. Control Inputs for Adaptive Control at 120 kts/1000 ft with Measurement Noise (σ = 0.25 ft/sec^2) and Process Noise (σ = 0.1°) Included

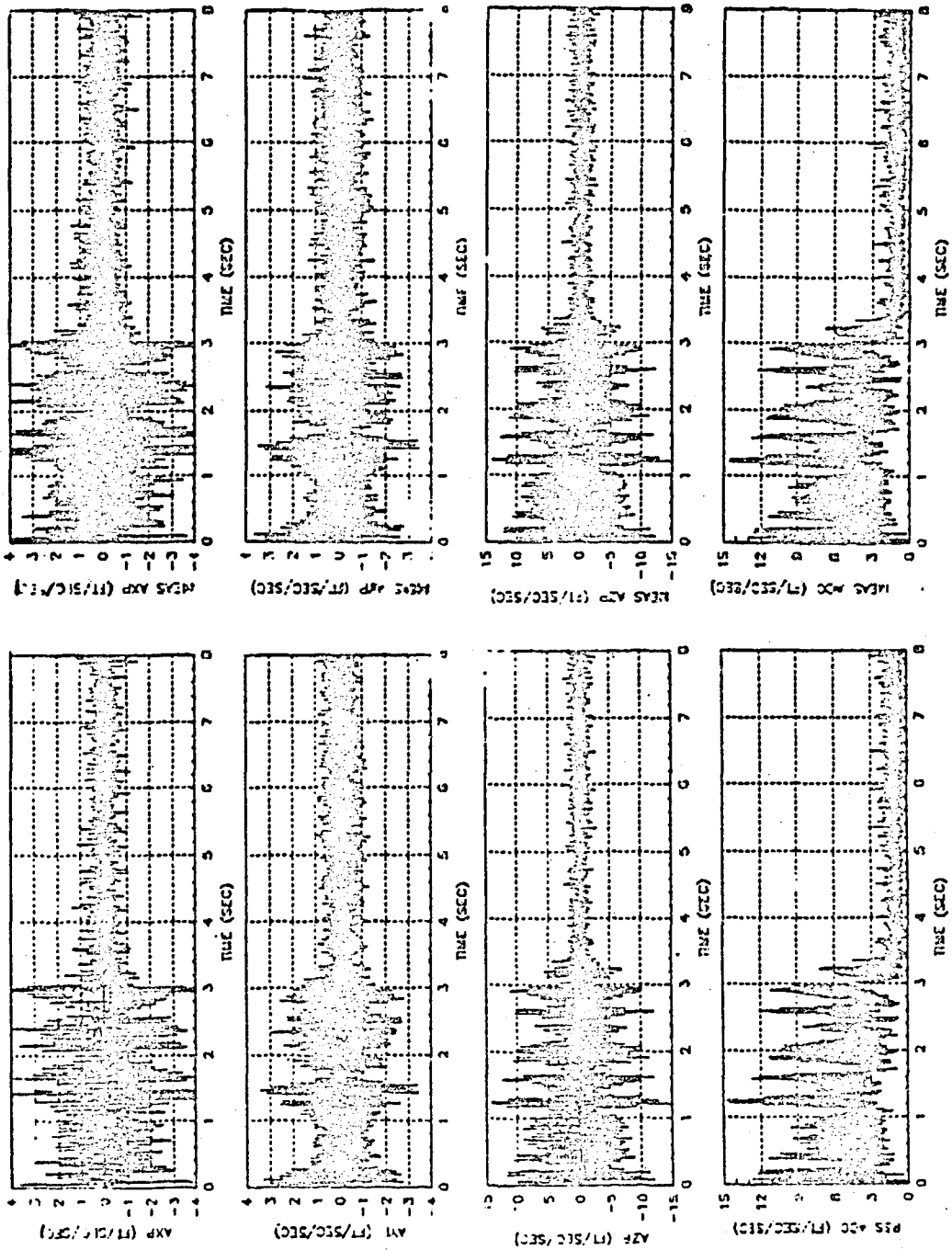

Figure 4-26. Accelerometer Outputs for Adaptive Control at 120 kts/1000 ft with Measurement Noise (σ = 0.25 ft/sec^2) and Process Noise (σ = 0.1°) Included

4.3.2 Discussion of Adaptive Controller Simulation Results

The simulation results of the adaptive controller applied to the GENHEL model of the RSRA helicopter indicate significant vibration reduction at all steady-state flight conditions tested. Significant vibration reduction was also achieved during changing flight conditions. Notably, the reduction was achieved with no unique a priori information about the helicopter or flight conditions. The algorithm initialization and tuning were independent of the flight conditions.

Adaptive controller performance under steady-state flight conditions without measurement noise or process noise included is shown in Figures 4-5 through 4-17. As discussed previously, the first second of the acceleration time histories indicates the uncontrolled, unforced vibration levels; from one to two seconds wide band noise is being added to the controls, but no feedback for vibration control is present; from two seconds on the control feedback is present. As can be seen by noting the times at which the vibration levels drop suddenly to their final values, the time from control feedback initiation to parameter identification disabling (and consequently wide band noise turn-off) is on the order of two to three seconds. This is, of course, a strong function of the ID-OFF threshold level. In Figure 4-16, the results for the flight condition 120 knots at 5000 feet indicate a transient time in excess of 4 seconds. For this flight condition, the ID-OFF threshold was lowered from 3.0 ft/sec^2 to 2.0 ft/sec^2.

For all the steady-state flight conditions, less collective is used than swashplate control. It was also noted during the algorithm tuning phase of the analysis, near the stability boundary large amounts of collective were used. Correspondingly larger amounts of swashplate deflection were used as well. Apparently, attempts to use more collective deflection to decrease the vertical vibration result in increasing amounts of power at N/rev cross-coupling into the lateral channels; thus requiring larger swashplate deflections. Incorporating cross-coupling terms in the MISO parameter identification algorithm might alleviate these problems. As far as the GENHEL simulation is concerned, however, it is seemingly necessary to keep the amount of main rotor collective used for vibration control small. Increasing collective deflections are indicative of impending instability.

During each of the steady-state flight condition tests, it was also noted that the RSRA simulation could not maintain the supposed trim condition. In each case, non-zero body angular rates developed which after several seconds caused slow divergence of the velocity and altitude profiles. The most common divergence was due to a small positive pitch rate and resulted in (initially) increasing altitude and decreasing velocity profiles. For the 120 knot/7000 feet flight condition, the divergence was rapid however, and over the eight second test interval, the flight condition varied significantly. After initially suppressing the vibration below the ID-OFF threshold, the vibration level increased to the point where the ID-ON threshold was surpassed. Increasing amounts of control authority were required throughout the eight second test. To prevent this divergence, the roll and pitch rates of the body were set to zero in order to prevent the divergence. Note this was required for the 120 knot/7000 feet flight condition only.

Table 4-2 summarizes the final steady-state vibration and control amplitudes for the various flight conditions without measurement or process noise. For the steady state conditions, the input amplitudes gradually increase for more demanding flight regimes, though not nearly as fast as for the fixed-gain controllers (cf. Table 3-1). These results are highly dependent upon the ID-ON/OFF thresholds and the time history of wide band noise input for robust parameter identification. This dependence is possibly a consequence of overparameterization/mismodeling as indicated by the large parameter correlations in Table 4-1.

The results of the adaptive control with time-varying Ω are shown in Figures 4-18 through 4-20. The rather abrupt change in Ω results in a significant decrease in velocity over the interval (θ_c was increased in an attempt to maintain altitude) as well. As can been seen in the output time histories, during the period of Ω-variation, the vibration suppression is less than impressive. This is a consequence of the time constants in the narrowband filters in the identifier and controller structures. The center frequency of the filters tracks the Ω-variations, but the bandwidth remains fixed. The time constants are too large for the filters to be effective when the center frequencies are changing rapidly. After the Ω-variation ceases, the filters reach steady-state and the controller performance improves substantially. The bandwidth of the filters could certainly be

TABLE 4-2. SUMMARY OF ADAPTIVE CONTROLLER STEADY-STATE ACCELERATION AND CONTROL AMPLITUDES FOR STEADY-STATE FLIGHT CONDITIONS

Flight Condition		Steady-State RSS ACC (ft/sec^2)	Steady-State Feedback Control Peak-to-Peak		
VEQ (knots)	Altitude (feet)		B_{1s}(deg)	θ_c(deg)	A_{1s}(deg)
5	100	0.8	0.2	0.3	0.7
	1000	1.0	0.5	0.3	0.7
40	100	1.0	0.7	0.6	1.8
	1000	1.0	1.2	0.4	1.6
120	100	1.2	0.3	0.4	1.5
	1000	1.0	1.0	0.1	0.4
	2000	1.0	1.0	0.2	0.6
	5000	1.2	0.9	0.3	1.1
	7000	1.5	1.0	0.6	1.6

increased somewhat during period of significant Ω-variation. However, more sophisticated logic would be required, and caution would have to be exercised so as not to excite the nonlinearities of the helicopter, thus invalidating the approximate model of the vibration dynamics.

The vibration results during transition from 80 to 125 knots are interesting (cf. Figures 4-21 through 4-23)). After the identification start-up procedure, the vibration is suppressed by a factor of 5-10 at 6 seconds when the maneuver begins. The controller is continuously operating and identification comes on when the vibration performance measure exceeds the ID-ON threshold about one tenth of a second after the start of the maneuver. There is a fair amount of dynamics due to pilot motion in the period from 6 to 10 seconds. By viewing parameter plots in Figure 4-22, it is evident that at during the maneuver, the model poles become more heavily damped (a_1 and a_2 decrease) and that the phase of the second-order transfer function is changing radically (b_0 and b_1 change symmetrically by significant amounts). The vibration level during this time is slightly less than the uncontrolled

vibration, even with the additive excitation. Note the pilot inputs during this period are severe enough that they have some contribution in the bandwidth around N/rev and thereby "fight" the vibration suppression controller. With more stable rigid body motion after ten seconds the parameters begin to stabilize and by sixteen seconds the vibration threshold is passed such that the identification turns off. As the control gains reach their steady-state values, the vibration level continues to decrease. Other small increases are due to some lateral acceleration at twenty and thirty-one seconds. The ID-ON threshold is not surpassed for the remainder of the test.

The results of the adaptive controller tests with measurement noise only (Figure 4-24) and with measurement and process noise (Figures 4-25 and 4-26) indicate that the algorithm performance does not degrade significantly with moderate amounts of noise added. Certainly, with broadband measurement noise only, little degradation is to be expected since the narrowband controller filters output most of the noise before generating the feedback signals. Process noise clearly is the dominant factor (unless powerful narrowband measurement noise is present), and for wideband noise with σ=0.1°, the performance degradation is minimal.

SECTION 5

SUMMARY OF FIXED-GAIN AND ADAPTIVE CONTROLLER RESULTS

The design of a fixed-gain controller for suppressing vibration in the model (GENHEL) of the RSRA helicopter was successfully accomplished using frequency shaped cost functionals and a linearized model of the vibration dynamics obtained by numerical calculation of stability derivatives in a fourteenth-order model of the vibration dynamics. The frequency shaping was necessary in order to prevent feedback at frequencies other than Ω (the region of model validity) which could cause instabilities. This controller was found to be destabilizing, however, when flexible fuselage modes were added to the simulation, resulting in the need for the inclusion of additional modes in the model. Noting that the model had grown too complex for control of nearly periodic disturbances, an approximate second-order autoregressive with exogenous input (ARX) model of the input-output relationships was identified instead. Based upon this approximate model of the vibration dynamics, a fixed-gain controller was designed at a flight condition of 120 knots forward speed and 100 feet altitude. The performance of the controller at and away from the design point was quite good.

The design of the adaptive controller employed a similar ARX model of the vibration dynamics and used the frequency shaping concept in the control design as well. The implementation was significantly more complex than the fixed-gain controller, involving on-line parameter identification, state estimation, and control gain calculation. The algorithm performed quite well at all flight conditions as well as during transients. Robustness to measurement and process noise was demonstrated as well.

Though the temptation to compare the results of the two algorithms is great, this should be done in the light of several important points. First, and most important is the fact that the underlying assumptions upon which the two algorithms are based are different. The fixed-gain controller is designed assuming that the model of the vibration dynamics is fixed and known for all future times, whereas the adaptive algorithm assumes the model form is fixed, but that the parameters in the model may vary with time.

This subtle difference is similar to the difference between causal and anti-causal filters. Knowledge of the future can always be used to great advantage in control design, and the fixed-gain controller is using such knowledge. The adaptive algorithm, on the other hand, attempts to identify the present system, estimate the current states, and control the future outputs based on the past and limited expectations concerning the future.

A second key difference in the controllers involved the set of controls used for vibration suppression. All four controls were used in the fixed-gain design whereas only three were used in the adaptive algorithm; tail collective was not used. Another important difference was that different models were used for system identification. The fixed-gain control design was based on a fully MIMO identified ARX model structure. The adaptive controller ignored the output coupling identifying parameters in three decoupled MISO ARX models.

However, in spite of all these important differences, there are a few general comments which can be made. First, the algorithms both performed equally well at all the flight conditions tested in terms of overall vibration suppression. Away from the design point of 120 knots/100 feet, the fixed-gain controller required more control authority than did the adaptive algorithm which is to be expected. However, the fixed-gain controller exhibited faster convergence than the adaptive controller at and near the 120 knots/100 feet design point. This is a direct consequence of the different assumptions discussed above..

As a final note, it should be remembered that both controllers were controlling a simulation and not a real helicopter. The nonlinearities of a real helicopter are most assuredly more severe than those in the GENHEL simulation of the RSRA, and real actuator dynamics (not modeled in the simulation) will certainly have an effect on the controller performance. However, the most important point with respect to unmodeled nonlinearities is that the objective is to control vibration at or near a few select frequencies only. Global validity of the models employed is not required. Approximate models, valid in the frequency ranges of interest, are sufficient for effective control designs, both fixed-gain and adaptive.

SECTION 6
RECOMMENDATIONS

The results of the adaptive controller tests are quite promising, however further analysis is warranted before stronger conclusions can be reached. A more extensive process and measurement noise sensitivity analysis should be conducted in order to ascertain the performance degradation with increasing measurement noise. Since the adaptive algorithm is nonlinear, there is little that can be done analytically; Monte Carlo analysis is appropriate for these investigations.

Further trade-off studies should be performed in which the effect of the bandwidth of the noise added for identification on the transient vibration levels is ascertained. Noise outside the controller bandwidth (which is significantly smaller than the noise filter bandwidth) is not controlled and adds to the vibration level during the ID process. On the other hand, as the noise filter bandwidth decreases, the identifiability of the model parameters decreases resulting in larger variance estimates and possible subsequent controller degradation.

As discussed in Section 4, the controller implemented used the filtered state estimates in the feedback loop. For real-time implementation, this will result in a delay in the control actuation due to the finite computation time. Use of the predicted state estimates eliminates the problem of the delay, but introduces states with a larger variance in the control loop. The effects of the delay versus the predicted state feedback should be investigated. The fundamental factor in determining which approach is superior is the adequacy of the second-order model of the helicopter dynamics around N/rev. If the model is not good, the predicted states will deviate significantly from the 'true' states and the controller performance will degrade.

Finally, further studies should be performed on a simulation including higher order aeroelastic nonlinear effects and, more importantly, with more realistic models of the actuators. It is anticipated that the later will have a more significant impact on the achievable performance than the former. Regardless of the magnitude of the nonlinearities, the second-order model employed is sufficiently accurate in the frequency ranges of interest for periodic disturbance suppression. However, control actuator lags and

limits could potentially limit severely the performance of both the fixed-gain and adaptive controllers.

In spite of the caveats discussed above, the autotuning type of adaptive controller successfully demonstrated in this study is quite attractive for an operational environment, where manufacturers will not want to do identification on each vehicle that is produced or 'retune' the controller during periodic maintenance to track changes in the flexibility effects of structual members. Thus, both the fixed-gain and adaptive frequency shaped control techniques analyzed here should be tested in wind tunnels. A logical sequence would be:

Wind tunnel testing

1) with a fixed-gain scheduled control law,
2) with a single-point robust fixed-gain control law, and
3) with an adaptive autotuning control law,

Should the tests prove successful, demonstrating sufficient robustness to disturbances of all types, flight tests would be warranted. A similar sequence as that outlined above would be appropriate.

REFERENCES

[1] Kaletka, J., 'Rotorcraft Identification Experience', AGARD Lecture Series No. 104, London, November 1979.

[2] McCloud, J.L., III, and Kretz, M., 'Multicyclic Jet-Flap Control for Alleviation of Helicopter Blade Stresses and Fuselage Vibration', Rotorcraft Dynamics, NASA SP-352, 1974, pp. 233-238.

[3] Johnson, W., 'Self-Tuning Regulators for Multi-Cyclic Control of Helicopter Vibration', NASA Technical Paper 1996, March 1982.

[4] Johnson, W., Helicopter Theory. Princeton University Press, Princeton, New Jersey, 1980.

[5] Gupta, N.K., 'Comparison of Frequency-Domain and Time-Domain Rotorcraft Vibration Control Methods', NASA Contractor Report under Contract NAS2-11271, Apr. 1984.

[6] Gupta, N.K., and DuVal, R.W., 'A New Approach to Active Control of Rotorcraft Vibrations', AIAA Journal of Guidance and Control, Nov.-Dec. 1981.

[7] Gupta, N.K., 'Frequency-Shaping of Cost Functionals: Extensions of LQG Design Methods', AIAA Journal of Guidance and Control, Vol. 3, No. 6, Nov.-Dec. 1980, pp. 529-535.

[8] Gregory, C.Z., Jr., and Gupta, N.K., 'Rotorcraft Vibration Controller Design and Evaluation,' ISI Report No. 14, Prepared by Integrated Systems, Inc. for NASA-Ames Research Center under Contract NAS2-10951, April 1982.

[9] Bierman, G.J., Factorization Methods for Discrete Sequential Estimation, Academic Press, New York 1977

[10] Bryson, A.E., and Ho, Y.C., Applied Optimal Control, Hemisphere Publishing Co., New York, 1975

[11] Franklin, G.F., and Powell,J.D., Digital Control of Dynamic Systems, Addison Wesley, Menlo Park, California, 1980

[12] Doyle, J. C. and Stein, G., 'Multivariable Feedback Design: Concepts for a Classical/Modern Synthesis', IEEE Trans. Automat. Contr., AC-26, pp 4-16, February 1981.

[13] Safanov, M. G., Laub, A. J. and Hartmann, G. L., 'Feedback Properties of Multivariable Systems: The Role and Use of the Return Difference Matrix', IEEE Trans. Automat. Contr., AC-26, pp 47-65, February 1981.

[14] Kosut, R. L., 'Robustness Issues in Adaptive Control', IFAC Workship on Adaptive Systems in Control and Signal Processing, San Francisco, CA, June 20-22, 1983.

[15] Molusis, J.A.,Hammond, C.E., and Cline, J.H.,'A Unified Approach to the Optimal Design of Adaptive and Gain-Scheduled Controllers to Achieve Minimum Helicopter Rotor Vibration', 37th Annual Forum of the American Helicopter Society, New Orleans, La., May 1981.

APPENDIX A

NASTRAN MODAL ANALYSIS OF RSRA FLEXIBLE FUSELAGE

The first 34 natural frequencies, generalized masses and generalized stiffnesses for the RSRA flexible fuselage are shown in Table A-1. The eigenvector of mode number 15, the closest mode to the rotor frequency N/rev is shown in Table A-2. In Table A-2, point ID number 11 is the rotor frame (HUB) and point number 546 is considered to be the pilot location.

Table A-1. MODAL ANALYSIS OF THE RSRA HELICOPTER MODEL
(MARCH 4, 1981 - NASTRAN 12/16/81)

REAL EIGENVALUES

MODE NO.	EIGENVALUE	RADIANS	CYCLES	GENERALIZED MASS	GENERALIZED STIFFNESS
1	0.0	0.0	0.0	4.e54792E+01	0.0
2	0.0	0.0	0.0	4.e54792E+01	0.0
3	0.0	0.0	0.0	4.523229E+01	0.0
4	0.0	0.0	0.0	1.779957E+01	0.0
5	0.0	0.0	0.0	1.921430E+02	0.0
6	0.0	0.0	0.0	1.293919E+02	0.0
7	7.621617E+02	2.760728E+01	4.393835E+00	1.622210E+00	1.236392E+03
8	9.630158E+02	3.103250E+01	4.938975E+00	1.267294E+00	1.220426E+03
9	2.308398E+03	4.804579E+01	7.646726E+00	1.712279E+00	3.952622E+03
10	3.559379E+03	5.966053E+01	9.495268E+00	1.565646E+00	5.572726E+03
11	4.190264E+03	6.473225E+01	1.030246E+01	2.872793E+00	1.203778E+04
12	6.577077E+03	8.109916E+01	1.290734E+01	1.859165E+00	1.222129E+04
13	8.738801E+03	9.348156E+01	1.487805E+01	1.872158E+00	1.636042E+04
14	9.494006E+03	9.743719E+01	1.550761E+01	2.873428E+00	2.728034E+04
15	1.230904E+04	1.109461E+02	1.765762E+01	3.987881E+00	4.902542E+04
16	1.369259E+04	1.170154E+02	1.862357E+01	2.866976E+00	3.925634E+04
17	1.448761E+04	1.203645E+02	1.915660E+01	3.575121E+00	5.179495E+04
18	1.591383E+04	1.261579E+02	2.007866E+01	4.220672E+00	6.717550E+04
19	1.732225E+04	1.316140E+02	2.094702E+01	3.160165E+00	5.474117E+04
20	1.980104E+04	1.407162E+02	2.239567E+01	4.230754E+00	8.377333E+04
21	2.452748E+04	1.566125E+02	2.492565E+01	2.129577E+00	5.223311E+04
22	2.753163E+04	1.659266E+02	2.640804E+01	3.311485E+00	9.117057E+04
23	2.805686E+04	1.675018E+02	2.665875E+01	1.987016E+00	5.574944E+04
24	2.888033E+04	1.699421E+02	2.704713E+01	2.277678E+00	6.578009E+04
25	3.316464E+04	1.821116E+02	2.898396E+01	3.017276E+00	1.000669E+05
26	3.497404E+04	1.870135E+02	2.976412E+01	3.317150E+00	1.160141E+05
27	3.673318E+04	1.916590E+02	3.050348E+01	5.228042E+00	1.920426E+05
28	4.007387E+04	2.001846E+02	3.186037E+01	2.818761E+00	1.129587E+05
29	4.709674E+04	2.170178E+02	3.453946E+01	3.761831E+00	1.771700E+05
30	5.053968E+04	2.248103E+02	3.577969E+01	3.510556E+00	1.774224E+05
31	5.095703E+04	2.257366E+02	3.592710E+01	5.241822E+00	2.671077E+05
32	5.638099E+04	2.374468E+02	3.779083E+01	3.847402E+00	2.169204E+05
33	5.698542E+04	2.387162E+02	3.799286E+01	4.731770E+00	2.696419E+05
34	5.939288E+04	2.437065E+02	3.878710E+01	8.698703E+00	5.166411E+05

Table A-2. EIGENVECTOR OF MODE 15 OF RSRA HELICOPTER MODEL
(MARCH 4, 1981 - NASTRAN 12/16/81)

EIGENVALUE = 1.239904E+04
CYCLES = 1.765762E+01 REAL EIGENVECTOR NO. 15

POINT ID.	T1	T2	T3	R1	R2	R3
1	-2.189307E-02	-2.332110E-02	-5.830057E-03	-1.112256E-03	-2.399986E-04	-4.626277E-05
2	-2.104183E-02	-2.520769E-02	-1.650842E-02	-1.112256E-03	-2.399986E-04	-4.626277E-05
3	-2.274430E-02	-2.520769E-02	2.442260E-02	-1.112256E-03	-2.399986E-04	-4.626277E-05
8	-3.012502E-02	1.389802E-02	-9.998965E-04	-1.415554E-03	-5.333254E-04	-5.634995E-05
9	-2.431705E-02	-1.301858E-02	-9.988717E-04	-1.112256E-03	-2.399784E-04	-4.626272E-05
10	-2.652504E-02	-2.785824E-03	-9.988851E-04	-1.112256E-03	-2.399986E-04	-4.626277E-05
11	-4.898098E-02	5.128137E-02	-1.001022E-03	-2.032791E-03	-1.130329E-03	-6.556213E-05
12	-2.456072E-02	6.768619E-03	4.114681E-02	-9.551572E-04	8.112236E-04	-1.456099E-04
13	-2.812669E-02	7.145563E-03	6.094339E-02	-1.475376E-03	6.445037E-04	-1.405402E-04
101	-6.249715E-03	1.418512E-01	-1.469113E-01	-2.445294F-02	-2.720051E-03	-1.056095E-03
527	-2.142667E-02	5.115862E-02	4.082010E-02	-2.393977E-03	-4.463514E-04	0.0
535	2.227910E-02	4.996913E-02	-7.478463E-02	-1.340232E-03	-1.667367E-03	0.0
538	2.210359E-02	3.473072E-02	-5.324562E-02	-1.481017E-03	-1.536200E-03	0.0
546	-2.113531E-02	3.709349E-02	5.521893E-02	-1.037675E-03	-5.100583E-04	0.0
647	2.195067E-02	2.683900E-02	-4.299799E-02	-6.666940E-04	-1.391693E-03	0.0
659	-2.033691E-02	2.998216E-02	5.895294E-02	-1.543560E-03	-5.512129E-04	0.0
1401	1.147524E-02	-2.848306E-02	-5.601325E-03	0.0	-3.534379E-04	0.0
1402	1.112423E-02	-3.056510E-02	-4.883300E-03	0.0	2.888741E-04	0.0
1403	1.150519E-02	-3.212431E-02	-4.830200E-03	0.0	2.776836E-04	0.0
1404	1.258090E-02	-3.333500E-02	-4.021813E-03	0.0	-1.319482E-04	0.0
1440	1.761409E-02	-2.337366E-02	1.162864E-02	0.0	3.470051E-04	0.0
1441	1.411692E-02	-2.462533E-02	5.954643E-03	0.0	4.503997E-04	0.0
1442	1.229327E-02	-2.626352E-02	5.827924E-04	0.0	3.683948E-04	0.0
1504	1.514671E-02	-3.134985E-02	-5.166459E-03	0.0	3.024370E-04	0.0
1540	2.324402E-02	-2.772009E-02	8.201866E-03	0.0	-3.217202E-04	0.0
1601	1.979644E-02	-2.525138E-02	-8.488368E-04	0.0	1.935107E-05	0.0
1602	1.866584E-02	-2.530770E-02	-5.227968E-03	0.0	4.982934E-04	0.0
1603	1.760415E-02	-2.551403E-02	-9.697185E-03	0.0	4.854839E-04	0.0
1604	1.631994E-02	-2.608518E-02	-1.640776E-02	0.0	6.136770E-04	0.0
1640	2.307229E-02	-2.929680E-02	2.410931E-02	0.0	-8.724071E-04	0.0
1641	2.142116E-02	-2.718537E-02	1.093953E-02	0.0	5.388239E-04	0.0
1642	2.043353E-02	-2.603326E-02	4.281957E-03	0.0	5.323228E-04	0.0
4913	6.149341E-02	8.517664E-01	1.570026E-01	0.0	0.0	0.0
5101	-4.586285E+00	1.724457E+00	-5.274023E+00	8.991367E-02	4.145254E-03	-6.650239E-02
5102	-4.586285E+00	1.164374E+00	-5.308935E+00	8.991367E-02	4.145254E-03	-6.650239E-02
5103	-4.586285E+00	2.108626E-01	-5.368349E+00	8.991367E-02	4.145254E-03	-6.650239E-02
5130	4.875851E+00	2.014762E-01	5.531722E+00	9.158336E-02	-1.527945E-03	-6.702738E-02
5131	4.875851E+00	1.162515E+00	5.509815E+00	9.158336E-02	-1.527945E-03	-6.702738E-02
5132	4.875851E+00	1.727019E+00	5.496946E+00	9.158336E-02	-1.527945E-03	6.702738E-02

APPENDIX B

LINEARIZED MODEL OF THE RSRA VIBRATION DYNAMICS

This appendix presents the dynamic matrices for the identified linear model of the RSRA vibration dynamics in steady-state flight at a 120-knot forward speed and 100 feet altitude flight condition. The discrete domain MIMO ARX model given in equation 3.1;

$$y_{k+i} = A_1 y_k + A_2 y_{k-1} + B_1 u_k + B_2 u_{k-1} + \Gamma w_k \qquad (3.1)$$

where u is the vector of control inputs, y is the vector of outputs and w is a vector of the sine and cosine of the rotor angle (ψ), was used to perform least-squares identification of the coefficient matrices. Transforming this equation into state-space form for controller design was performed in detail in Section 3 (cf. equations 3.21 through 3.23). Using the notation employed in Section 3.2, the following matrices represent the identified model of the RSRA vibration dynamics (i.e. the plant) coupled with the frequency shaping filter dynamics.

```
         COLUMNS  1 THRU  6
       1.9840D+00   8.6314D-03   2.3410D-03   1.0000D+00   0.0000D+00   0.0000D+00
      -7.7307D-03   1.9815D+00   2.1024D-03   0.0000D+00   1.0000D+00   0.0000D+00
       2.4753D-04  -5.2800D-02   1.9790D+00   0.0000D+00   0.0000D+00   1.0000D+00
      -9.9139D-01  -9.9747D-03  -2.6493D-03   0.0000D+00   0.0000D+00   0.0000D+00
       0.4532D-03  -9.9550D-01  -2.5781D-03   0.0000D+00   0.0000D+00   0.0000D+00
F =    2.8754D-03   4.3141D-02  -9.9049D-01   0.0000D+00   0.0000D+00   0.0000D+00
       1.2146D-02   5.2842D-05   1.4332D-05   6.1221D-03   0.0000D+00   0.0000D+00
       2.4267D+01   1.0559D-01   2.8635D-02   1.2232D+01   0.0000D+00   0.0000D+00
      -4.7328D-05   1.2131D-02   1.2871D-05   0.0000D+00   6.1221D-03   0.0000D+00
      -9.4560D-02   2.4238D+01   2.5716D-02   0.0000D+00   1.2232D+01   0.0000D+00
       1.5157D-06  -3.2324D-04   1.2116D-02   0.0000D+00   0.0000D+00   6.1221D-03
       3.0283D-03  -6.4583D-01   2.4207D+01   0.0000D+00   0.0000D+00   1.2232D+01

         COLUMNS  7 THRU 12
       0.0000D+00   0.0000D+00   0.0000D+00   0.0000D+00   0.0000D+00   0.0000D+00
       0.0000D+00   0.0000D+00   0.0000D+00   0.0000D+00   0.0000D+00   0.0000D+00
       0.0000D+00   0.0000D+00   0.0000D+00   0.0000D+00   0.0000D+00   0.0000D+00
       0.0000D+00   0.0000D+00   0.0000D+00   0.0000D+00   0.0000D+00   0.0000D+00
       0.0000D+00   0.0000D+00   0.0000D+00   0.0000D+00   0.0000D+00   0.0000D+00
       0.0000D+00   0.0000D+00   0.0000D+00   0.0000D+00   0.0000D+00   0.0000D+00
       9.9388D-01   9.9796D-04   0.0000D+00   0.0000D+00   0.0000D+00   0.0000D+00
      -1.2232D+01   9.9388D-01   0.0000D+00   0.0000D+00   0.0000D+00   0.0000D+00
       0.0000D+00   0.0000D+00   9.9388D-01   9.9796D-04   0.0000D+00   0.0000D+00
       0.0000D+00   0.0000D+00  -1.2232D+01   9.9388D-01   0.0000D+00   0.0000D+00
       0.0000D+00   0.0000D+00   0.0000D+00   0.0000D+00   9.9388D-01   9.9796D-04
       0.0000D+00   0.0000D+00   0.0000D+00   0.0000D+00  -1.2232D+01   9.9388D-01
```

```
      -1.3753D-02  -2.2317D-01   1.9015D-01  -4.1865D-03
       7.1973D-02  -1.[illegible]55D-01   4.6902D-02  -1.2116D-02
       2.0029D-01  -1.9127D-01   9.4816D-02   2.5011D-02
       9.8085D-03   2.1322D-01  -1.8756D-01   6.0758D-03
      -7.2618D-02   1.0875D-01  -3.9058D-02   1.2015D-02
G =   -2.1661D-01   1.5871D-01  -8.0228D-02    .9114D-02
      -8.4195D-05  -1.3663D-03   1.1641D-03  -2.5630D-05
      -1.6822D-01  -2.7298D+00   2.3259D+00  -5.1208D-02
       4.4063D-04  -6.6457D-04   2.8714D-04  -7.4185D-05
       8.8035D-01  -1.3278D+00   5.7369D-01  -1.4922D-01
       1.2262D-03  -1.1711D-03   5.8047D-04   1.5312D-04
       2.4499D+00  -2.3398D+00   1.1598D+00   3.0593D-01
```

This model was used for control design as discussed in Section 3.2. The control gains used and the open-loop and closed-loop eigenvalues of the linearized vibration dynamics are:

Open-Loop Eigenvalues

σ (1/sec)	ω (rad/s)	ω_n (Hz)	ζ
4.2566D+00	1.2461D+02	1.9834D+01	3.4140D-02
2.5967D+00	8.7334D+01	1.3913D+01	2.9720D-02
4.4022D+00	1.0011D+02	1.5936D+01	4.3932D-02
4.2566D+00	-1.2461D+02	1.9834D+01	3.4140D-02
2.5967D+00	-8.7334D+01	1.3913D+01	2.9720D-02
4.4022D+00	-1.0011D+02	1.5936D+01	4.3932D-02
-1.0238D-07	1.1071D+02	1.7629D+01	-9.2478D-12
5.8703D-12	1.1071D+02	1.7629D+01	5.3024D-14
3.8927D-11	1.1071D+02	1.7629D+01	3.5161D-13
-1.0232D-07	-1.1071D+02	1.7629D+01	-9.2417D-12
5.9674D-12	-1.1071D+02	1.7629D+01	5.3902D-14
3.8302D-11	-1.1071D+02	1.7629D+01	3.5069D-13

Closed-Loop Eigenvalues

σ (1/sec)	ω (rad/s)	ω_n (Hz)	ζ
7.1415D+00	1.2640D+02	2.0159D+01	5.6411D-02
7.1415D+00	-1.2640D+02	2.0159D+01	5.6411D-02
4.4536D+00	8.6572D+01	1.3804D+01	5.1376D-02
4.4536D+00	-8.6572D+01	1.3804D+01	5.1376D-02
6.6755D+00	9.8342D+01	1.5696D+01	6.7724D-02
6.6755D+00	-9.8342D+01	1.5696D+01	6.7724D-02
5.9024D+00	1.1240D+02	1.7923D+01	5.2440D-02
5.9024D+00	-1.1240D+02	1.7923D+01	5.2440D-02
4.9943D+00	1.0967D+02	1.7481D+01	4.5493D-02
4.9943D+00	-1.0967D+02	1.7481D+01	4.5493D-02
1.8250D+00	1.1080D+02	1.7646D+01	1.6469D-02
1.8250D+00	-1.1080D+02	1.7646D+01	1.6469D-02

C =

COLUMNS 1 THRU 6

5.2392D-02	3.9459D-01	-1.2831D-01	7.6333D-02	3.2285D-01	-1.4201D-01
-2.5550D-01	6.2625D-01	-1.8679D-01	-2.3961D-01	7.0790D-01	-1.9097D-01
-4.3921D-02	5.0004D-01	-2.5159D-02	-6.8761D-02	4.9968D-01	-2.2637D-02
5.0362D-02	-1.4042D-02	-3.0547D-02	5.7812D-02	2.0260D-03	-3.5999D-02

COLUMNS 7 THRU 12

-3.0376D-04	-6.9425D-06	1.5228D-02	7.3513D-05	3.0940D-03	2.5415D-05
3.8086D-03	5.9148D-06	-9.1967D-03	-1.1579D-04	2.2726D-03	3.6610D-05
-8.9000D-03	4.0230D-05	-6.0302D-03	3.6339D-06	1.1363D-03	9.7865D-06
-1.4216D-03	-1.9195D-05	3.9101D-03	-1.9569D-05	-2.3552D-05	1.1047D-05

APPENDIX C

DIRECT FEEDTHROUGH MODIFICATION TO LQR COST FUNCTIONAL

In this appendix, a derivation is presented indicating the modifications to the standard LQR cost function in regulator design required to account for a direct feedthrough term, i.e. the presence of a component of the inputs in the outputs. The derivation is given in the continuous domain to simplify notation. Including the direct feedthrough term, the dynamical model of the system to be controlled can be written:

$$\begin{aligned} \dot{x} &= Fx + Gu \\ y &= Hx + Du \ . \end{aligned} \tag{C.1}$$

The cost function to be minimized is the standard quadratic functional:

$$J = \frac{1}{2} \int [y^T A y + u^T B u] \, dt \ .$$

Minimizing J subject to the constraints of the dynamical model by the method of Lagrange multipliers leads to the defintion of the Hamiltonian and the Euler-Lagrange equations:

$$\bar{H} = y^T A y + u^T B u + \lambda^T (Fx + Gu), \tag{C.2}$$

$$\frac{\partial \bar{H}}{\partial x} = \dot{\lambda} = - x^T H^T A H - u^T D^T A H - \lambda^T F \ , \tag{C.3}$$

$$\frac{\partial \bar{H}}{\partial u} = 0 = x^T H^T A D + u^T B + \lambda^T G + u^T D^T A D \ . \tag{C.4}$$

Defining:

$$\begin{aligned} \bar{B} &= B + D^T A D \ , \\ \bar{A} &= A - A D \bar{B}^{-1} D^T A \\ \bar{F} &= F - G \bar{B}^{-1} D^T A H , \end{aligned} \tag{C.5}$$

equation C.4 can be solved for u to give:

$$u = - \bar{B}^{-1} G^T \lambda - \bar{B}^{-1} D^T A H x \ . \tag{C.6}$$

Substituting equation C.6 into C.4, the Euler-Lagrange equations can be written in the standard form:

$$\dot{x} = \bar{F}x - G\bar{B}^{-1}G^T\lambda \ ,$$

$$\dot{\lambda} = -\bar{F}\lambda - H^T\bar{A}Hx \ . \qquad (C.7)$$

Thus, with the substitutions given in C.5, the LQR design with direct feedthrough of inputs to outputs can be cast in the standard cost functional form which which leads to the forward Ricatti equation and associated feedback gains:

$$\dot{S} = S\bar{F} + \bar{F}^TS - SG\bar{B}^{-1}G^TS + H^T\bar{A}H \ ,$$

$$\bar{C} = -\bar{B}^{-1}G^TS \ , \qquad (C.8)$$

$$\bar{u} = \bar{C}x \ .$$

In order to obtain the feedback appropriate for the original system in terms of the regulator gains computed in C.8, equation C.3 is rewwritten as follows:

$$u = -\bar{C}x - \bar{B}^{-1}D^TAHx = -Cx \ ,$$

$$C = \bar{C} + \bar{B}^{-1}D^TAH \ . \qquad (C.9)$$

It should be emphasized that even in the case of time-invariant system matricies (F,G,H,D), the steady-state solution to the forward regulator problem will not be the same as the fixed-gain regulator solution discussed in Section 3. They are solving two DIFFERENT problems! In the forward, or causal regulator solution, only knowledge of the past is assumed. The fixed-gain regulator assumes knowledge of the system over the entire interval which is usually assumed to be infinite.

1. Report No.	2. Government Accession No.	3. Recipient's Catalog No.
NASA CR-177344		

4. Title and Subtitle	5. Report Date
Fixed Gain and Adaptive Techniques for Rotorcraft Vibration Control	May 1985
	6. Performing Organization Code
7. Author(s)	8. Performing Organization Report No.
R. H. Roy, H. A. Saberi, R. A. Walker	
	10. Work Unit No.
9. Performing Organization Name and Address	Job Order # T4713D
Integrated Systems Inc. 101 University Avenue Palo Alto, CA 94301	11. Contract or Grant No. NAS2-11548
	13. Type of Report and Period Covered Contractor Report
12. Sponsoring Agency Name and Address National Aeronautics and Space Administration Washington, D.C. 20546	14. Sponsoring Agency Code 505 42 51

15. Supplementary Notes

Point of Contact: Technical Monitor, Peter D. Talbot
M.S. 237-5, Ames Research Center
Moffett Field, CA 94035 (415)694-5108

16. Abstract

This report presents the results of an analysis effort performed to demonstrate the feasibility of employing approximate dynamical models and frequency-shaped cost functional control law design techniques for helicopter vibration suppression. Both fixed-gain and adaptive control designs based on linear second-order dynamical models were implemented in a detailed Rotor Systems Research Aircraft (RSRA) simulation to validate these active vibration suppression control laws. Approximate models of fuselage flexibility were included in the RSRA simulation in order to more accurately characterize the structural dynamics. The results for both the fixed-gain and adaptive approaches are promising and provide a foundation for pursuing further validation in more extensive simulation studies and in wind tunnel and/or flight tests.

17. Key Words (Suggested by Author(s))	18. Distribution Statement
Higher Harmonic Control, Vibration Control of Helicopters, Adaptive Techniques, Helicopter Controller Algorithms	Unclassified - Unlimited Star Category 02

19. Security Classif. (of this report)	20. Security Classif. (of this page)	21. No. of Pages	22. Price*
Unclassified	Unclassified	116	

*For sale by the National Technical Information Service, Springfield, Virginia 22161

END

DATE

FILMED

OCT 22 1985

End of Document